

Drops: Controlled crystallization of organic crystals and their use as matrix materials for encapsulation of volatiles

Présentée le 30 août 2022

Faculté des sciences et techniques de l'ingénieur
Laboratoire de la matière molle
Programme doctoral en science et génie des matériaux

pour l'obtention du grade de Docteur ès Sciences

par

Aysu Ceren OKUR

Acceptée sur proposition du jury

Dr J. C. Plummer, président du jury
Prof. E. Amstad, directrice de thèse
Dr Ph. Erni, rapporteur
Prof. A. Fink, rapporteuse
Dr A. Magrez, rapporteur

İlim ilim bilmektir, ilim kendin bilmektir
Sen kendin bilmezsin, ya nice okumaktır
—Yunus Emre

To my family...

Acknowledgements

I would like to express my sincere gratitude to the people who have benevolently provided their support during this PhD thesis.

First, I would like to thank my supervisor, Esther Amstad for giving me the opportunity to pursue this thesis, and for introducing me to the amazing field of bio-inspired materials. Her encouraging attitude led me to discover and pursue challenging projects, dwell upon new areas of science. She has not only been a supervisor, but also a role model for me with her kindness, discipline and driven enthusiasm for science. I am very grateful for her support during rough times of pandemic which held a big part of the time this thesis being executed. I definitely learned a lot from her, and I am very grateful for this experience.

I would like to thank Philipp Erni, Lahoussine Ouali, Daniel Benczedi for collaborations, fruitful discussions, critical evaluations and technical support in Firmenich. I also thank Firmenich SA, as the projects in this thesis are funded by them. I also would like to thank all the jury members for their time, critical evaluations and positive and constructive feedbacks.

I have spent the majority of this period with my labmates from SMaL group. Gianluca Etienne and Antoine Vian have become the very first mentors and transferred their technical know-how to me. I would like to thank them for their time. I also thank them with former group members Jui-Chia Chang, Bjorn Schulte, Thomasz Szymborski, Irvine Ong for setting a joyful atmosphere in the group. I specifically would like to thank Huachuan Du, as he has been very supportive. We had numerous fruitful discussions on science and philosophy. He has been a person whom I can talk to anytime I intellectually struggle. I am very grateful for his presence during this study.

When I look back, I see that I have learnt at least one remarkable thing from each group member. I am very happy that I met these unique people and they contributed both this thesis and also my life. I would like to thank Alvaro Charlet for being very considerate, Michael Kessler for introducing self-respect, Matteo Hirsch

Acknowledgements

for chess sessions, Mathias Steinacher for SAW device setup. I must acknowledge Chuen-Ru Li for her perseverance, Ran Zhao for her wisdom and maturity, and Gaia De Angelis for her nurturing nature.

I enjoyed Pauline Pradal's delightful dark humor and Alexandra Thoma's kindness, understanding and open minded nature. I also thank both for awesome french sessions we have had. Alex has become one of the best office mate I ever had. I am very grateful for her presence, she brought a very fresh spirit to our office and the lab and have become a great support.

I also would like to thank recent members of SMaL. I will remember Francesca Bono with her courage and boldness, Lorenzo Lucherini with his empathy and sincerity, Tianyu Yuan with her cheerful nature and Eva Baur with her creativity. I would like to thank our secretary, Mercedes Quintas, as she has always been very cheerful, helpful, lovely and warm.

In addition, I thank all the students worked with me, namely Luc Monnier, Buse Tatli, Andrea Calamida, Rodolphe Henri. It has been very joyful experience for me to teach and collaborate with each of them. Their self-disciplined nature hence brilliant work helped to advance this thesis.

I also would like to thank several people for technical support. Without their diligent support to tackle challenges, it would be very difficult to proceed. I thank for their supports to David Bi and Arnaud Magrez on crystallographic characterization, Daniele Laub, Fabienne Bobard, Lucie Navratilova, Gregoire Baroz on electron microscopy and Jacques Morisod and Yann Lavanchy on IR and TGA measurements.

This PhD journey introduced fascinating features of nature as well as great friends to me. I would like to thank my collaborator, yet more than that, a close friend, Nina Kolln Wittig. Being aside it was a joyful journey to work with her, she has been an incredible support with her sincerity, cheerful and beautiful spirit. I feel very lucky to meet her. I would like to send my sincere gratitude for their presence to Louis Martin-Monier, William Esposito and Sarah Wehrle for board game parties and gatherings we have. It was very fun to share memories with them. In addition, I would like to thank my very kind fellows Suiyang Liao and Francesca Olgiati, they both have been very helpful, kind and altruistic. It was a real pleasure to meet them.

I would like to especially thank Lukas Riemer for his continuous, unconditional friendship. He, whom I met as a new PhD like me on a breezy Bern morning and he, who told me that he knows me because he heard me singing while doing the

experiments regularly, has become a very close friend. He was the shoulder across the corridor whenever I needed. Someone has never let me alone, no matter where and when. My words are just insufficient when it gets to express my gratitude for his friendship. I'm greatly indebted to him. As he introduced me to other awesome people I would like to name some of them as well. Marge, Sergio and Jorge have been very warm and welcoming people during these years. I truly enjoyed the time we spent together, and very much appreciated their support and lovely environment they set.

I would like to thank some of my Turkish friends, which helped me to alleviate the homesickness especially during difficult covid times. Isinsu Katircioglu and Hande Kabil have formed cheerful girl band. Being around them has always been fun. I sincerely thank them. I also thank Merve Demir as we shared the PhD experience simultaneously but only few thousand miles away.

I also would like to thank Bilal Demir. He has become a second family to me in Lausanne. We went through good and bad, easy and very difficult times. He has taken part in most of my memories in Lausanne, and I am deeply grateful that he provided me a place of trust and full support with his presence. He has been a teacher to me in the most challenging parts of my PhD and I learned tremendously from him. I send my sincere thanks to him.

Last but not least I would like to thank my best friends, Ayfer Sarac and Gulay Kart for their unconditional love and support. They have been with me more than 20 years and I found their support with me under every circumstance. I feel very blessed to have them in my life. Finally, I would like to thank my family. During my PhD I understood once more, they have been my real treasure. I have always felt their heart next to mine and I am so thankful that they now witness of a long-dreamed achievement of mine. I thank my mom and dad, Nuran and Aykut Okur and my beloved sister Aysenur Okur, for being my family. And the most, I am so grateful to almighty Allah, who made it all possible.

Lausanne, April 19, 2022

A.C. O.

Abstract

Nature possesses a fascinating control over the size, structure, and orientation of crystals such it can form gleaming surfaces with excellent optical properties and high mechanical strength. This ability is exploited to form strong and tough skeletons or to enable animals to adapt their properties to their environment. To form synthetic crystals with similar sets of properties, we must understand the crystallization in much more detail. One way nature controls the crystal structure is through confinement. Crystals are formed in designed spaces with well-defined dimensions or within cells that are specialized solely for crystallization. Inspired by the techniques nature has, drops have been exploited as confinements. Using drops, we can investigate how the different crystallization parameters influence the size and structure of crystals.

This thesis is dedicated to gaining an understanding on the influence of processing parameters on the structure of a low molecular weight organic compound, succinic acid, that is used as a matrix to encapsulate volatile substances. To achieve this goal, I employ emulsion drops and aerosols to study the crystallization kinetics of succinic acid and other biologically relevant crystals. In the **3rd chapter**, I demonstrate that the structure of succinic acid crystals can conveniently be tuned with the parameters used to spray dry these particles. For example, the crystal structure of succinic acid strongly depends on the initial solute concentration and solvent type used to formulate them from because these two parameters determine the time crystals have to form while drops dry. In the **4th chapter**, I study how the initial solute concentration and solvent type influence the encapsulation efficiency of a model volatile, vanillin, and its release kinetics. Succinic acid forms a polycrystalline matrix that exhibits excellent encapsulation efficiencies for vanillin. Thereby, I demonstrate that crystalline matrices composed of a low molecular weight organic compound can successfully retain volatiles and control their release kinetics, as they exhibit a low permeability towards them.

Abstract

Finally, in the **5th chapter**, I end my thesis by demonstrating that drops can also be used to control the formation of other biologically relevant crystals, such as $CaCO_3$, guanine and calcium oxalate. Single and double emulsions are employed as pico-liter sized crystallization vessels that slow down the crystallization kinetics, and thereby enable studying the formation of these crystals with a higher temporal and spatial resolution. These findings open new routes to understand and mimic the formation of biogenic crystals that display remarkable properties.

Keywords: drops, biogenic crystals, spray-drying, surface acoustic wave atomization (SAW), microfluidics, volatile encapsulation, crystallization

Résumé

La nature possède un contrôle extraordinaire sur la taille, la structure et l'orientation des cristaux de sorte qu'il lui est possible de former des surfaces brillantes possédant d'excellentes propriétés optiques et mécaniques. Cette aptitude est notamment exploitée pour former des squelettes extrêmement rigides et résistants ainsi que pour permettre aux animaux une parfaite adaptation à leur environnement. Pour synthétiser de tels cristaux, il est essentiel de comprendre en profondeur le phénomène de cristallisation. Une des méthodes utilisées par la nature pour contrôler la structure des cristaux est le confinement. Ces derniers sont en effet formés soit dans un espace clos prédéfini, soit dans une cellule spécialisée pour la cristallisation. Basé sur les techniques observées dans la nature, les gouttes ont été utilisées comme source de confinement. Nous pouvons ainsi étudier comment les différents paramètres de cristallisation influencent la taille et la structure des cristaux confinés dans une goutte.

Cette thèse est dédiée à l'approfondissement de la compréhension de l'influence des paramètres sur la structure d'un composé organique de faible masse molaire, l'acide succinique, utilisé comme matrice pour encapsuler des substances volatiles. Ainsi, j'utilise des émulsions et aérosols pour d'abord étudier la cinétique de la cristallisation de l'acide succinique, puis celle d'autres cristaux biologiques. Au cours du **chapitre 3**, je démontre que la structure cristalline de l'acide succinique peut aisément être modifiée en jouant sur les paramètres utilisés lors du séchage par pulvérisation des particules. En effet, celle-ci dépend fortement de la concentration initiale du soluté ainsi que du type de solvant utilisé, puisque ces deux paramètres déterminent le temps que les cristaux ont pour se former lors du séchage des gouttes. Dans le **chapitre 4**, j'étudie comment la concentration initiale de soluté et le type de solvant influencent l'efficacité d'encapsulation d'une molécule volatile, la vanilline, ainsi que sa cinétique de libération. L'acide succinique forme une matrice

Résumé

polycristalline qui présente d'excellente efficacité d'encapsulation de la vanilline. Ainsi, je démontre que la faible perméabilité des matrices cristallines constituées de composés organiques de faible masse molaire permet de contenir avec succès des substances volatiles et de monitorer leur cinétique de libération.

Finalement, au cours du **chapitre 5**, je finis ma thèse en démontrant que les gouttes peuvent aussi être utilisées pour contrôler la formation d'autres cristaux biologiques, tels que le $CaCO_3$, la guanine et l'oxalate de calcium. Les émulsions simples et doubles sont employées comme des vaisseaux de cristallisation de l'ordre du femtolitre qui ralentissent la cinétique de cristallisation et permettent ainsi l'étude de la formation de ces cristaux avec une meilleure résolution spatio-temporelle. Ces découvertes ouvrent de nouvelles portes quant à la compréhension et la reproduction de cristaux biosynthétiques présentant de remarquables propriétés.

Mots-clefs : gouttes, cristaux biosynthétiques, séchage par pulvérisation, atomisation d'ondes acoustiques de surface (SAW), microfluidique, encapsulation de substances volatiles, cristallisation.

Contents

| | |
|--|----------|
| Acknowledgements | v |
| Abstract | ix |
| Résumé | xi |
| 1 Introduction | 1 |
| 1.1 Advances and Challenges in Applied Crystals | 3 |
| 1.1.1 Volatile Encapsulation | 3 |
| 1.1.1.1 Volatile Classifications | 4 |
| 1.1.1.2 Conventional Matrices for Volatiles | 5 |
| 1.1.2 Pharmaceuticals | 7 |
| 1.2 Kinetic Control on Crystals | 8 |
| 1.2.1 Reaction Parameters and Relative Supersaturation | 9 |
| 1.2.2 Confinement | 12 |
| 1.3 Techniques for Crystallization Control | 17 |
| 1.3.1 Bulk Crystallization | 17 |
| 1.3.2 Micron-size Templated Crystallization | 21 |
| | xiii |

Contents

| | | |
|-------------|--|-----------|
| 1.3.2.1 | Microfluidics | 21 |
| 1.3.2.2 | Drops | 24 |
| 1.3.2.2.1 | Emulsions | 24 |
| 1.3.2.2.2 | Aerosols | 27 |
| 1.3.2.2.2.1 | Spray Chilling | 27 |
| 1.3.2.2.2.2 | Electrospraying | 28 |
| 1.3.2.2.2.3 | Spray Drying | 29 |
| 1.3.2.2.2.4 | Surface Acoustic Wave Atomiza- tion | 36 |
| 2 | Materials & Methods | 39 |
| 2.1 | SAW Atomization | 40 |
| 2.1.1 | SAW Device Microfabrication | 40 |
| 2.1.2 | Operation of the SAW Device | 41 |
| 2.2 | Microfluidic PDMS Device | 42 |
| 2.2.1 | PDMS Device Fabrication | 42 |
| 2.2.2 | Surface Treatment | 43 |
| 2.3 | Characterization Tools | 43 |
| 2.3.1 | Scanning Electron Microscopy (SEM) | 43 |
| 2.3.2 | X-Ray Diffraction (XRD) | 43 |
| 2.3.3 | Thermogravimetric Analysis (TGA) | 44 |
| 3 | Use of Aerosols as Crystallization Template | 45 |

| | | |
|----------|---|-----------|
| 3.1 | Abstract | 46 |
| 3.2 | Introduction | 47 |
| 3.3 | Experimental Section | 48 |
| 3.3.1 | Solution Preparation | 48 |
| 3.3.2 | Particle Formation | 49 |
| 3.3.3 | Characterization | 49 |
| 3.3.3.1 | Scanning Electron Microscopy (SEM) | 49 |
| 3.3.3.2 | X-Ray Diffraction (XRD) | 50 |
| 3.4 | Results & Discussion | 50 |
| 3.4.1 | Spray Drying of Succinic Acid Nanoparticles | 50 |
| 3.4.2 | Influence of Solute Concentration and Solvent on Morphology & Crystal Structure | 50 |
| 3.4.3 | Stability of Crystal Structure During Storage | 56 |
| 3.4.4 | Influence of Additives on Crystal Structure of Succinic Acid | 58 |
| 3.5 | Conclusion | 62 |
| 4 | Implementation of Crystallization Control: Vanillin Encapsulation in Crystalline Particles | 63 |
| 4.1 | Abstract | 64 |
| 4.2 | Introduction | 65 |
| 4.3 | Experimental Section | 67 |
| 4.3.1 | Solution Preparation | 67 |
| 4.3.2 | Particle Formation | 67 |

Contents

| | | |
|----------|--|-----------|
| 4.3.3 | Characterization | 67 |
| 4.3.3.1 | Scanning Electron Microscopy (SEM) | 67 |
| 4.3.3.2 | X-Ray Diffraction (XRD) | 69 |
| 4.3.3.3 | Thermogravimetric Analysis (TGA) | 69 |
| 4.4 | Results & Discussion | 69 |
| 4.4.1 | Influence of Solute Concentration on Size & Morphology | 69 |
| 4.4.2 | Influence of Solute Concentration on Phase Separation | 72 |
| 4.4.3 | Vanillin Retention in Crystalline Particles | 75 |
| 4.4.3.1 | Vanillin Loading in Succinic Acid and Tartaric Acid Particles | 75 |
| 4.4.3.2 | Release Kinetics | 78 |
| 4.5 | Conclusion | 80 |
| 5 | Emulsion Templated Crystallization | 81 |
| 5.1 | Abstract | 82 |
| 5.2 | Introduction | 83 |
| 5.3 | Experimental Section | 85 |
| 5.3.1 | Materials | 85 |
| 5.3.2 | Methods | 85 |
| 5.3.2.1 | Single Emulsion Production via Tip Sonication . | 85 |
| 5.3.2.2 | Production of Single Emulsions and Their Trapping | 85 |
| 5.3.2.3 | Microfluidic Device Production for Double Emulsions | 86 |

| | | |
|----------|--|------------|
| 5.3.2.4 | Double Emulsion Production | 86 |
| 5.4 | Results & Discussion | 87 |
| 5.4.1 | Crystal Formation in Single Emulsions | 87 |
| 5.4.2 | Crystal Formation in Trapping Device | 88 |
| 5.4.3 | Crystal Formation in Double Emulsions | 89 |
| 5.4.4 | Influence of Reactant Concentration on Morphology & Size | 91 |
| 5.4.5 | Influence of Osmotic Pressure on DE Core Size & Morphology of the Particles | 94 |
| 5.5 | Conclusion | 96 |
| 6 | Conclusion | 97 |
| | Bibliography | 121 |
| | Acronyms | 123 |
| | Symbols | 125 |
| | List of Figures | 125 |
| | Curriculum Vitae | 134 |
| | Christmas Cards | 136 |

1 Introduction

In this chapter, I give an overview of potent applications arising from establishing kinetic control over the crystal formation, the parameters used to control the crystallization kinetics focusing on relative supersaturation and confinement and finally the techniques, including drop formation to control aforementioned parameters.

Contents

| | | |
|-------------|--|----|
| 1.1 | Advances and Challenges in Applied Crystals | 3 |
| 1.1.1 | Volatile Encapsulation | 3 |
| 1.1.1.1 | Volatile Classifications | 4 |
| 1.1.1.2 | Conventional Matrices for Volatiles | 5 |
| 1.1.2 | Pharmaceuticals | 7 |
| 1.2 | Kinetic Control on Crystals | 8 |
| 1.2.1 | Reaction Parameters and Relative Supersaturation | 9 |
| 1.2.2 | Confinement | 12 |
| 1.3 | Techniques for Crystallization Control | 17 |
| 1.3.1 | Bulk Crystallization | 17 |
| 1.3.2 | Micron-size Templated Crystallization | 21 |
| 1.3.2.1 | Microfluidics | 21 |
| 1.3.2.2 | Drops | 24 |
| 1.3.2.2.1 | Emulsions | 24 |
| 1.3.2.2.2 | Aerosols | 27 |
| 1.3.2.2.2.1 | Spray Chilling | 27 |
| 1.3.2.2.2.2 | Electrospraying | 28 |
| 1.3.2.2.2.3 | Spray Drying | 29 |
| 1.3.2.2.2.4 | Surface Acoustic Wave Atomiza- tion | 36 |

1.1 Advances and Challenges in Applied Crystals

The structure of crystals strongly influences their properties such as optical appearance [1–3], dissolution kinetics [4–6], or mechanical properties [7–9]. A possibility to control the structure of crystals is to form them in drops. Indeed, the use of drops to achieve such control is beneficial for the formulation of drugs and their delivery. As we discover nature further, it becomes obvious that crystallization in compartments has a lot more to offer. Nature frequently forms crystals under confinement and these crystals display astonishing properties such as mechanical and optical properties. By employing drops, we can mimic the techniques that nature applies to produce crystals with remarkable properties. Crystallization studies in drops have the potential to control crystal structure and morphology and hence properties. Such basis can open up routes to alternative uses of crystals. For instance, crystals composed of densely packed molecules can be used as a matrix to encapsulate active ingredients such as volatiles, which requires ultimate control on permeability.

Within this scope, in this section, the challenges and recent applications on crystallization control in several fields will be discussed.

1.1.1 Volatile Encapsulation

Fragrances are volatile substances that are used as active ingredients in a wide range of commonly used products including food [10, 11], cleaning products [12, 13], perfumery and even in fashion [14–16]. Aside from the inherent volatility of fragrances which makes it difficult to preserve them during storage, they span a large range of partition coefficients. Thereby, they cover a wide range of hydrophobicity and hence, tendency to phase separate from the medium they have been dispersed in. Their inherent volatility and tendency to phase separate limit the shelf-life of products containing them. To mitigate these limitations, fragrances are often encapsulated to delay their evaporation and disperse them in water- based products.

1.1.1.1 Volatile Classifications

Volatile oils are mixtures of hydrocarbon terpenes, sesquiterpenes and polyterpenes and their oxygenated derivatives obtained from various parts of the plant. Volatile oils have high vapor pressures such that they evaporate already at room temperature. From ancient times, they have been considered as medicines and their antibacterial and antioxidant properties are proven by modern science.

However, it is very rare to find their use in products in unprocessed forms as they are very fragile. When they are exposed to light, air or heat, they oxidize easily hence, the odours attributed to their natural chemical structures are compromised. To prolong their shelf life, they must be encapsulated.

Chemically volatiles can be divided into 8 classes;

- (i) Hydrocarbon volatiles,
- (ii) Alcohol volatiles,
- (iii) Aldehyde volatiles,
- (iv) Ketone volatiles,
- (v) Phenol volatiles,
- (vi) Phenolic ether volatiles,
- (vii) Oxide volatiles, and
- (viii) Ester volatiles

Except of some aliphatic hydrocarbons and phenolic groups, most of the volatiles are either sparingly soluble or insoluble in water. They possess good solubility or miscibility in alcohols and various organic solvents. Their solubility in different solvents determines their formulation.

Their interaction with fats and proteins makes them suitable to be encapsulated in solid lipid carriers, yet they require special storage and transportation. Therefore, more stable, dried formulations are preferred. Carbohydrates and their derivatives such as maltodextrin are heavily used for their encapsulation. However, the volatile

substances require an encapsulating matrix that possesses a very small mesh size to prevent their loss during storage.

1.1.1.2 Conventional Matrices for Volatiles

Natural and synthetic polymers are heavily exploited as matrix materials for volatile encapsulation. Gum acacia is an attractive natural matrix material that displays a low permeability towards many volatiles and hence, retains them for a prolonged time [17–19]. Unfortunately, this material is expensive such that it is only used in selected products [20]. More price sensitive products frequently contain capsules made of dextrin derivatives, mainly maltodextrin and cyclodextrin [20]. Maltodextrin is popular due to its neutral taste and good barrier properties towards many volatiles. It also results in solutions with a low viscosity if dissolved below five dextrose equivalency (DE) [21]. This high molecular weight sugar can thus be readily processed into particles and capsules through spray drying [22, 23]. While 10-20 DE maltodextrin is best suited for encapsulation and exhibits the best retention, it has a poor emulsifying capacity, making the fabrication of capsules from emulsion drops difficult [24]. The emulsion drop stability increases if maltodextrin is mixed with whey protein, sodium caseinate and gum acacia [22, 25]. The variability in their properties between the batches is common to natural polymers, which makes it difficult to closely control the dimensions, stiffness, and release profile of volatile substances contained in them. Alternative matrices that are frequently exploited for the encapsulation of volatiles include proteins and fats. Sodium caseinate and lactose have been used as good emulsifiers, especially when fats are used to encapsulate lipophilic volatile compounds [25–27]. Furthermore, whey protein and pectin are used as wall materials thanks to their flow properties [28, 29]. However, these macromolecular actives can impose some restrictions on the choice of active ingredients as they may have unwanted interactions with certain volatiles and their intrinsic nature is vulnerable to create sensitivities such as allergies and intolerance in their consumers [30–32].

A better reproducibility is achieved if synthetic polymers are employed as matrix materials. For example, microparticles [33, 34] made of poly(lactic-co-glycolic acid) (PLGA), and capsules [35–37] made of polycaprolactone (PCL), polyurethane and polybutylcyanoacrylate (PBCA) are well-suited carriers for volatile substances because they are biocompatible and the release kinetics can be tuned via crosslinking

density [38]. If made out of PCL, these capsules slowly degrade, resulting in a diffusion limited release of reagents that lasts for up to 24 months, rendering them well-suited for detergent and textile applications [38, 39]. The degradation rate and hence, release kinetics depends on the crosslinking density and the degree of crystallinity of these materials, which are strongly related to their processing.

To further slow down the release rate, capsules have been made from inorganic materials possessing a higher density than polymers, such as SiO_2 or $CaCO_3$ and the phosphates [40–42]. The loading efficiency of these inorganic particles is dependent on pore size and chemical interaction of volatiles with the inorganic matrix which is typically significantly higher than that of polymeric counterparts. The release kinetics is strongly influenced by the size, type of pores and the density of the defects; these parameters depend on the processing conditions and templates hence need to be tailored for each application [43, 44]. To render these capsules less susceptible to defects, they are often strengthened with polymeric materials.

Overall, the use of high temperatures required to process such macro-molecular matrices reduces the encapsulation efficiency of volatiles as a significant fraction is lost during its formulation. Therefore, alternative technologies such as the use of molecules with higher packing densities, e.g crystals and compounds with lower molecular weights have been explored [45, 46]. To facilitate the fabrication of capsules and thereby improve the control over the release kinetics while increasing the scalability of the process, capsules have been produced from low molecular weight organic compounds that easily crystallize to minimize their permeability towards volatiles, such as erythritol [45]. In this case, erythritol is processed through spray chilling and the release of encapsulants is typically triggered by temperature changes that melt the capsule material. Low molecular weight compounds such as erythritol exhibits an appropriate temperature range for processing, unlike previously used molecules such as sorbitol [47] and mannitol [48, 49]. The encapsulation efficiency strongly depends on the volatility of the encapsulant, which is influenced by the processing temperature. Since the processing temperature for spray chilling is around 130°C, a significant fraction of volatiles is lost during the processing. Encapsulation efficiencies range from 60% for volatile substances up to 90% for non-volatile counterparts if loaded in erythritol capsules [45]. Erythritol rapidly crystallizes such that it has the potential to encapsulate volatiles within crystalline domains, thereby demonstrating a good retention control. However, the high processing temperatures required to melt erythritol limit the use of spray chilling to

formulate these capsules. Liquid volatiles can be trapped within crystal boundaries yet, a more suited process and processing parameters that offer control over this encapsulation remain to be discovered.

1.1.2 Pharmaceuticals

Pharmaceuticals are another field where crystallization control gains utmost importance. Control of polymorphism in drugs is crucial as exemplified by the scandalous thalidomide use in pregnant women that caused irreversible natal defects over 10000 newborns [50]. The drug had been produced via a route where the two polymorphs were in a racemic mix, however the β form was causing some mutagenic effects. Nevertheless, the presence of polymorphs in drugs can also be beneficial, as the conformation can enhance the interaction of drugs with their receptor [51]. Therefore, polymorphism control is an interesting topic in pharmaceuticals.

Aside from molecular aspects of drug crystallization, controlled polymorphism attracts attention in pharmaceutical industry because it possesses a better compressibility and bioavailability in certain drugs. Amorphisation of the compound enhances the drug compressibility which is especially important for orally administered active compounds. While polymeric excipients are used to ameliorate their mechanical properties, these additives typically dilute the active compounds and can cause phase separations. These shortcomings can be overcome if the active compounds are formulated as amorphous phases because they possess a better compactability compared to their crystalline counterparts.

An increase in bioavailability is another advantage of introducing polymorphs in pharmaceuticals. Poor bioavailability is mainly due to the hydrophobic nature of the drugs. It is known that almost 80% of the drugs are poorly soluble in water [52]. This renders drug formulation challenging, as almost 70% of the body is water. Therefore, there is a serious risk for these drugs to precipitate in the body, causing side effects. In addition, administration of high doses of drugs to overcome the bioavailability limitation and to fulfill their function can cause toxicity. The solubility and hence bioavailability of hydrophobic drugs can be increased with excipients. However, finding suitable excipients that do not cause unwanted side reactions is laborious. Moreover, the selected excipient should have adequate miscibility with the bioactive substance to prevent phase separations that

eventually diminish the efficacy of the drug formulation. Alternatively, hydrophobic drugs have been formulated as emulsions or vesicles. However, these approaches only moderately increased the bioavailability of these drugs.

The bioavailability of these drugs can be more efficiently increased through micronization of the drugs as the precipitation of them is less likely to occur. Moreover, micronization can result in metastable polymorphs that may exhibit better solubility profiles. Such micronization can be established via aerosol-based techniques such as spray-drying. For example, chloramphenicol palmitate that is processed through spray-drying transformed into particles with small sizes and specific polymorphs that influence the solubility, dissolution rate, and hence the bioavailability of this drug [53]. To advance these properties, fundamentals of crystallization should be studied in-depth, and relevant processing parameters should be identified to achieve control over the crystallization kinetics.

1.2 Kinetic Control on Crystals

Crystallization is one of the oldest fields in process engineering, which has played an immense role on the rise of the chemical industry. It allows to purify and separate compounds that enabled numerous technological advancements in ceramics, semiconductors and pharmaceutical applications. Despite the long history, industrial needs require novel solutions for the control of the crystal structure of certain materials including drugs, proteins and photonics.

These solutions could be found thanks to technological advancements on microscopy and spectroscopy techniques. These techniques enabled crystallization studies on the sub-micron scale, leading to discoveries of many morphologies as well as polymorphs of crystals which differ in their magnetic, optical and mechanical properties [3, 54–57]. Such studies enabled us to understand the formation of crystals as well as the properties of them in more depth; today critically pertaining to applications for high-tech materials. For instance, the existence of polymorphs resolves the limitations of hydrophobic drugs since different polymorphs exhibit distinct solubility and dissolution kinetics. Photonic crystals, if engineered accordingly, could enable high reflection coatings or mirrors. Hence, control over morphology and crystal structure has gained high importance over the last few decades.

In nature there are crystalline structures that show remarkable properties yet the formation mechanism is still largely unknown. Once such mechanisms are resolved and can be mimicked, we would get materials that have properties with potentials that we have not reached yet. Most of these crystals are formed under non-equilibrium conditions because the metastable crystal forms are kinetically arrested.

1.2.1 Reaction Parameters and Relative Supersaturation

The kinetic control over the crystallization can be achieved by adjusting the formation parameters of crystalline compounds. According to the classical nucleation theory, crystallization starts from nucleation, which is followed by the growth of nuclei. Under equilibrium conditions, nucleation is a process driven by the chemical potential difference $\Delta\mu$ (Equation (1.1)), that is dictated by temperature T and, if crystals are formed from solution, the relative supersaturation S .

$$\mu_1 - \mu_2 = \Delta\mu = -kT\ln S \quad (1.1)$$

While a low S is more suitable for the thermodynamically controlled crystallization, a kinetically controlled crystallization usually occurs at high S . S is defined as the concentration of a solute c divided by its solubility product k_{sp} (Equation (1.2)). The different polymorphs of crystalline materials can have very different solubilities. Hence, the crystal structure should be taken into consideration in the determination of S . The solubility of a compound also depends on the temperature, pressure and pH of the environment. Hence, these parameters change the relative supersaturation and ultimately the nucleation rate.

$$S = \frac{c}{k_{sp}} \quad (1.2)$$

Once the supersaturation exceeds 1, the first nuclei can start to form. However, the formation of a nucleus involves overcoming the energy penalty caused by the creation of a surface. Once the nuclei reach a critical size, the energy gain from the formation of a bulk solid overcompensates the surface energy penalty such that the nuclei become stable. This interplay in volume vs. surface energies is

Chapter 1. Introduction

expressed in Equation (1.3) where the Gibbs free energy ΔG relates to the chemical potential $\Delta\mu$, radius of nuclei r_n , volume per molecule V_m and surface energy γ . The formation of stable nuclei can be accelerated by any impurity that is found in the system that can act as a heterogeneous nucleation site, which decreases the energy penalty due to creating additional surface, hence making it easier for nuclei to form (Equation (1.3)): This is called *heterogeneous nucleation*. In this case, the nucleation rate I is controlled by the number of nucleation sites n_0 , the critical Gibbs free energy ΔG^* , temperature T and the hopping velocity v_h (Equation (1.4)). In *heterogeneous nucleation* nucleation rates are faster and critical radii are smaller compared to those formed through *homogeneous nucleation*, where precipitation occurs in a pure system with no impurity.

$$\Delta G = -\frac{4}{3}\pi r_n^3 \cdot \frac{\Delta\mu}{V_m} + 4\pi r_n^2 \cdot \gamma \quad (1.3)$$

$$I \propto n_0 \cdot \exp\left(-\frac{\Delta G^*}{kT}\right) \cdot v_h \quad (1.4)$$

The stable nuclei start to grow after the critical threshold value in radius is reached. Classical nucleation theory assumes that the growth of these nuclei progresses such that one atom/molecule is incorporated into the nucleus per unit time. Hence, in this simplistic case, the growth rate u is determined by the rate of atoms or molecules that attach to and detach from the nuclei, which is governed by the migration enthalpy as the nuclei are assumed to be spherical. This is shown in simplified (Equation (1.5)) where ΔG_m is the migration energy, a_0 is a prefactor and v is the attachment frequency.

$$u = va_0[1 - \exp(-\frac{\Delta G_m}{kT})] \quad (1.5)$$

The initial assumption of the classical nucleation theory was that nucleation is a one-step process where the initial nuclei display the structure of the final crystal and kinetic control over the crystallization process was maintained solely by one free energy barrier. This assumption has been contradicted by many examples in nature, hence the theory has been extended by the Ostwald's step rule. According to this rule, instead of a representative initial crystal structure, there can be many

metastable structures that have different phases other than the thermodynamically most stable one, as can be seen in Figure 1.1.

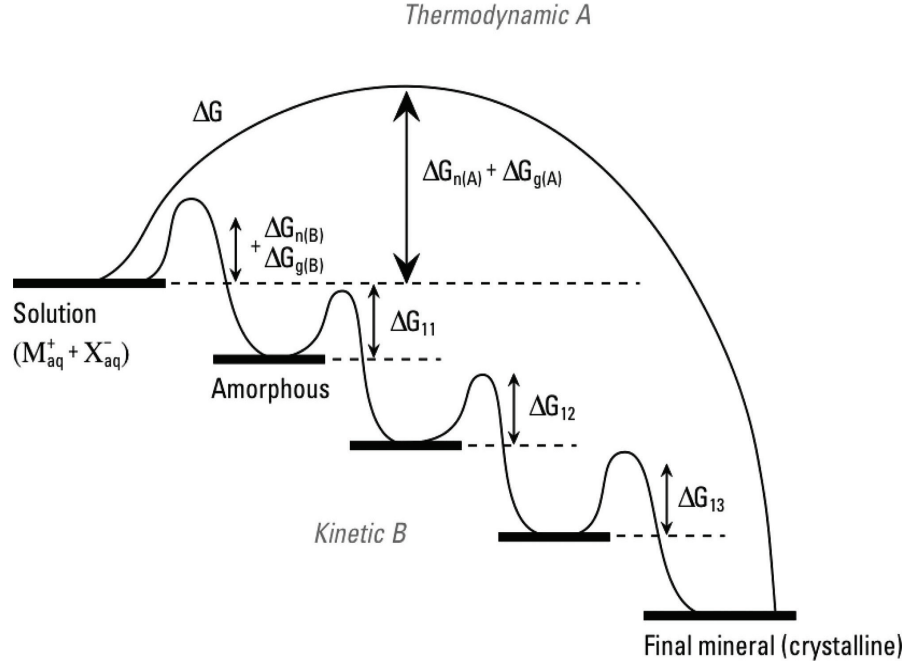


Figure 1.1: Ostwald step rule, adapted with permission from [58].

Over the years many examples of crystals have been reported whose formation path cannot be explained by the classical nucleation theory [59–61]. The non-classical theories make the prediction of which phase dominates under which condition more difficult because each individual system presents a complex energy profile. Especially in biogenic crystals, such as CaCO_3 , there are multiple short-lived metastable phases that transform via non-classical pathways as exemplified in Figure 1.2, yet for many of the pathways, control mechanisms are still unknown. Nonetheless, factors such as the thermodynamic parameters: *temperature*, *pH*, *pressure*, and confinement effect are used as tools to control the crystallization.

Environmental factors such as temperature, pH and pressure influence the free energy profile which determines the most stable polymorph. They also influence the supersaturation, and hence the chemical potential, opening up possibilities to control nucleation. For example, temperature is a well-known parameter to control the size and size distribution of particles. It is used for ceramic processing to prepare rough ceramics through dynamic ripening which requires grain growth control that is achieved by temperature programming. Temperature also enables the selective growth of certain crystals as it may change the Gibbs free energy and

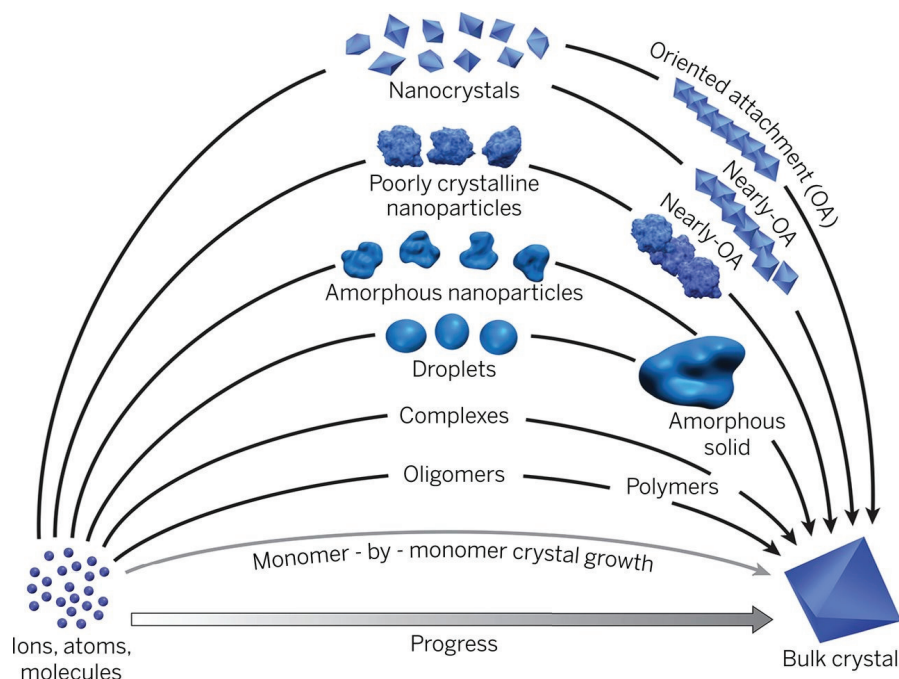


Figure 1.2: Non-classical nucleation pathways adapted with permission from [62].

hence the most stable phase. Pressure is another factor that is used to control the growth rate of several high molecular weight crystalline compounds such as polymers [63] and proteins [64] and for polymorph screenings of pharmaceuticals [65–67]. Pharmaceutical compounds can also be processed in different polymorphs via pH modulation, as pH shows the strongest effect on the surface energies of these compounds and hence their growth kinetics [68].

1.2.2 Confinement

Classical nucleation theory suggests supersaturation as a primary tool to control crystallization kinetics, and hence to determine the morphology, polymorphs and their kinetic stability, yet, many examples of biomineralization show that this is not the only way. The marvelous designs of natural biocrystals such as shells [69], teeth [70] and bone [71] demonstrate the importance of confinement on the final morphology and crystal structure.

Confinement is considered to be the environment within which crystallization occurs with spatial restriction in one or multiple directions. In nature, calcium phosphate and calcium carbonate are popular examples of confinement controlled

crystallization in living species. Under these conditions, nucleation rates are expected to decrease as the probability of nucleation scales with the volume. For finite volumes, the supersaturation degree will drop over time as the ion species are depleted. Therefore, nuclei form and grow at much lower rates under confinement compared to bulk systems [60, 72].

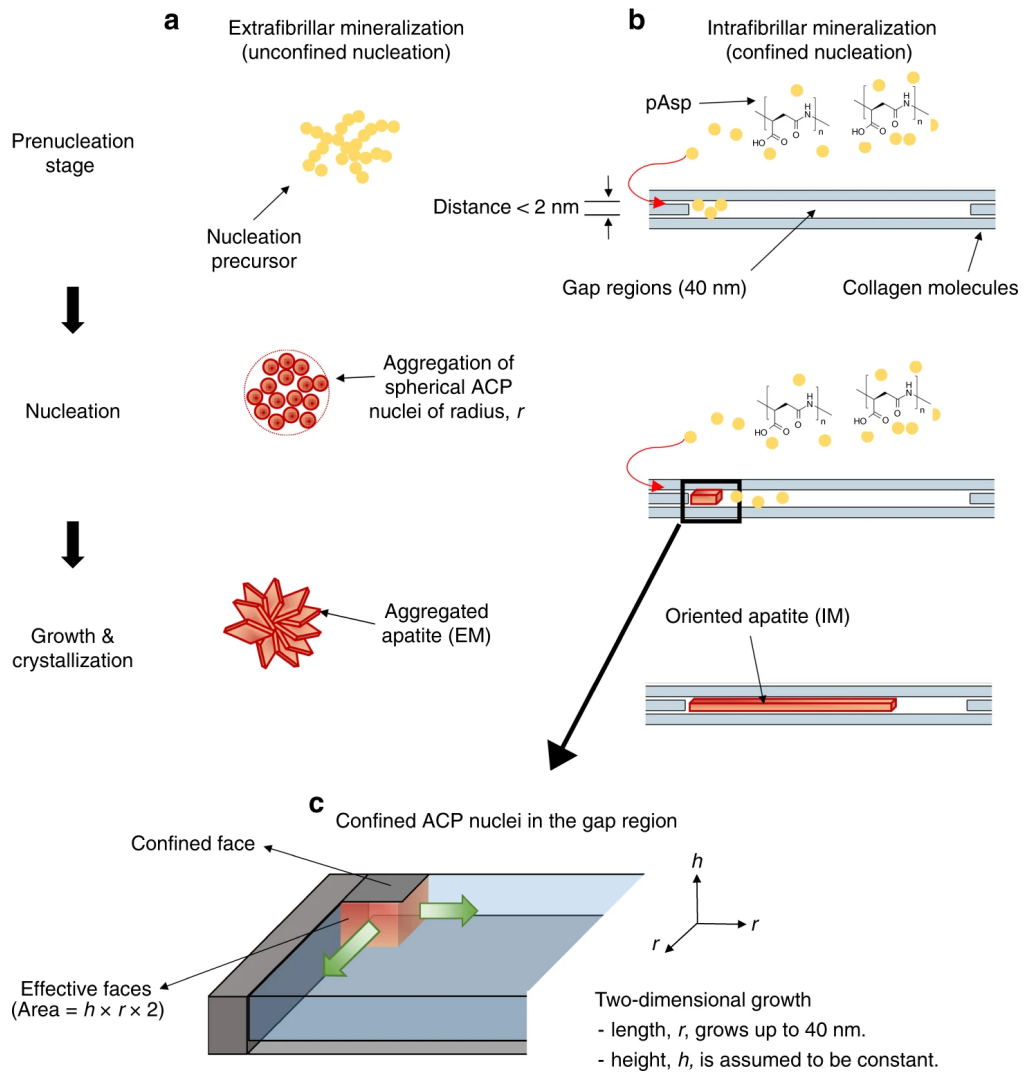


Figure 1.3: Schematic illustration of two different nucleation models for collagen mineralization. a) Extrafibrillar nucleation in unconfined space and b) intrafibrillar nucleation in a confined gap region. c) Geometry of confined amorphous calcium phosphate (ACP) nuclei in the gap region. Adapted with permission from [71] under the license of CC BY 4.0.

In biology, confinement is caused by the matrix morphology. For instance, hydroxy

apatite crystals are one of the primary constituents of bone and teeth. They are responsible for the load bearing properties and mechanical strength. Such crystals are formed within the cylindrical collagen matrix where crystals are nucleated within pores with diameters between 20-40 nm [71]. In this case, one face is confined allowing the formation of apatite with a specific orientation, as can be seen in Figure 1.3. The resulting crystal orientation and morphology are very different compared to crystals that nucleated in bulk. Hence, confinement yields unique organization of the crystals that impart the crystals distinct mechanical properties [7, 73].

Another fascinating confinement example of nature is guanine crystals. These crystals very efficiently reflect light once produced and arranged in a specific way and with a specific phase. Accordingly, these crystals give the materials unusual optical properties allowing several species including deep sea fish and spiders, to possess remarkable optical properties. Several studies show that those species have one thing in common: they present in their body anhydrous guanine, which is a metastable form of guanine that has been impossible to synthetically obtain from aqueous systems until very recently [74]. Scientists observe similar confinement effects on ACP in scallop eyes where guanine crystals are limited to layers that have thicknesses of a few hundred nm, as shown in Figure 1.4 [75]. Spiders and koi fishes are found to grow these crystals slightly differently than bone. Their approach to have confinement is established through specific cells that perform crystallization such that each cell could carry approximately 10 crystals in them, as shown in Figure 1.5 [75].

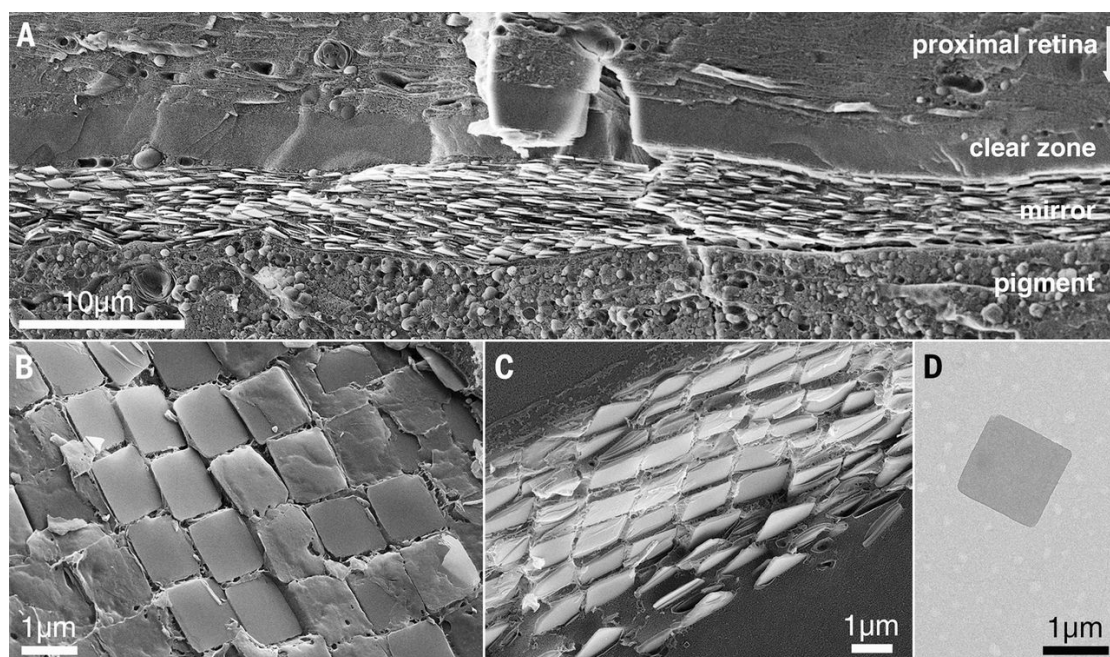


Figure 1.4: Micrographs of scallop eyes where mirrors composed of guanine layers to maximize and manipulate the light reflection. Adapted with permission from [76].

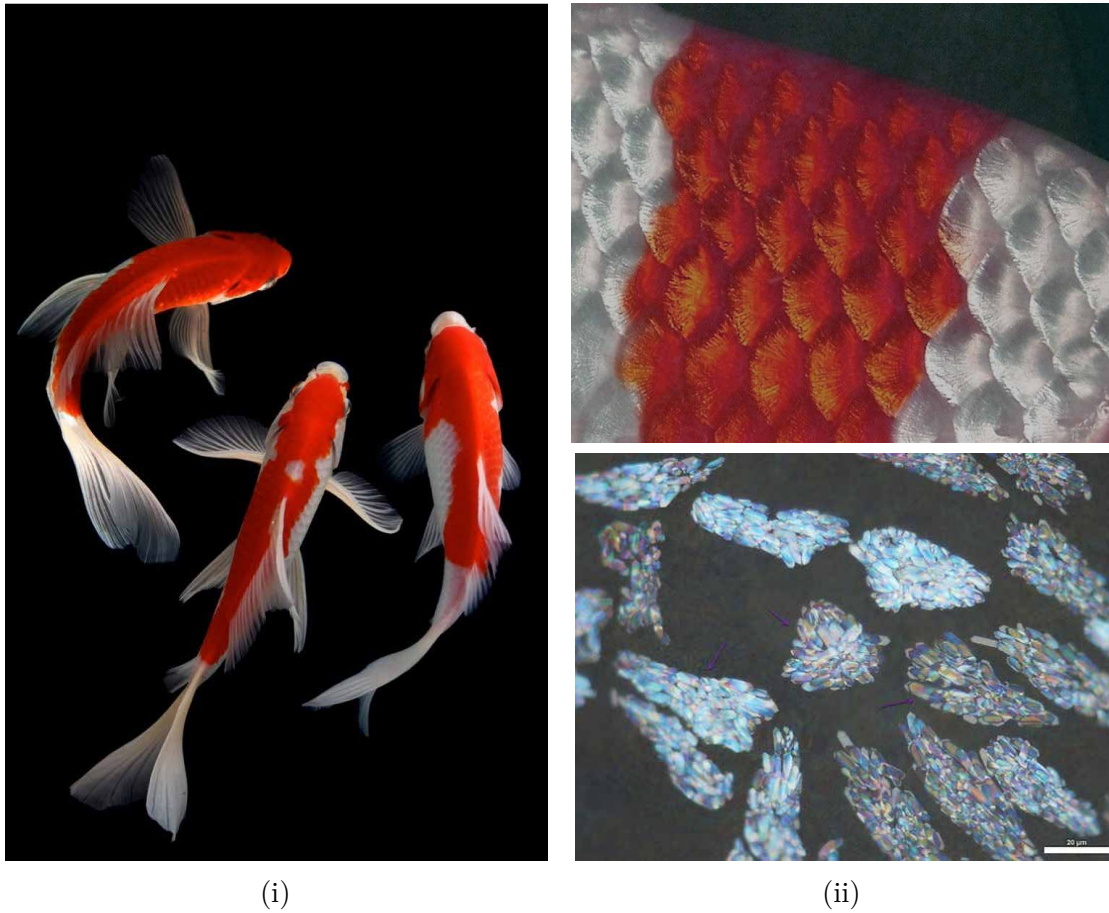


Figure 1.5: (i) koi fish (ii) koi fish scale and iridophores composed of guanine crystals from the skin of koi fish. Reproduced with permission from [77].

These examples demonstrate the potential of controlling the crystal structures for a diverse range of applications. Processes that facilitate crystallization opens up new possibilities to make novel composite materials with distinct properties, such as good mechanical and optical performances, that so far conventional techniques can not provide. Indeed, the biomineralization field inspired many researchers to develop new tools and applications to improve or transform the existing processing techniques accordingly to mimic the strategies of nature to create high-tech composite materials. Therefore, it is valuable to have a summary on this emerging technology with a perspective on tools and techniques to achieve such control.

1.3 Techniques for Crystallization Control

Historically, control over crystallization aimed to establish processes that narrow down the size distribution of particles, as summarized in Figure 1.6. This endeavor is followed by the demand to precisely control the crystal growth of inorganic materials to manufacture semiconductor crystals in the 1950s. This milestone enabled tremendous achievements thanks to tremendous advances in electronics. Starting from early 2000s, the control over crystal structure gained also importance in the field of proteins. In addition, nucleation and growth control have required in-depth understanding of processes, which allow the synthesis of many types of nanoparticles possessing well-defined structures. The control over the structure of crystals enabled the control of properties such as optical, electronic, magnetic properties, chemical stability, and solubility.

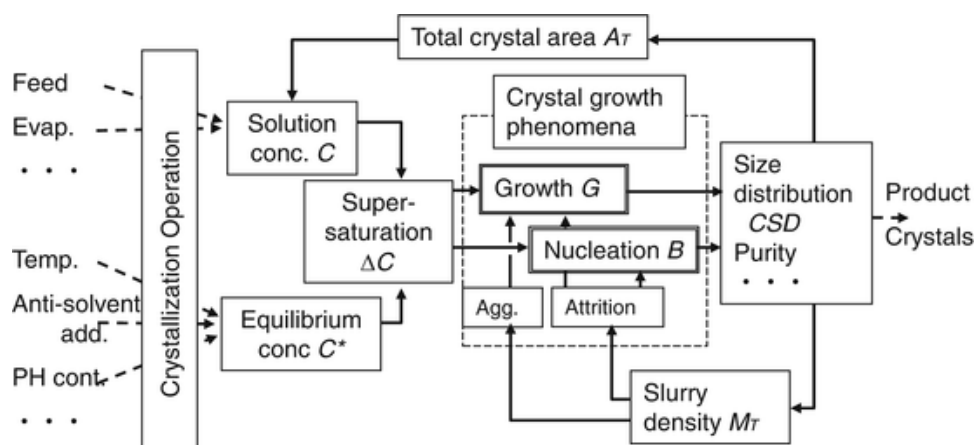


Figure 1.6: Crystallization operation scheme. Adapted with permission from [78].

1.3.1 Bulk Crystallization

Industrial crystallization started with batch crystallization where the prime objective was the synthesis of pure crystals with a narrow size distribution. This required a good control over the nucleation. Verneuil is considered to be the founder of industrial crystallization as, by 1902, he developed the first process named *flame fusion*: in this process, the feeding powder is melted upon passing by the flame

and delivered onto the surface of the seed crystal to grow bulk crystals, as seen in Figure 1.7 [79]. *Flame fusion* is one of the fastest crystal growing techniques, yet was able to control nucleation to a significant extent. Hence with a pioneering investment it has been used to grow Al_2O_3 based bulk crystals for ruby and sapphire production for artificial gems in Paris, and for watch industry in Switzerland by Djevahirdjian. However, the products have a large dislocation density, which needs to be decreased for later advances in semiconductor and nanomaterial synthesis. The Czochralski method can be used to produce crystals with fewer dislocations, which are more suitable for semiconductors, and optical applications [54]. Hydrothermal synthesis is another method that has been used for bulk crystals and nanoparticle formation [79–81]. During the following decades, numerous techniques followed the Verneuil method, as only few of them are mentioned above. Most of the techniques and famous theories for crystallization by Nernst and Volmer that are still used today, have been developed before the 1950s and variations of them have been established for the semiconductor technology. By the year 2000, approximately 60% of bulk crystals were semiconductors (Figure 1.8).

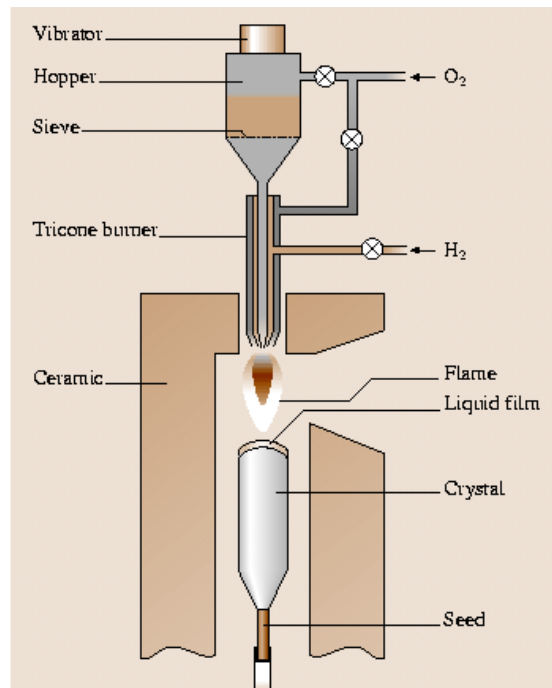


Figure 1.7: Verneuil method adapted with permission from [79].

This has changed during the last few decades. Advances in colloidal science and biology opened up a new area of crystallization studies as the structure of the resulting materials, such as proteins, drugs and colloids, are directly related to

1.3 Techniques for Crystallization Control

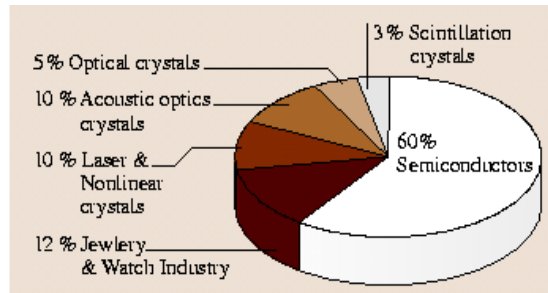


Figure 1.8: Estimated share of the world production of 20000t of bulk crystals (1999). Adapted with permission from [82].

their performances. To obtain a good control over the size, seeded crystallization is heavily used to take the system into the *metastable zone*, where no new nuclei form, since the surface of the presented seeds lowers the energy barrier for the crystal growth. Therefore, controlled growth can be achieved on top of the seeds, resulting in crystals displaying a narrow size distribution, as shown in Figure 1.9 [78].

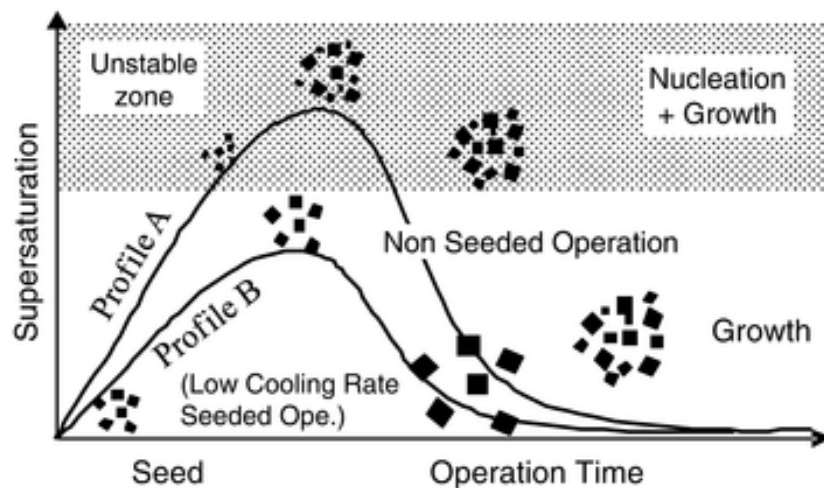


Figure 1.9: Schematics of seed crystallization. Two regimes of crystallization where Profile A shows a poor control over the size distribution and Profile B good control growth over on the size. Adapted with permission from [78].

In addition to the size and size distribution control, crystal phase control has been investigated for more intricate and complicated applications. For instance, depending on their processing, one can influence the phase of superparamagnetic iron oxide nanoparticles (SPIONs) which can then be used as magnetic resonance imaging (MRI) agents [81]. Phase-controlled synthesis of metallic nanomaterials

Chapter 1. Introduction

has a high potential, as it allows to control physicochemical properties such as chemical stability, optical, electrical and magnetic properties and bandgaps [56]. Hydrothermal synthesis in which high pressure and temperature is applied, is used as a popular route to achieve control over the crystal structure. It is reported that experimental conditions such as *temperature*, *pressure*, *solvent* and *precursor concentration* are used to fine tune crystal structure of the resulting nanomaterials, allowing increased performances in various applications [56, 83].

The use of controlled crystallization is not limited to inorganic materials. Controlled crystallization also accelerated the discovery of new drugs and screening assays which have transitioned from library-based to structure-based. This brought up the urge of protein crystallization, as the crystallographic data became a fundamental part of simulations aimed to identify protein-ligand interactions [84]. The structure of such macromolecules is tuned by various routes, as demonstrated in Figure 1.10 [85].

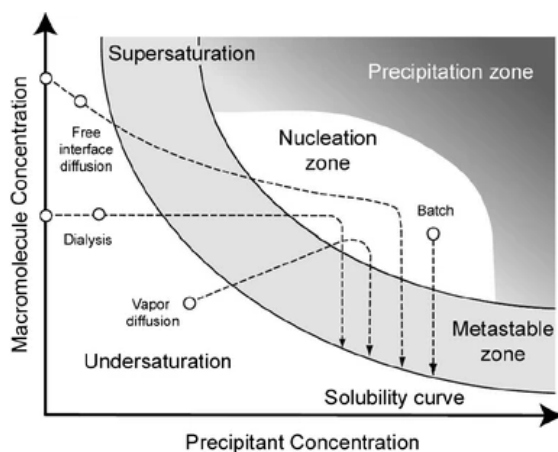


Figure 1.10: Scheme of protein crystallization routes for controlled precipitation and growth. Adapted with permission of the International Union of Crystallography from [86].

There is still a large potential in crystal engineering to discover new materials. However, it would be extremely expensive and hence not competitive, especially for bio-derived molecules such as proteins, to screen the different crystal structures through bulk crystallization. Therefore, *templated crystallization* that uses limited volumes, for example if liquids are formulated as airborne drops or emulsions, is attractive for these applications.

1.3.2 Micron-size Templated Crystallization

1.3.2.1 Microfluidics

Within microfluidic devices, minute amounts of liquids in the range between nanoliter (nL) and microliter (μL), that can impose confinement on crystallization, can be manipulated through microchannels with dimensions varying from 1 to 1000 μm . Such systems display low Reynolds numbers, hence allowing controlled laminar flows that minimize the mixing and hence reduce the reaction rates [87, 88]. Thanks to the low flow rates and low Reynold numbers, controlled flow can be exploited for many applications including, drop formation [89], reaction kinetics [90–92], and analytics [93].

Valves and wells have been widely used to screen proteins with microfluidics. The amount of reagents added and the precipitation speed can be controlled by co-flowing different fluids, optionally containing different reagents at defined rates, as shown in Figure 1.11 [91]. Additionally, microwells enable trapping drops such that reactions occurring within them can be monitored for a prolonged time. One commercialized example of this technology is known as *Slipchip*. This system enables versatile mixing and formation of different conditions simply by attaching two microfluidic chips filled with different reagents and connected to different wells, as shown in Figure 1.12 [94]. Thanks to this advancement, screening processes become less time and resource consuming.

The laminar flow interface dictated by microfluidics also introduces a platform for nucleation and growth of crystals. Such stable interfaces minimize the probability of mixing of different reagents such that nucleation and growth is governed by the diffusion kinetics. In this case, diffusion kinetics is dictated by the initial solute concentration, flow rate and the dimensions of the microfluidic device [90, 96]. Such continuous crystallization has been used to screen short-lived metastable phases. If performed via batch crystallization, it is not possible to quench them and observe such phases due to the fast reaction kinetics. On the contrary, microfluidics decreases the crystallization rate significantly, as it confines fluids. The control on mixing and reaction rate microfluidics possesses makes it attractive for such crystallization studies.

As crystallization can be achieved through many different methods, including the

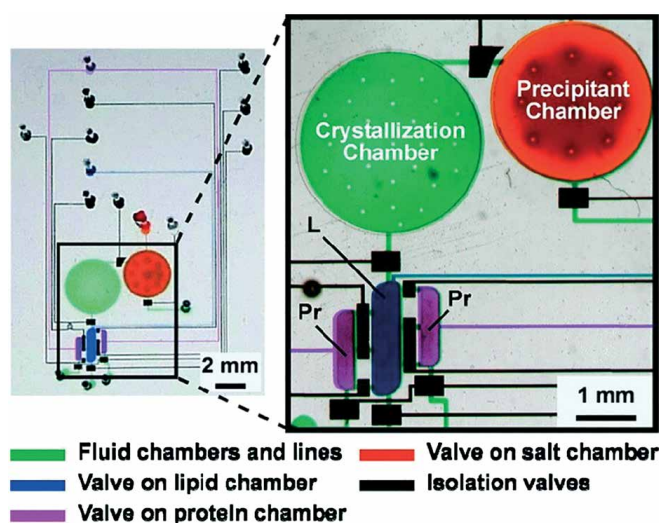


Figure 1.11: Optical micrograph of a microfluidic chip capable of mixing lipids (L) and aqueous protein (Pr) solutions by pneumatic actuation. Adapted with permission from [95].

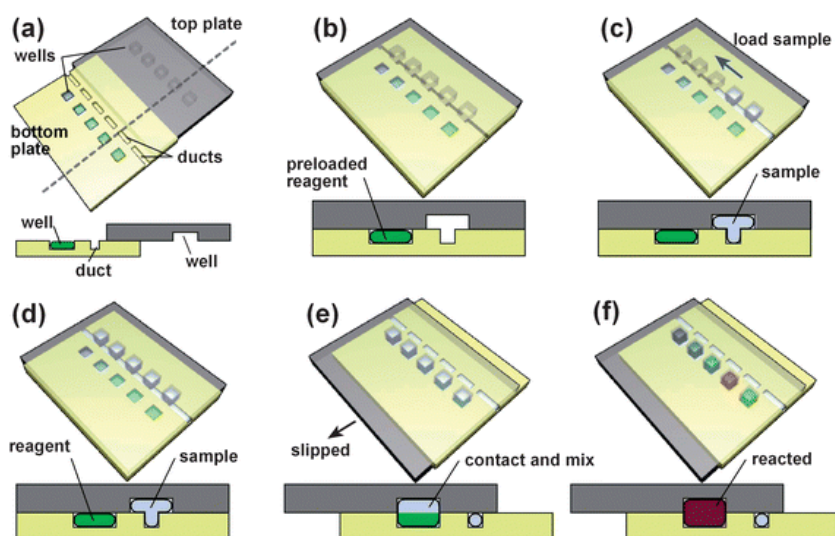


Figure 1.12: Step-by-step 3D schematic drawings with cross-sectional views that describe the operation of the SlipChip. (a) Off-set view that shows the preloaded wells of the bottom plate, the ducts of the bottom plate, and the wells of the top plate. (b) View of the device available to the user, in which the top and bottom plates are aligned. (c) and (d) Loading of a single sample through the overlapping ducts of the bottom plate and wells of the top plate. (e) Slipping of the top plate relative to the bottom plate disconnects the sample wells of the top plate from the ducts of the bottom plate, and then exposes the sample wells to the wells of the bottom plate containing reagents. (f) The red well schematically shows a reaction taking place after mixing and incubation. Adapted with permission from [94].

1.3 Techniques for Crystallization Control

use of anti-solvents or precipitants, mixing within the microfluidic device plays an important role for anti-solvent induced precipitation and reactive crystallization. As a result, the structure of microfluidic channels has a strong influence on the nucleation and growth. For instance, capillaries are mostly used for spherical crystallization of proteins yet these structures are not suitable for anti-solvent crystallization or reactive crystallization as the laminar flow makes mixing very slow such that very long capillaries are needed to complete the process [93, 97].

Mixing of reactants can be accelerated with Y or T junctions. Zeng et al. used this technique to study the formation of $CaCO_3$, as the crystallization time can be tuned with the capillary length of the outlet channel. They observed several phases from amorphous calcium carbonate at the proximity of the junction to the most stable calcite observed at the proximity of the outlet as seen in Figure 1.14. This technique is handy to observe the morphology and even perform Raman spectroscopy if coupled to a confocal microscope. However, *in-situ* structural characterization requires diligent sample preparation and *ex-situ* structural characterization is limited. Most of the time, crystals start to adhere to the microchannel surfaces, thereby preventing retrieval of crystals for proper analysis [89]. These limitations can be addressed if emulsion drops are formed within microfluidic devices, as discussed in the next section.

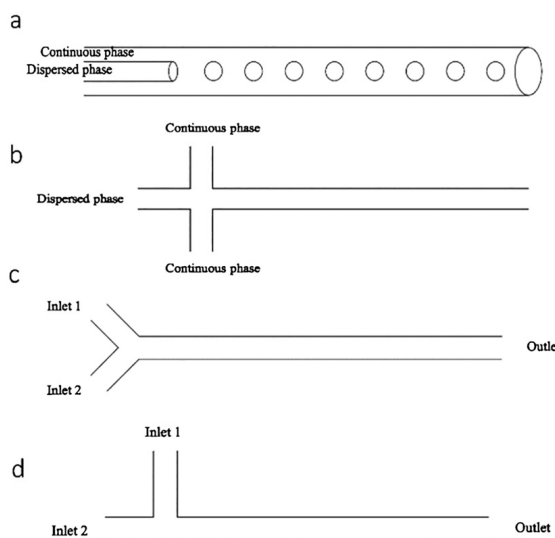


Figure 1.13: Design of drop generation structures in microfluidics based on (a) capillaries; (b) flow-focusing; (c) Y-junctions; and (d) T-junctions. Adapted with permission from [97].



Figure 1.14: Formation of branched ACC at the center of the Y-junction when directly mixing solutions containing equimolar concentrations of $CaCl_2$ and Na_2CO_3 (20 mM) in microfluidics. Adapted with permission from [88].

1.3.2.2 Drops

1.3.2.2.1 Emulsions

Emulsions are drops dispersed in another immiscible fluid. In the simplest case, single drops are dispersed in a second fluid. These are called *single emulsions*. If small drops are contained in larger drops contained in a third fluid, they are called *double emulsions*. The dispersed phase can either be water based or oil based. Most of the crystallization studies in emulsions are performed in the core of aqueous drops that are surrounded by a continuous oil phase. In the early 2000's emulsions were mainly used to control the crystal size distribution of macromolecules such as fats and proteins [98, 99]. However, the lack of control on the size of emulsions formed with bulk techniques, such as shaking, has prevented their further use to screen crystallization parameters [100]. Additives, such as surfactants and nanoparticles, needed to stabilize the emulsions, act as heterogeneous nucleation sites and thereby increase the nucleation rate and limit the growth rate [100, 101].

Drops with a narrow size distribution can be formed in flow focusing microfluidic devices. These drops are suitable for crystallization screening since they can be treated as identical crystallization vessels. The low volume needed to perform drop-based screening assays also enables the screening of expensive substances. In addition, the large number of drops that can be formed and analyzed allows for statistical analysis (Figure 1.15) [102]. These advantages allow to screen and monitor multiple crystallization conditions simultaneously.

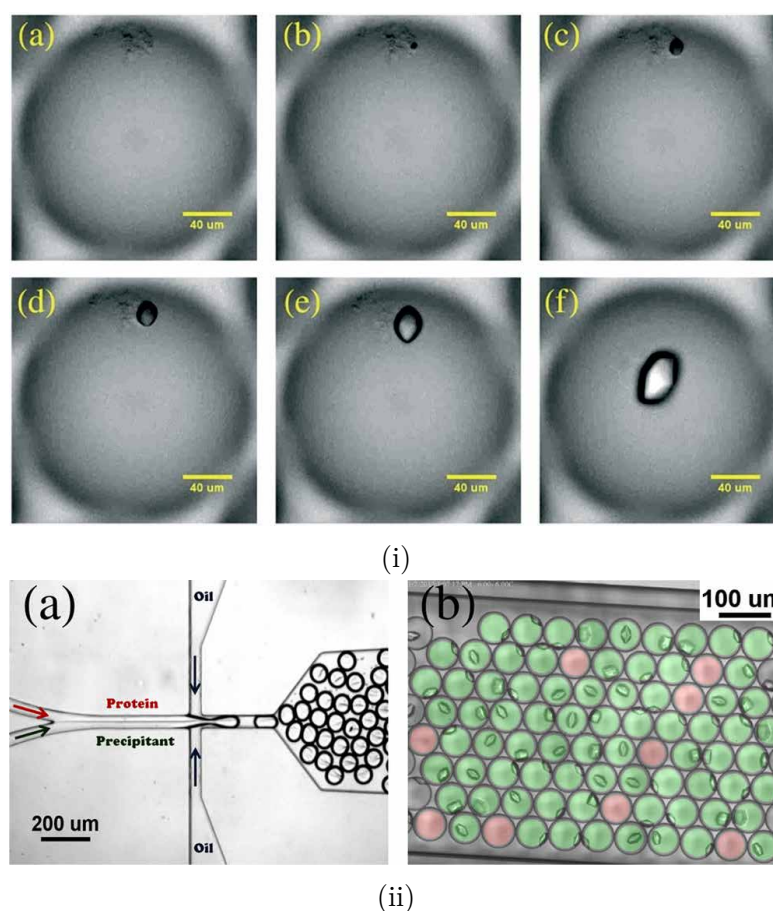


Figure 1.15: (i) Nucleation and growth of a crystal from a protein dense aggregate at (a) $t = 0$, (b) $t = 15$ s, (c) $t = 45$ s, (d) $t = 75$ s, (e) $t = 120$ s, and (f) $t = 300$ s. (ii) (a) Drop generation using a co-flow microfluidic device fabricated using PDMS (b) Detected drops with crystals highlighted in green and without crystals highlighted in red. Reproduced with permission from [102]. Copyright 2014, American Chemical Society

To monitor crystallization for a prolonged time, trapping devices have been introduced [103, 104]. Drops with diameters larger than the channel height are squeezed into a channel. The channel contains areas where its height abruptly increases. When the drops reach such an area, they relax, thereby lowering their surface area. The energy gain associated with the reduction in surface area is equal to the trapping energy that immobilizes the drops at these locations [105, 106]. Cavanaugh *et al.* utilized this system to study CaCO_3 crystallization as shown in Figure 1.16. As these devices are made either from polydimethylsiloxane (PDMS) or glass, they are transparent and permit the *in-situ* observation and to some extent characterization of crystallization [90]. The main limitation of these systems is

the stability of the emulsions during crystal formation. Crystallization conditions may require changes in pH, osmotic pressure and temperature that diminish the emulsion stability. Recent studies demonstrated that w/o/w double emulsions produced with microfluidics can be used for studying protein crystallization with minimal shape distortion of the emulsions, as demonstrated in Figure 1.17 [101]. Alternatively, separation of drops with air-liquid interfaces through levitating the drops or aerosol formation can be used to avoid drop coalescence.

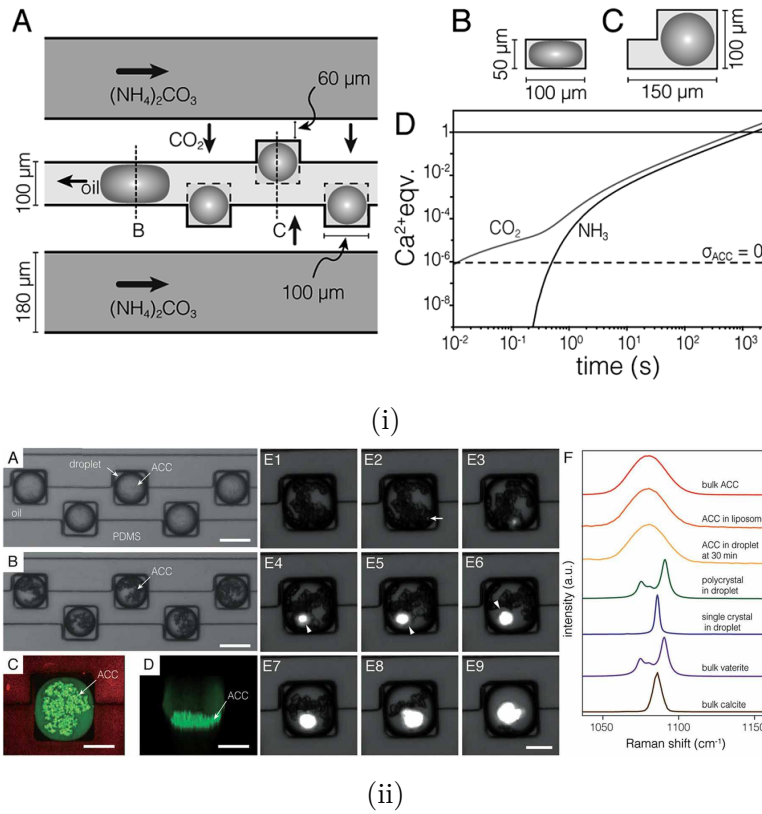


Figure 1.16: (i) (A) Schematic drawing of the trapping device. In the oil channel, drops display an ellipsoidal shape (B), but can relax on entering the wells (C). (D) Plot of stoichiometric equivalents of CO_2 and NH_3 delivered to the drop versus time, predicted by finite element modeling. (ii) Observed phase transformations in the trapping device. Raman spectroscopy demonstrates the potential to observe multiple short-lived metastable phases. Adapted with permission from [90].

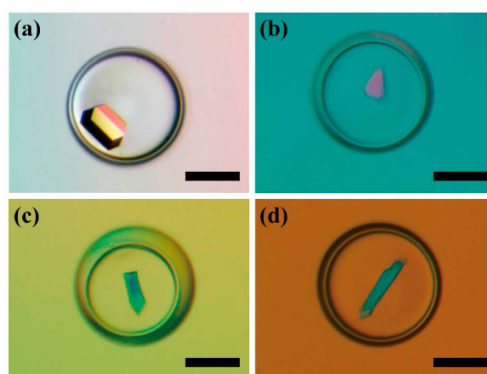


Figure 1.17: Protein crystallization using the double emulsion-based approach on various compounds including (a) Lysozyme; (b) Thaumatin; (c) Trypsin; (d) Horseradish peroxidase. Scale bars: 300 μm . Adapted with permission from [101].

1.3.2.2.2 Aerosols

One of the main routes to form micrometer-sized crystals is through aerosols. By controlling the drying time of drops, the crystallization time and hence the crystal structure can be controlled. *The drying time* can be controlled through the solvent choice, drying temperature and the initial size of aerosols. Such control can be established via several techniques.

1.3.2.2.2.1 Spray Chilling

Spray chilling is a process where molten liquid is atomized into aerosol drops that are rapidly cooled down to form prills or powders [107]. Such rapid cooling helps restricting the crystallization time since the mobility of molecules has become limited within a short period of time. Spray chilling or congealing can otherwise be used as a technique to form metastable or amorphous particles [108].

The viscosity of liquids to be processed through spray techniques must be low. This limits the amount of reagents that can be dissolved in the solution. This limitation can be overcome by spray chilling pure, undiluted materials. However, the processing temperature should be chosen such that the melt viscosity is in the range where aerosols can be produced [109]. Therefore, materials suited for spray chilling are low molecular weight compounds that have relatively low melting points and exhibit fast crystallization [49, 110, 111]. Aerosols formed through

spray chilling are used to fabricate amorphous/nanocrystalline metal coatings as a barrier material against extreme thermal conditions, abrasive wear, and creep as sprayed drops deposit as particles with controlled crystal structure [112, 113]. Another application is the use of low molecular weight organic crystals, such as sugars like erythritol and mannitol used to retain volatile fragrances and sensitive food ingredients. It is possible to produce polycrystalline matrices out of these materials to encapsulate fragrances, as shown in Figure 1.18, thereby increasing their storage and release control [45, 46, 49]. However, the use of high temperatures to formulate volatiles is not desired due to a high loss of volatiles during processing.

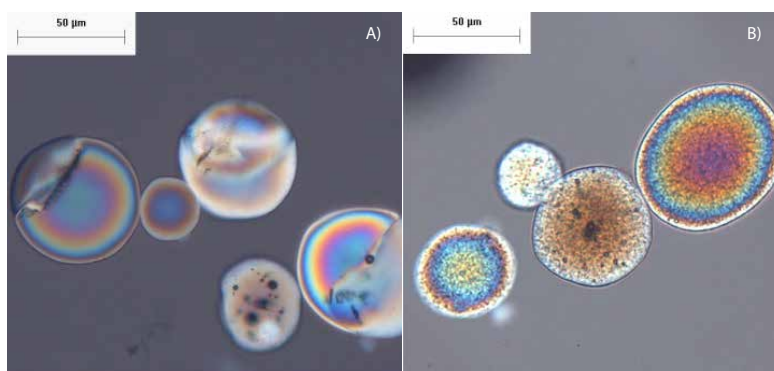


Figure 1.18: Fine crystalline particles formed by spraying (A) pure erythritol and (B) an erythritol/limonene emulsion as imaged by slightly uncrossed (75°) polarized light. While several gas bubbles are seen within one of the particles of A, particles in B also contain a multitude of fine oil droplets dispersed throughout the structure. Adapted with permission from [45].

1.3.2.2.2 Electrospraying

Electrospraying is a promising technique to fabricate aerosols with small sizes that can be translated into small particles [114–116]. In electrospraying, a high voltage is applied to a metal nozzle where the conductive solution is delivered with a controlled flow rate by a syringe pump. At the nozzle, the liquid is broken into drops that are collected on a grounded substrate, as shown in Figure 1.19 [117]. Due to the high voltage applied on the conductive solution, a Taylor cone is formed, which then transformed into a jet with high charge density. If high molecular weight polymers are included in the solution, the jet is able to carry a high tension. This tension distorts the jet into a spindle form, creating nano or micronscale polymeric fibers that reach the collector. If the electrospray setup is used for the formulation of pharmaceuticals, the aim is to form tiny drops that

can be collected as nano or micron sized particles on the collector. The size of the drops depends on the flow rate, the applied voltage, electrical conductivity of the solution and its dielectric constant [118].

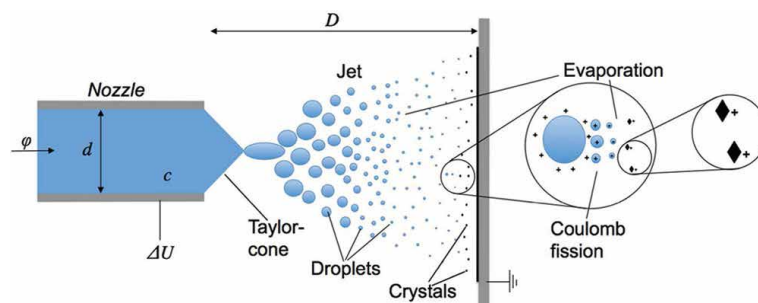


Figure 1.19: Schematics of electrospray process, adapted with permission from [117].

Since with electrospraying, drops with diameters on the order of micrometers can be produced, this technique can be used to form small drops. Rapid drying may also allow kinetic quenching of metastable structures if the drying time is shorter than the time needed to form the most stable crystal phase. Hence this technique is used to formulate amorphous active pharmaceutical ingredients (API) [114, 116, 119]. It has the advantage that substances can easily be produced at room temperature. However, compounds that are sensitive to high electric fields and accumulated charge density in the drops cannot be processed through electrospraying. Moreover, during the powder processing, evaporation of drops increases the charge density to a point, where Rayleigh disintegration can occur. Above this limit, the accumulated charge repulsion overcomes the surface tension, so that the drop emits highly charged offspring droplets that stay separated. Such a system naturally forms a bimodal distribution of droplet sizes and nanoparticles thereby, comprising the control on the crystal structure. Therefore, nebulization with a better size distribution such as spray drying can be used to study crystallization.

1.3.2.2.3 Spray Drying

Spray-drying is a technique that has mainly been exploited in food industry to formulate capsules for flavors [47, 120], fragrances [16, 121], food compounds [122, 123] and many more [124–126]. In addition, in pharmaceutical industry it is used to produce drugs [127] and to embed them in a matrix [128] or an excipient

Chapter 1. Introduction

[129] to ameliorate their delivery and bioavailability [51, 130]. It is a technique used to process solutions into drops and, subsequently dries them during their flight within a temperature controlled chamber. The resulting particles are collected within a separate collection chamber [131, 132].

The conventional setup mainly consists of an atomizer that forms aerosols, a drying chamber where drops are dried through the temperature-controlled gas flow to form solidified particles, and a cyclone that neutralizes the particles and separates them into another chamber called collector, as shown in Figure 1.20. The most common nozzle type is a two nozzle system, however, nozzles can be varied to specific applications that require high viscosity and low shear, high temperatures and pressures and so on.



Figure 1.20: The photo of a spraydryer.

Spray-drying is a very powerful technique, because it is a flexible, one-step process to directly transform liquids into solid particles with a high scalability and versatility. The technique demonstrates ease of processing, simplicity and low operating costs [133]. Compared to its competitors, it is also energy efficient [134]. As a result, spray-drying has become the dominating approach to form powder at high throughputs in many areas, especially in food industry, where spray-drying accounts for almost 80% of the flavor encapsulation (Figure 1.21) [135].

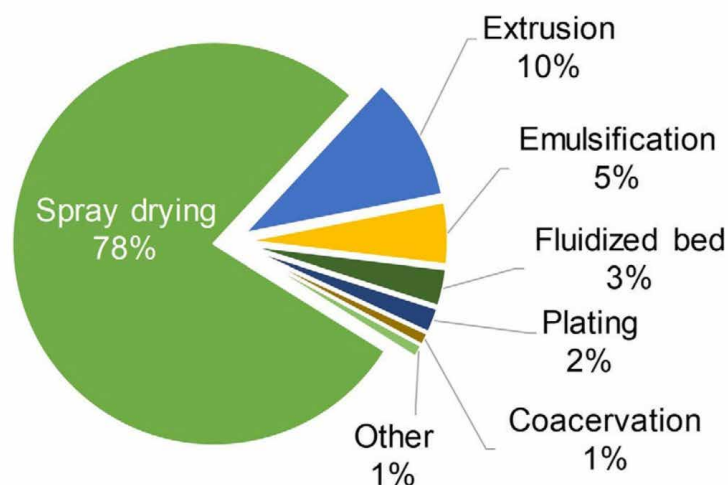


Figure 1.21: Statistics demonstrating the processes of flavor encapsulation, adapted with permission from [135].

Conventional spray dryers form drops with diameters of 10 to couple of hundreds of micrometers [131]. Their size inversely scales with the nozzle pressure [136, 137]. While commercial spray driers can process solutions up to 10L/hour, spray-dryers that are used for scientific purposes, named *mini spray-driers* exhibit feed rates of a few liters per hour. Temperature is an important parameter that determines the drying rate of the solution and the amount of solvent residues in the spray dried particles. The latter is especially important, since the amount of solvent that remains in the powder dictates the shelf life of the final product. Industrial scale spray-dryers dry drops at temperatures up to 500 °C, while the ones that are used for scientific purposes can increase the temperature up to 250 °C [138]. The drops produced by regular spray-dryers are completely dried within 1s. However, an early skin formation due to primary drying on the surface of the drop can occur within 10 ms, as demonstrated in Figure 1.22. Whether such a crust forms is determined by the Peclet number (Pe). The value of Pe indicates whether the evaporation rate is faster compared to the diffusion of the solutes. The interplay between solute diffusion and evaporation rate influences the final particle morphology. By tuning Pe, the processing parameters can be tuned in a way that encapsulants are homogeneously distributed within matrix or core-shell structures are obtained [139].

As the Pe number depends on the drop size, nanospray-drying received high visibility to improve this parameter by decreasing the drop size, especially in the last decade.

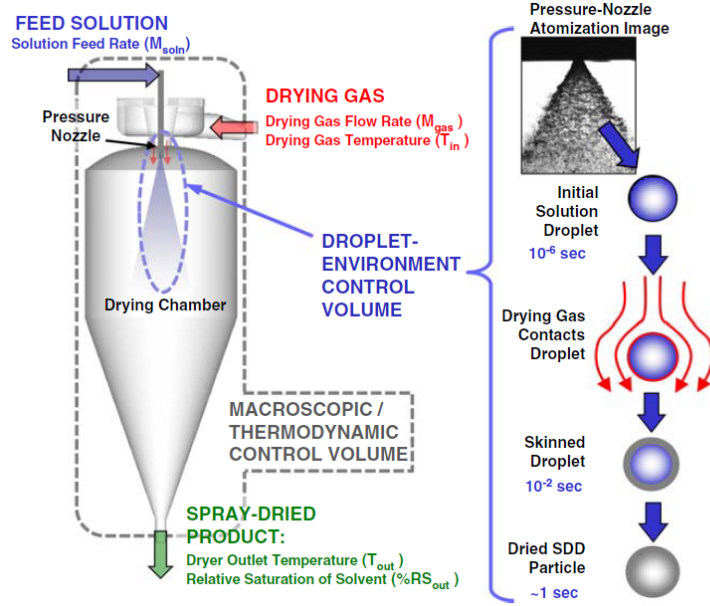


Figure 1.22: Schematics of drying process demonstrating the main processing parameters and time scale of drying, adapted with permission from [139].

While the working principle is fundamentally similar to conventional spray-dryers, there are some essential differences. To produce particles in the nano regime, the drops must be smaller compared to drops produced by conventional spray-dryers. Assuming one drop forms one particle, with the average solid concentration C_s in the order of 0.1 to 0.01 g/mL and a density ρ around 0.9 to 1.5 g/cm³ nanometer sized particles can only be produced if the drop diameter d_D is below 10 μm as determined with Equation (1.6), where d_p is the particle diameter. Drops with such small sizes cannot be obtained with the two nozzle system where the drop size is determined by the gas pressure. In this case, by increasing the gas pressure the drop size can be reduced down to 10-20 μm [140]. To form smaller drops, nanospray-dryers use a different atomizer called *vibration mesh technology*.

$$d_p = d_D \cdot \left(\frac{C_s}{\rho}\right)^{\frac{1}{3}} \quad (1.6)$$

This new droplet generator uses an electronically driven piezoelectric actuator that vibrates the thin spray mesh, as shown in Figure 1.23. The mesh contains 1000-2000 laser drilled micron-sized holes with conical shapes for fluid supply [141, 142]. The

1.3 Techniques for Crystallization Control

ultrasonic vibration frequency ranges between 80 to 140 kHz. The vibrating mesh breaks the fluid into drops that fly into the drying chamber. With this method, droplets with a very narrow size distribution can be produced. Approximately 100 million precisely dimensioned droplets are produced per second, given the average feed rate is 10 mL/h, the vibration frequency is 100 kHz and 1000 active holes are found in the spray mesh [140]. The uniformity of the droplet size is mainly defined by the uniformity of the holes. The droplet size depends on the mesh size and the physicochemical properties of the fluid, such as viscosity and surface tension [140]. The diameter of droplets produced through these holes varies between 5-10 μm [143]. The droplets are dried within a laminar flow of gas to prevent that they merge such that the droplets are transformed into nanoparticles once completely dried. The residence time for these droplets is 3–6 s in the short setup and 7 to 15 s in the tall setup [140]. However, collecting nanoparticles is more difficult than collecting microparticles as their impact on the substrate can easily be hindered by the gas flow. Yet, with more advanced filters and more effective collecting units, particles with controlled sizes and structures can be obtained and collected.

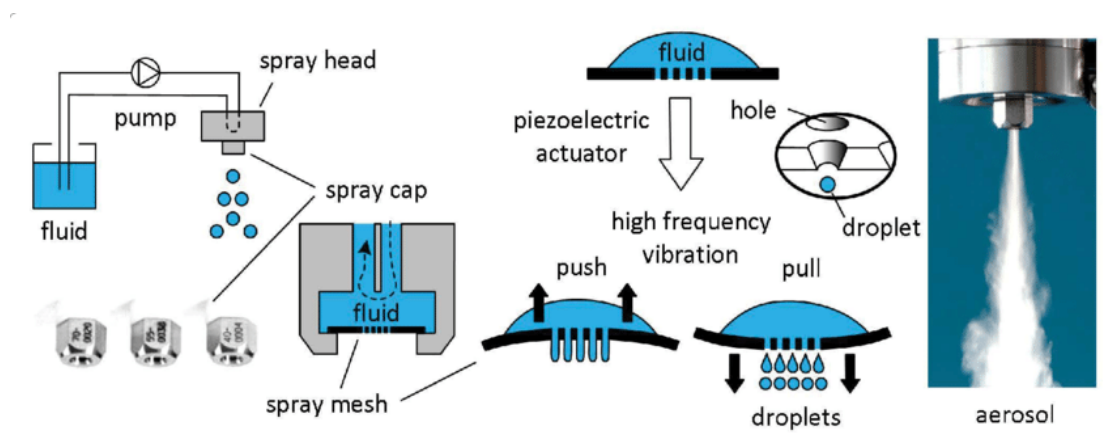


Figure 1.23: Schematics of drying process demonstrating the main processing parameters and time scale of drying, adapted with permission from [126].

To achieve control over the size and crystal structure, there are several processing parameters that can be explored and tuned, as shown in Figure 1.24 and Table 1.1. One of the main parameters to control the structure is the drying time. As the size of the drops gets smaller, the time required to dry them is reduced. This may limit the time for molecules to arrange into the most stable phase. Therefore, these dryers are well-suited to formulate pharmaceutical, biomedical and food related compounds as for example, metastable or amorphous phases. The drying time can

be controlled with the *drop size*, which is governed by the spray mesh size and vibration frequency, *temperature*, as it influences the evaporation rate, and *solvent type*, since the evaporation rate is intrinsically determined by the vapor pressure of the solvent.

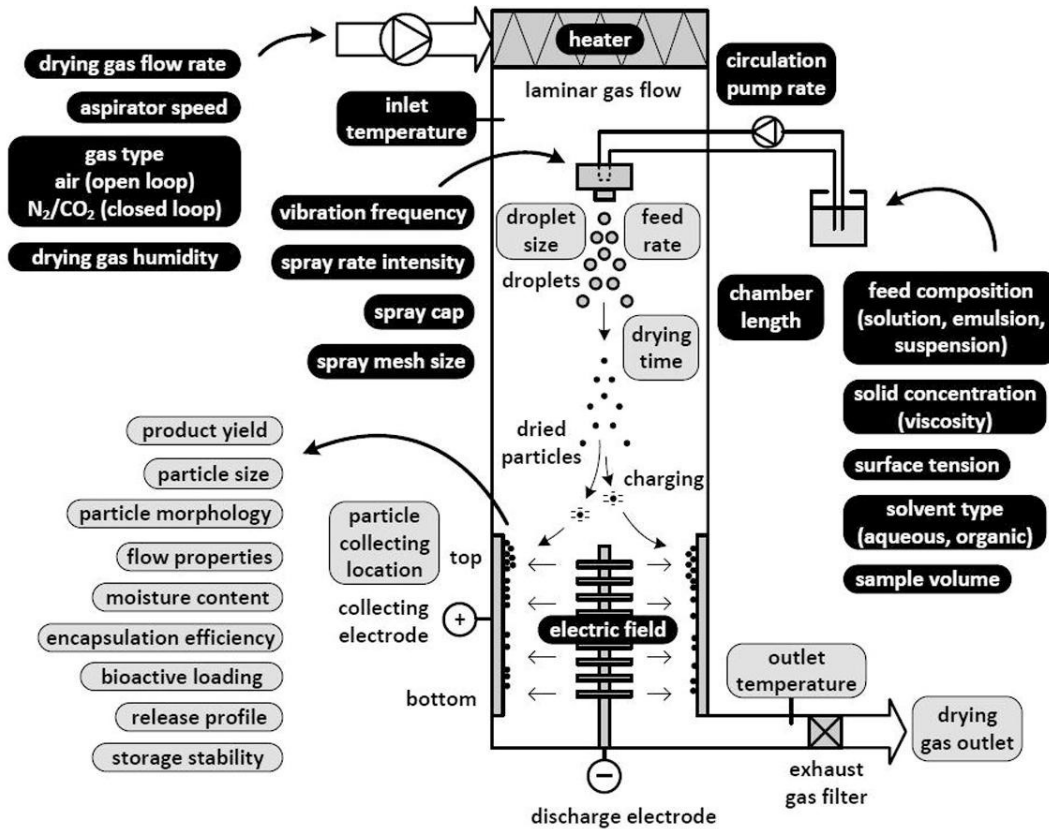


Figure 1.24: Process parameters and formulation variables for the production of bioactive food-loaded nanoparticles by nano spray drying, adapted with permission from [141].

Table 1.1: Influence of spray drying process parameters on the properties of the final product. Adapted with permission from [126].

| Process parameter | Outlet temperature | Droplet size | Particle size | Feed size | Moisture rate | Yield content | Stability |
|-----------------------------------|--------------------|--------------|---------------|-----------|---------------|---------------|-----------|
| Drying gas flow rate ↑ | ↑ | - | - | - | ↓ | - | - |
| Drying gas humidity ↑ | ↑ | - | - | - | ↑ | ↓ | - |
| Inlet temperature ↑ | ↑ | - | ↑ | - | ↓ | ↑ | ↓ |
| Spray mesh size ↑ | ↓ | ↑ | ↑ | ↑ | - | - | ↑ |
| Spray frequency ↑ | ↓ | ↑ | ↑ | ↑ | ↑ | - | ↓ |
| Circulation pump rate ↑ | - | ↑ | ↑ | ↑ | - | - | ↑ |
| Solid concentration (viscosity) ↑ | ↑ | - | ↑ | ↓ | ↓ | ↑ | - |
| Surfactant / stabilizer in feed ↑ | - | ↓ | ↓ | ↑ | - | ↑ | ↑ |
| Organic solvent ↑ | ↑ | ↓ | ↓ | ↑ | ↓ | ↑ | - |

Spray drying has been applied to many food and pharmaceutical compounds where crystal structure determines their performance. For instance, chitosan which is used as wall material for encapsulation is formulated as amorphous phase via nanospray-drying to encapsulate and better embed levofloxacin, a respiratory system drug [144]. Moreover, crystalline compounds such as acidifiers like potassium bitartrate and colorants such as sodium sulfite are processed to demonstrate the advantages of their amorphous structures [141]. In addition, many pharmaceutical compounds and excipients such as succinic acid have been formulated as amorphous phases to increase their bioavailability and dissolution rate [145]. Despite the many advantages, the risk of clogging of spray meshes limits the use of this technique. This can be resolved with a nozzle-free production of aerosols via techniques such as surface acoustic wave atomization.

1.3.2.2.4 Surface Acoustic Wave Atomization

Another way to form aerosols with small diameters is through the use of *Surface Acoustic Wave (SAW) atomization*. SAWs are sound waves that travel parallel to the surface of piezoelectric materials, with decaying amplitude into the piezoelectric material, in a way that the waves are kept confined to the surface (approximately one wavelength) [146]. SAWs can be generated on the piezoelectric material with an alternating voltage that is applied onto an *interdigitating transducer (IDT)*, as shown in Figure 1.25. The pitch of this IDT determines the wavelength of the SAW.

The SAW can interact with liquid and transport it on the piezoelectric chip surface. If focused on a specific point on the chip, it can cause capillary waves through streaming, which eventually creates a Rayleigh instability and forms droplets. The diameter of the droplet can only be as large as the *capillary wavelength* λ . The *capillary wavelength* and the size of the droplets are determined by the frequency of capillary wave f_c , surface tension γ and density ρ of the liquid as shown in Equation (1.7) [148]. In case of continuous liquid delivery with a flow rate that is similar to the atomization rate, a continuous formation of droplets is achieved. Upon drying of these droplets, a continuous formation of nanoparticles is possible. With such a system, drops with diameters up to 10 μm can be produced; these droplets dry within a few hundred ms. The applicability of this technique for the formation of particles with controlled crystal structures has been demonstrated

1.3 Techniques for Crystallization Control

with some organic salts and hydrophobic drugs [149]. Because this atomizer does not possess any nozzle, it does not risk clogging, thereby increasing its operation robustness.

$$\lambda = \left(\frac{2\pi\gamma}{\rho f_c^2} \right)^{\frac{1}{3}} \quad (1.7)$$

Microfluidics based SAW spray-drying can open up new routes to produce novel materials with controlled microstructure, thanks to their production of kinetically controlled nano-sized powders. This feature can be used in pharmaceutical processing, as the bioavailability and solubility of these compounds strongly depends on their crystal structure. In addition, compactability of these compounds is a critical parameter to form pellets for orally administered drugs and it is also influenced by the crystal structure of the compound. Such control in bulk methods is challenging, due to the difficulty to achieve control over the nucleation in large volumes, as it requires compatible additives and laborious processes to achieve ultimate pharmaceutical product. However, through the use of microfluidic SAW device, it is possible to limit the crystallization volume into micron sized airborne drops enabling control over the crystal structure thus, physicochemical and mechanical properties of the pharmaceuticals. It is also possible to control phase separation and tailor the resulting particles as matrix systems for volatiles. Unlike conventional encapsulation systems where high molecular weight compounds are spray-dried with elevated temperatures that are detrimental for volatile compounds, microfluidic spray dryer has the advantage of rapid drying of tiny drops, quickly arresting volatile substances within low molecular weight matrix compounds in milder temperature conditions. Such control can be achieved through the control of processing parameters such as drying time and supersaturation of solutions such that volatile substances can be kinetically trapped within matrices composed of low molecular weight compounds. While conventional matrix materials with high molecular weight and relatively large mesh sizes lack control over volatile release, with this technique low molecular weight crystalline compounds can be processed to form low mesh size matrix with controlled phase separation hence, presenting control over volatile release.

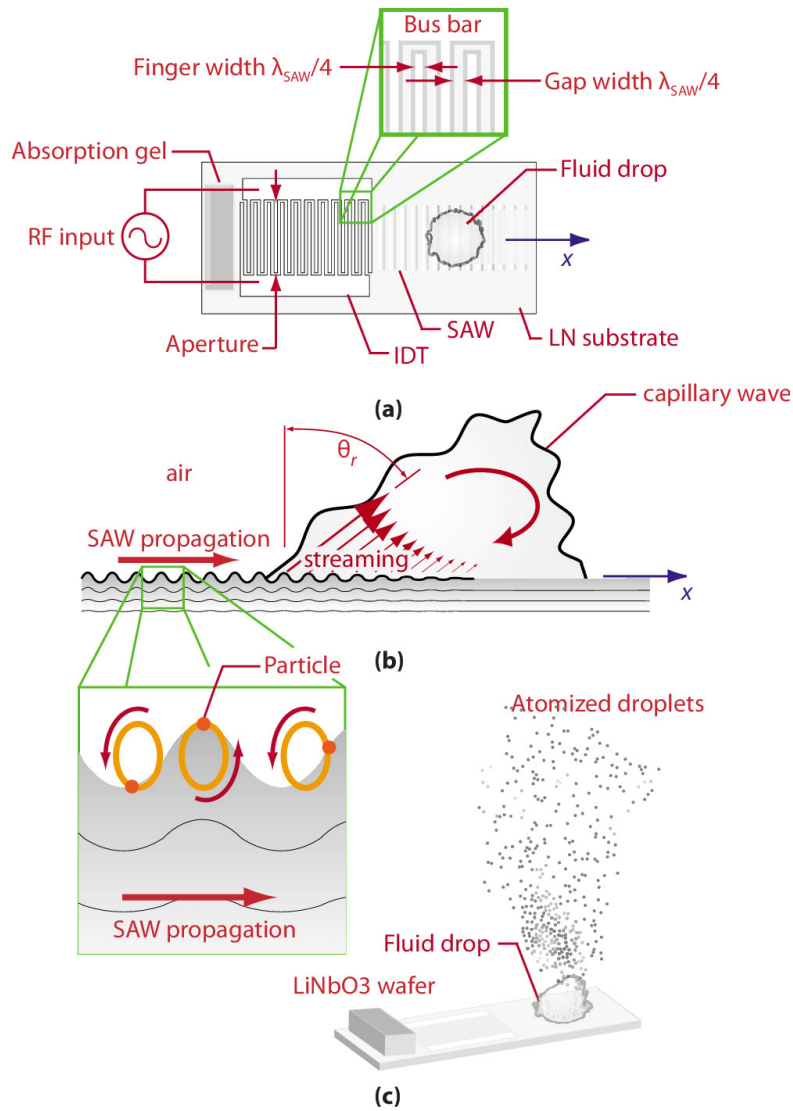


Figure 1.25: SAW propagation along a piezoelectric substrate. (a) Configuration of the SAW device and the IDT electrode deposited on the piezoelectric substrate to generate the SAW. (b) Interaction of the SAW with a fluid causes drop deformation through acoustic streaming. The SAW amplitude is reduced by the interaction with the drop due to viscous dissipation. (c) Schematic representation of atomization occurring from the free surface of the drop. Adapted with permission from [147].

2 Materials & Methods

In this chapter, I present the experimental methods used in the projects. I elaborate on the fabrication of SAW and microfluidic PDMS devices, the production of emulsions and characterization tools.

Contents

| | | |
|-------|--|----|
| 2.1 | SAW Atomization | 40 |
| 2.1.1 | SAW Device Microfabrication | 40 |
| 2.1.2 | Operation of the SAW Device | 41 |
| 2.2 | Microfluidic PDMS Device | 42 |
| 2.2.1 | PDMS Device Fabrication | 42 |
| 2.2.2 | Surface Treatment | 43 |
| 2.3 | Characterization Tools | 43 |
| 2.3.1 | Scanning Electron Microscopy (SEM) | 43 |
| 2.3.2 | X-Ray Diffraction (XRD) | 43 |
| 2.3.3 | Thermogravimetric Analysis (TGA) | 44 |

2.1 SAW Atomization

2.1.1 SAW Device Microfabrication

The surface acoustic wave (SAW) device is composed of a piezoelectric $LiNbO_3$ chip onto which an interdigitating transducer (IDT) pattern is printed. To deliver fluid to the right location, I employ PDMS-based microfluidic channels. The device is fabricated in the clean room facility (Center MicroNanotechnology (CMi)) at EPFL. A clean lithium niobate $LiNbO_3$ wafer with a YX cut at 128° (Roditi) is used as a piezoelectric substrate [150].

The lift-off process is used to form IDT patterns on piezoelectric substrates [149]. First, negative photoresist AZ nlof 2020 (Merck) is deposited onto the wafer through spin coating by automated resist processing (EVG 150) to form a layer with the thickness of $2\ \mu m$. This is followed by a soft-baking step at $110\ ^\circ C$ for 75 seconds. The wafer is then exposed to a laser with 335 nm and a dose of $21.6\ mJ/cm^2$ by a direct laser writer (VPG 200, Heidelberg Instruments). The equipment illuminated the wafer with a write head of 10 mm focal length according to the desired design of IDT. Upon 75 seconds of development, the wafer is washed with AZ 726 MIF

(MicroChemicals) and rinsed with water to strip the regions, resulting in IDT patterns surrounded by unexposed photoresist.

Conductive metal deposition is performed via electron beam evaporation (EVA 760, Alliance-Concept) to complete the IDT patterning. A titanium layer with 5 nm thickness is deposited as an adhesion layer, followed by the deposition of 200 nm of aluminum layer. Finally, the remaining photoresist is removed through incubation of the wafer in Remover 1165 for 12 h and subsequent rinse with isopropanol and DI water. The dried wafers are diced into chips of 2 cm x 3 cm such that each chip has one IDT pattern. This is performed by an automated dicing saw (DAD321, Disco).

To control the amount and location of fluid supplied to the SAW chip, I attach poly-(dimethylsiloxane) (PDMS) (Sylgard 184, Dow Corning) based microfluidic channels that are 40 μm tall and 50 μm wide are produced using soft lithography, as detailed in Section 2.2. To form the outlet, the channel is cut on one side and bonded on a LiNbO_3 chip using an oxygen plasma (PlasmaPrep 2, Gala Instrumente) such that the channel outlet is aligned with the focal point of the SAW to maximize the atomization throughput.

2.1.2 Operation of the SAW Device

To operate the SAW device, the fabricated chip containing the IDT is interconnected via Printed Circuit Board (PCB) to the SAW Generator BSG (Belektronig), which provides AC voltage. The SAW Generator is a specific device designed to produce SAWs. It acts as a network analyzer to determine the SAW resonance frequency of the IDT pattern, and an AC function generator with a radio frequency amplifier to provide AC waves with the determined resonance frequency of the chip to form SAWs. The chips used for the studies presented in the thesis have resonance frequencies around 32.5 MHz and 64.5 MHz. I used 64.5 MHz to produce SAWs and the output power has been set to 4W, which can create atomization. In the meantime, liquid to be atomized is delivered through the microfluidic PDMS inlet at a flow rate of 1.5 mL/hr, controlled by a syringe pump (Cronus Sigma 1000, Labhut).

2.2 Microfluidic PDMS Device

2.2.1 PDMS Device Fabrication

The master wafer that is used to produce PDMS microfluidic devices is fabricated using soft lithography [151] in the clean room facility (Center MicroNanotechnology (CMi)) at EPFL. The negative photoresist SU-8 (Series 3000, Microchem, USA) is spin coated onto a silicon wafer. The wafer coated with photoresist is pre-baked on a hotplate at 95°C. The photomask (OutputCity, USA) with the print of the targetted channel layout constructed by AutoCAD is placed onto the wafer and exposed to UV-light. The transparent parts of the photomask allow the exposure of certain parts that are thereby crosslinked. After exposure to UV light, the wafer is post-baked on a hotplate at 95°C. For double emulsion devices, two additional layers are spin coated onto the wafer. In between each step, the photomask is aligned using a mask aligner (Suss MJB4). Once all layers are completed, unreacted photoresist is dissolved by propylene glycol methyl ether acetate (PGMEA, Sigma-Aldrich). The master wafer is dried and treated with a solution of 2 wt% of trichloro(1H,1H,2H,2H-perfluorooctyl)silane (Sigma-Aldrich, USA) dissolved in HFE-7500 for 2 minutes. This is important to facilitate the PDMS removal from the wafer.

To produce PDMS devices from this master wafer, uncured PDMS and a crosslinker (Sylgard 184 silicone elastomer kit, Dow Corning) are mixed in a 10:1 ratio, and poured onto the wafer. The wafer containing the PDMS and crosslinker was degassed for several minutes and placed in an oven at 70°C overnight. Upon completion of curing, PDMS pieces with the desired microfluidic geometry on their surface were cut and peeled off. Holes are punched to be used as inlets and the outlet using a 1 mm hole puncher. Finally, the PDMS surfaces with the pattern is activated using oxygen plasma (GaLa Instrumente) for 45 s to bond to them either a glass slide or another PDMS piece. In case of flow focusing devices that are used for double emulsion production, PDMS pieces are bonded to each other to be used as 3D-microfluidic device.

2.2.2 Surface Treatment

To form drops in microfluidic devices, channels must be non-wetting to the inner phase. To form w/o single emulsions, the channel walls are made fluorophilic by injecting an HFE-7500-based solution containing 2 wt% of trichloro(1H,1H,2H,2H-perfluorooctyl)silane (Sigma-Aldrich, USA) for 10 min.

To produce double emulsions, the channels that polyvinyl alcohol (PVA) is delivered through are treated to be hydrophilic, while the channels designed to transport HFE-7500 with the surfactants through should be rendered fluorophilic to prevent wetting of the inner phase on the PDMS walls. To achieve this, first, all the channels are activated through filling them with 1M NaOH solution. After 10 minutes of incubation, NaOH is rinsed with DI water and channels are dried with compressed air. To render the main channel downstream the 3D junction hydrophilic, I treat it with an aqueous solution containing 2 wt% polydiallyldimethylammonium chloride (Sigma-Aldrich, USA). Subsequently, I render the middle phase channels fluorophilic, as I treat them with an HFE-based solution containing 2% (v/v) of trichloro(1H,1H,2H,2H-perfluorooctyl)silane (Sigma-Aldrich, USA). The solutions are kept in the channels for 30 min and the channels were dried with compressed air.

2.3 Characterization Tools

2.3.1 Scanning Electron Microscopy (SEM)

To characterize the size and morphology of particles, they are imaged with a scanning electron microscope (Zeiss Merlin field emission SEM) that is operated at an acceleration voltage of 2 kV and 100 pA using an in-lens detector. Particles are collected on a one-side polished silicon wafer. To avoid charging effects, the samples are coated with a 4 nm thick iridium film (Quorum Q 150).

2.3.2 X-Ray Diffraction (XRD)

The structure and the structural stability of spray dried particles are characterized as a function of time using powder X-ray diffraction (pXRD). To maximize the signal-to-noise ratio, the grazing incident configuration is used with an angle of 1°

over 2θ ranging from 10-30°. Particles are collected on a one-side polished single crystal silicon wafer that does not yield any 2θ peak in the region of interest and stored under ambient conditions. They are characterized with an Empyrean X-ray diffractometer (PANalytical) with PIXcel-1D detector using a Cu K α source with a wavelength of 1.5405 Å.

2.3.3 Thermogravimetric Analysis (TGA)

The amount of vanillin contained in particles is quantified using thermogravimetry analysis (TGA 4000 from Perkin Elmer). The sample is heated from 30 to 250 °C at a rate of 1 °C/min before the temperature is maintained for 2 min. To determine the release kinetics of vanillin, I perform isothermal TGA measurements. The samples are heated from 30 to 65 °C at 35°C/min and maintained at this temperature for 300 min. To ensure all vanillin is released and to quantify the amount of capsules contained in the crucible, I subsequently heat the sample from 65° to 250° at 1°C/min.

3 Use of Aerosols as Crystallization Template

In this chapter, I describe the influence of microfluidic spray dryer processing parameters on crystalline succinic acid nanoparticles. I demonstrate that the solute concentration and the solvent type strongly influence the crystal structure and crystal structure stability.

This chapter is adapted from the paper in preparation entitled “Controlling the Crystal Structure of Spray-dried Succinic Acid Particles” authored by Aysu Ceren Okur, Philipp Erni, Lahoussine Ouali, Daniel Benczedi, and Esther Amstad. A. Okur performed all the experiments. A. Okur and E. Amstad analyzed all data and wrote the manuscript.

Contents

| | | |
|---------|--|----|
| 3.1 | Abstract | 46 |
| 3.2 | Introduction | 47 |
| 3.3 | Experimental Section | 48 |
| 3.3.1 | Solution Preparation | 48 |
| 3.3.2 | Particle Formation | 49 |
| 3.3.3 | Characterization | 49 |
| 3.3.3.1 | Scanning Electron Microscopy (SEM) | 49 |
| 3.3.3.2 | X-Ray Diffraction (XRD) | 50 |
| 3.4 | Results & Discussion | 50 |
| 3.4.1 | Spray Drying of Succinic Acid Nanoparticles | 50 |
| 3.4.2 | Influence of Solute Concentration and Solvent on Morphology & Crystal Structure | 50 |
| 3.4.3 | Stability of Crystal Structure During Storage | 56 |
| 3.4.4 | Influence of Additives on Crystal Structure of Succinic Acid | 58 |
| 3.5 | Conclusion | 62 |

3.1 Abstract

Many properties of materials, including their dissolution kinetics, hardness, and optical appearance, depend on their structure. Unfortunately, it is often difficult to control the structure of low molecular weight organic compounds that have a high propensity to crystallize if they are formulated from solutions where they have a high mobility. This limitation can be overcome by formulating these compounds within small airborne drops that rapidly dry, thereby limiting the time molecules have to arrange into the thermodynamically most stable phase. Such drops can be formed with a surface acoustic wave (SAW)-based spray-drier. In this chapter, I demonstrate that the structure of a benign, pharmaceutically relevant low molecular weight compound, succinic acid, can be readily controlled with the time these

molecules have to solidify during the drying of the drop. Succinic acid particles preserve the metastable structure over at least 3 months if the initial succinic acid concentration is below 2% of its saturation concentration. I demonstrate that also the stability of the metastable phases against their transformation into the most stable phase increases with decreasing initial solute concentration of the spray-dried solution. These results open up new opportunities to control the crystal structure and therefore properties of low molecular weight compounds that have a high propensity to crystallize.

3.2 Introduction

Many physicochemical properties of materials, such as their color [152–154], conductivity [155], density [156] and solubility [5, 51] depend on their structure. For example, the dissolution kinetics and hence bioavailability of many poorly soluble drugs increases if formulated as a metastable phase. The structure of materials is often controlled with additives. However, these additives typically increase product cost and reduce the efficiency of active ingredients because they dilute them.

The structure of materials can also be controlled through their processing. For example, active pharmaceutical ingredients (APIs) have been processed into amorphous particles through ball milling [157–159] or freeze drying [160]. However, these techniques are time consuming and hence costly. A cheap, high throughput method that offers some control over the structure of the resulting particles is bulk recrystallization. This technique was used, for example, to formulate carbamazepine (CBZ) as a metastable phase [4]. However, even if formulated as a metastable phase, its dissolution kinetics is slow such that its bioavailability is compromised.

This shortcoming can be addressed by co-crystallizing the active ingredient with more soluble low molecular weight excipients such as succinic acid. Unfortunately, the high propensity of low molecular weight excipients to crystallize risks phase separations and ultimately disproportionation which makes bulk processing time consuming, and costly. A means to overcome this limitation is spray drying [161, 162].

Indeed, many active ingredients including carbamazepine [163, 164], nicotinamide [164, 165] and salbutamol sulfate [166, 167] are co-spray dried with low molecular

weight additives such as succinic acid [163] and some excipients such as lactose [166, 168] and mannitol [169–172]. The structure of these compounds can be tuned with the processing temperature, initial solute concentration, solvent evaporation rate, and solvent quality [27, 103, 173].

The structure of active ingredients is often controlled to tune their dissolution kinetics. By contrast, the structure of the carrier matrix strongly influences the compressibility of the formulation that is directly related to its disintegration kinetics if put into aqueous solutions, a parameter that is of particular importance for tableted drugs. This parameter is frequently tuned through the addition of low molecular weight substances that are co-spray dried with the active ingredients [168, 172]. The structure of these low molecular weight additives depends on their initial concentration, the drying rate of the drops, as well as the inlet temperature. However, systematic studies on the influence of the spray drying conditions on the structure of low molecular weight matrix materials and their storage stability remain to be shown.

In this chapter, I investigate the influence of the spray-drying conditions on the structure of a model low molecular weight matrix material, succinic acid. Succinic acid is a dicarboxylic acid that has three polymorphs. It is a well-suited matrix material for the encapsulation of volatile compounds, and co-crystallization of pharmaceuticals [129, 174]. Here, I demonstrate that the structure of succinic acid and its stability against crystallization during storage under ambient conditions can readily be controlled with the time it has to solidify if formulated through spray-drying. The solidification time can conveniently be tuned with the initial solute concentration and the type of solvent used to formulate the particles. This finding might open up new avenues for the formulation of carrier particles that efficiently retain low molecular weight substances, including volatiles, without the need for costly additives or time-consuming processes.

3.3 Experimental Section

3.3.1 Solution Preparation

All reagents are used as received. Vanillin, maltol, acetone (technical grade), and ethanol (absolute grade) are purchased from Sigma Aldrich, succinic acid from

Merck. I employ deionized water from Direct-Q Merck Millipore 25°C, 0.05 $\mu\text{S}/\text{cm}$. Succinic acid-based particles are formulated from acetone, ethanol or deionized water (DI)-based solutions containing 10 -100 mM succinic acid. To test the influence of active ingredients on the morphology of succinic acid particles, an ethanol-based solution containing various amounts of vanillin and maltol and 100 mM of succinic acid is co-spray dried. To test the influence of active ingredients on the structural stability, ethanol-based solutions containing 100 mM succinic acid and either 20-60 mM vanillin or 60 mM maltol is spray dried.

3.3.2 Particle Formation

Particles are produced through spray-drying using a surface acoustic wave (SAW) based microfluidic device [149]. The SAW-based microfluidic device is composed of a piezoelectric LiNbO_3 wafer (Roditi) onto which an interdigitating transducer (IDT) pattern is printed. Unidirectional IDT with a focused eccentricity of 30° is patterned on a LiNbO_3 wafer by vapor depositing a 5 nm thick titanium and 200 nm thick aluminum layer. The produced wafer is diced into $2 \times 3 \text{ cm}^2$ pieces [149]. The chip is connected to a Power SAW Generator that is operated at 3.3 W (Belektronig GmbH) via a printed circuit board (PCB). To guide the solution to the appropriate location on the SAW, I employ a microfluidic channel composed of PDMS that is bonded onto the piezoelectric wafer using oxygen plasma (GaLa Instrumente). The solution is injected into the device at a flow rate of 1.5 mL/h using a syringe pump (Cronus Sigma 1000, Labhut). The particles are dried in a stream of co-flowing room temperature air that is introduced into the drying unit at 4 bar before they are collected on a one-side polished silicon wafer that is placed close to the top end of the drying tube [149].

3.3.3 Characterization

3.3.3.1 Scanning Electron Microscopy (SEM)

Samples are imaged with a scanning electron microscope (Zeiss Merlin field emission SEM) that is operated at an acceleration voltage of 2 kV and 100 pA using an in-lens detector. To avoid charging effects, the samples are coated with 4 nm thick iridium film (Quorum Q 150).

3.3.3.2 X-Ray Diffraction (XRD)

The structural stability of spray dried particles is characterized as a function of time using powder X-ray diffraction (pXRD). Particles are collected on a one-side polished single crystal silicon wafer that does not yield any 2θ peak in the region of interest (10-30 degree) and stored under ambient conditions. They are characterized with an Empyrean X-ray diffractometer (PANalytical) with PIXcel-1D detector using a Cu K α source with a wavelength of 1.5405 Å.

3.4 Results & Discussion

3.4.1 Spray Drying of Succinic Acid Nanoparticles

To control the formation time of particles, they are formulated with a surface acoustic wave (SAW)-based spray-drier. The SAW device produces airborne drops with diameters between 1 and 10 μm that dry within a few hundred ms [96], if operated at a frequency of 64.5 MHz [149]. These drops are guided into a drying unit within which room temperature air co-flows with the drops before the dry particles are collected on a silicon wafer that is placed close to the top end of the drying tube within few seconds [149].

The time needed for low molecular weight solutes to diffuse the length of the initial radius of the drop is similar to the time needed to dry it. Hence, I approximate the solute concentration within the drop to be constant such that I expect to obtain solid spray-dried particles. Under these conditions, solutes start to solidify when their overall concentration exceeds their saturation concentration and their formation is arrested when the drop is dried [175].

3.4.2 Influence of Solute Concentration and Solvent on Morphology & Crystal Structure

The time when the saturation concentration is reached within the drying drop depends on the solubility of the solute and its initial concentration. To test the influence of the formation time on the structure of low molecular weight organic matrix materials, I employ succinic acid as a model substance. Succinic acid has

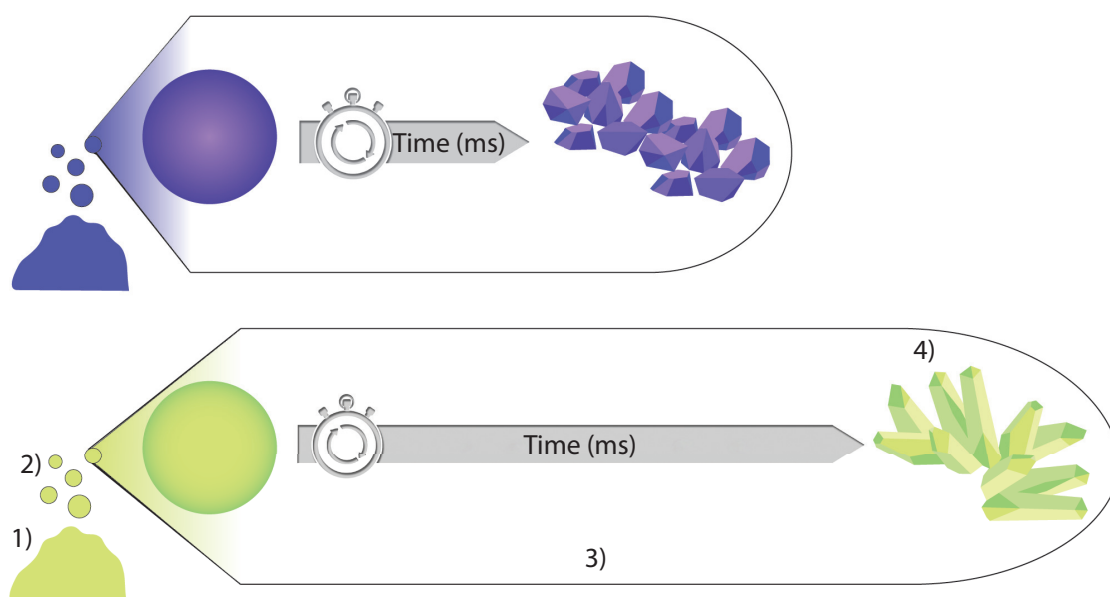


Figure 3.1: Schematic illustration of succinic acid particles spray dried from solvents with different vapor pressures that result in particles displaying different crystal structures. Solvent delivered onto the SAW device is broken into (1) aerosols (2) that are guided into the drying unit (3) where solutes start to solidify to form spray-dried particles that are deposited on a substrate (4).

three polymorphs, the metastable α and γ and the stable β polymorph [104, 176].

I dissolve succinic acid in ethanol and vary its initial concentration from 10 mM to 100 mM, corresponding to 2-20% of its saturation concentration. This solution is injected into a poly(dimethyl siloxane) (PDMS)-based channel that guides it onto a SAW-based spray-drier at a rate of 1.5 mL/h. The SAW device breaks the solution into airborne drops that dry within a few hundred ms.

The resulting spray dried particles are rather spherical, independent of the initial solute concentration, as shown in the scanning electron micrograph in Figure 3.2A and Figure 3.2B. Because each drop forms exactly one particle, the size of these particles scales with the initial solute concentration: Particles produced from solutions containing 10 mM succinic acid have an average diameter of 150 nm whereas those produced from solutions containing 100 mM succinic acid have an average diameter of 250 nm. The good correlation between the initial solute concentration and the size of spray-dried particles confirms that these particles are solid.

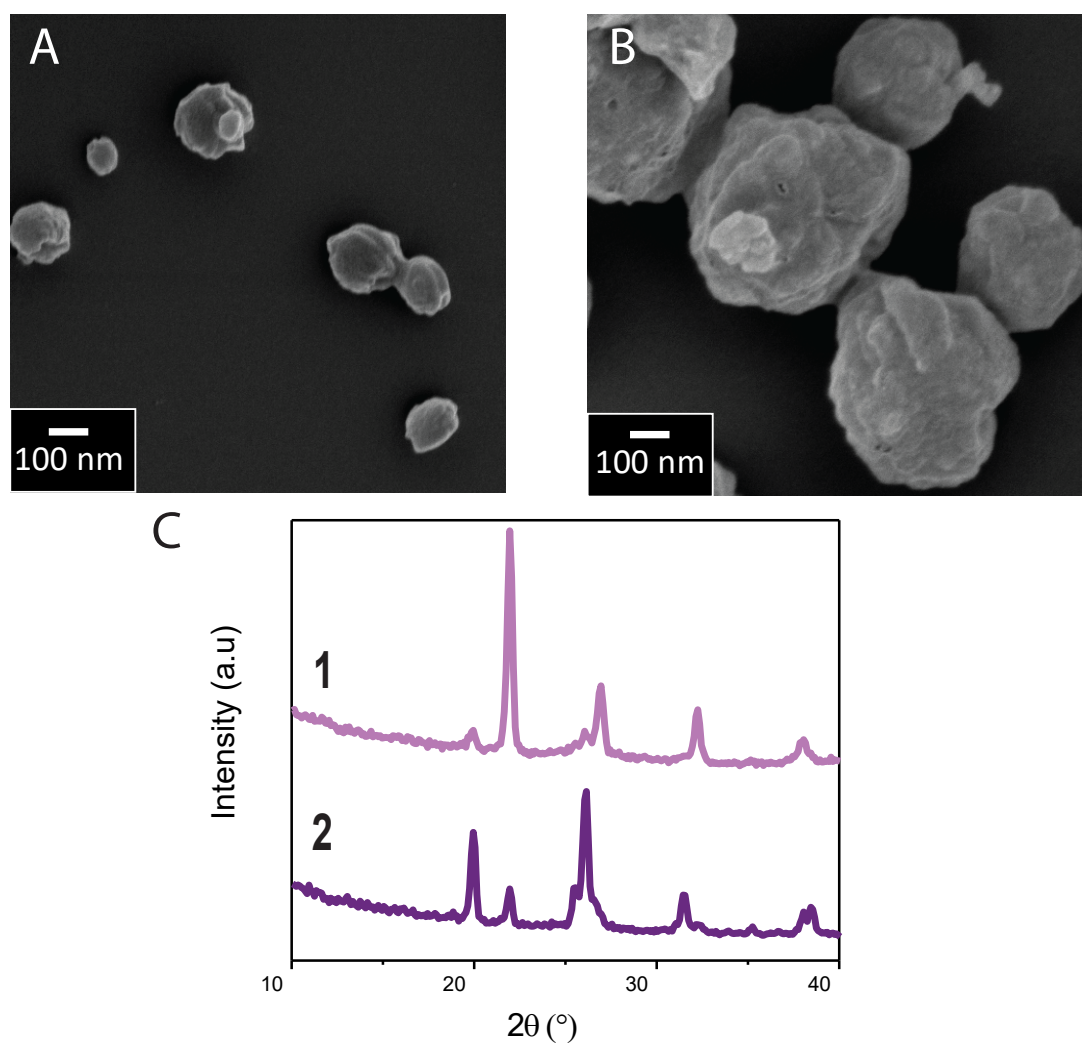


Figure 3.2: Structure and morphology of succinic acid particles. SEM image of succinic acid particles produced from ethanol-based solutions initially containing (A) 10 mM and (B) 100 mM succinic acid. (C) Crystal structure of spray-dried particles produced from solutions initially containing (1) 10 mM and (2) 100 mM succinic acid.

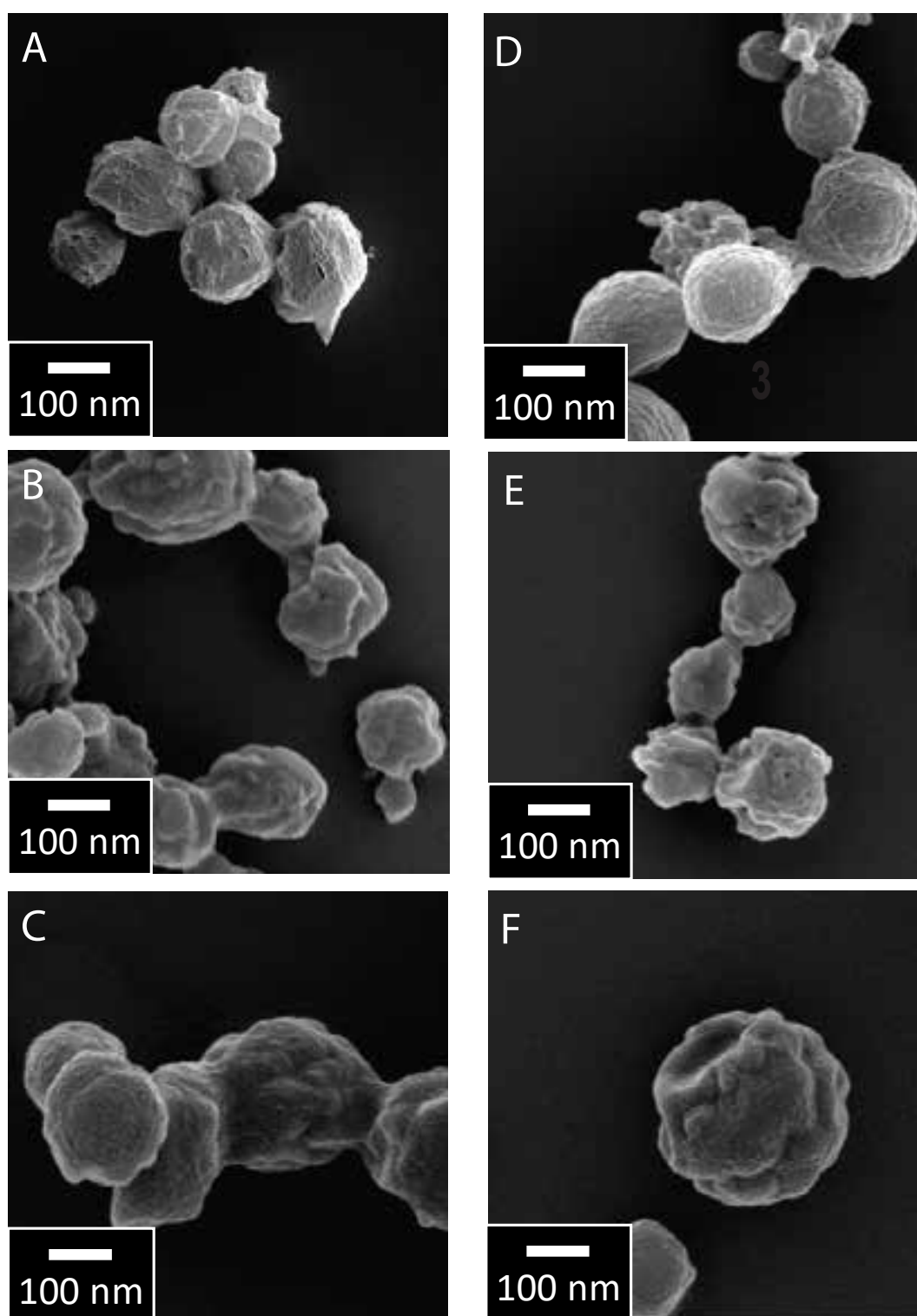


Figure 3.3: (A-C and D-F) Morphology of spray-dried succinic acid particles produced from (A, D) DI water, (B, E) ethanol, and (C, F) acetone. The initial succinic acid concentration is (A-C) 10 mM and (E-G) 100 mM.

To test the influence of the initial solute concentration on the structure of the resulting particles, I perform XRD analysis. Particles produced from 10 mM succinic acid containing solutions predominantly display the metastable α phase, as demonstrated by the diffraction peak at $2\theta = 22^\circ$. By contrast, particles formulated from 100 mM succinic acid containing solutions display predominantly the stable β phase, as shown by the diffraction peak at $2\theta = 20^\circ$ in Figure 3.2C [176]. If the crystals are precipitated from 10 mM succinic acid containing solutions under ambient conditions instead of spray drying, they mainly form β phase as shown in Figure 3.4. These results indicate that the structure of spray-dried succinic acid particles depends on their formation time which can be tuned with the initial solute concentration.

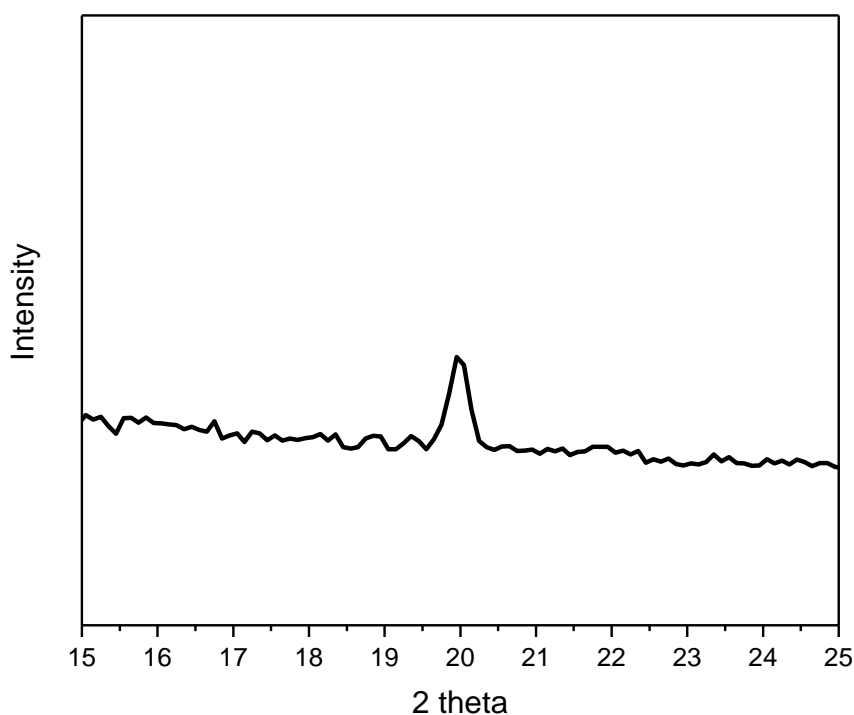


Figure 3.4: XRD of crystals that is precipitated under ambient conditions from ethanol solution containing 10 mM succinic acid.

Our results suggest that the structure of succinic acid particles depends on their formation time. This parameter is closely related to the drying time of the drops that is directly linked to the vapor pressure of the solvent they are made of. To

test if the structure of spray-dried succinic acid particles indeed depends on the drying time of the drops, I formulate them from solvents that have different vapor pressures, namely deionized water, ethanol and acetone. All spray-dried particles are spherical, as shown in Figure 3.3.

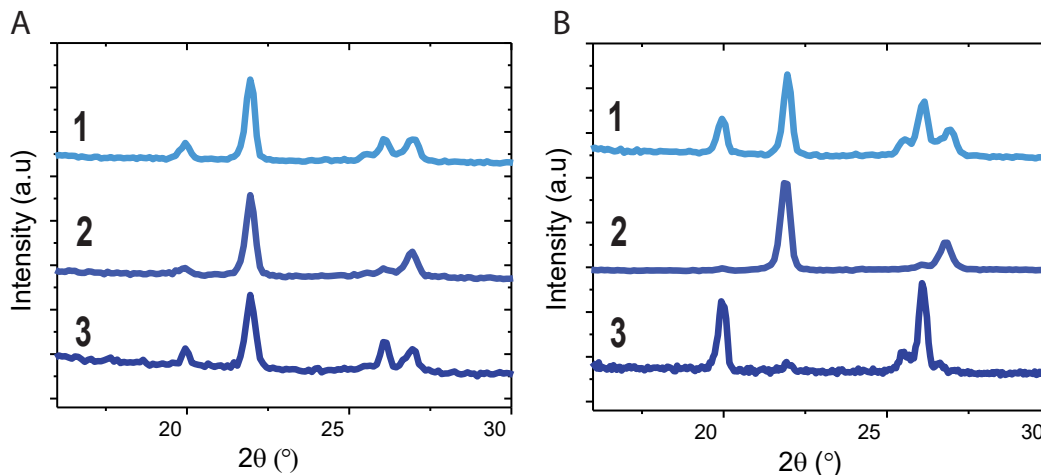


Figure 3.5: XRD traces of succinic acid particles spray-dried from (1) acetone, (2) ethanol and (3) DI water with initial succinic acid concentrations of (A) 10 mM and (B) 100 mM

Particles produced from solutions initially containing 10 mM succinic acid are predominantly metastable, independent of the solvent used, as shown in Figure 3.5A. The initial succinic acid concentration corresponds to 1.5 – 4% of its saturation concentration. If formulated from such diluted solutions, succinic acid has very little time to solidify during the final stages of the drop drying such that the formation of the stable β phase is kinetically prevented even if solvents with high vapor pressures are used. If I increase the initial solute concentration to 100 mM, particles are still predominantly metastable if formulated from ethanol-based solutions.

The initial succinic acid concentration in ethanol corresponds to 20% of its saturation concentration such that the time it can solidify within the drying drops is still very limited. By contrast, if formulated from acetone-based solutions, where the initial succinic acid concentration corresponds to 40% of its saturation concentration, a significant fraction of the particles displays the stable β phase. The fraction of stable particles is even higher if formulated from aqueous solutions, where the initial concentration corresponds to 15% of its saturation concentration, as shown in Figure 3.5B3. I assign this difference in structure to the different

drying rates of the solvents: water has a lower vapor pressure of 3.16 kPa at room temperature [177], compared to ethanol, whose vapor pressure is 7.87 kPa [178], such that aqueous drops dry much slower. The slower drying leaves more time for succinic acid molecules to arrange into the stable phase, such that the fraction of stable particles is much larger than if formulated from ethanol-based solutions even if particles start precipitating later during the drop drying process. It is important to note that, if particles are produced from acetone-based solutions with 100 mM succinic acid, a mixture of metastable and stable phase is observed, as shown in Figure 3.5B1. This is attributed to increased supersaturation of succinic acid due to significantly decreased solubility of succinic acid in acetone. In this case, the effect of increase in vapor pressure and increase in supersaturation on crystallization time counterbalances each other.

3.4.3 Stability of Crystal Structure During Storage

Metastable structures typically tend to transform into the stable phase over time. The rate at which this phase transformation occurs depends on the mobility of the molecules within the metastable phase. In addition, it depends on the density and size of nuclei possessing the stable phase that might be present within the metastable matrix but are invisible with XRD because their size or density is below its detection limit.

I expect the density of nuclei possessing the stable phase to increase with increasing time the molecules have to solidify and hence, with increasing initial solute concentration. To test this expectation, I compare the stability of succinic acid particles spray-dried from ethanol-based solutions initially containing 10 and 100 mM succinic acid. Indeed, particles produced from solutions initially containing 10 mM succinic acid preserve their metastable structure for more than three months if stored at 25°C and 40% humidity. By contrast, if sprayed from solutions initially containing 100 mM succinic acid, the majority of particles transforms from the metastable to the stable phase within 20 h if stored under identical conditions, as shown in Figure 3.6B. These results indicate that metastable particles, that have been formulated from concentrated solutions, encompass nuclei possessing the stable phase that are not detectable with XRD if analyzed within a few hours after production.

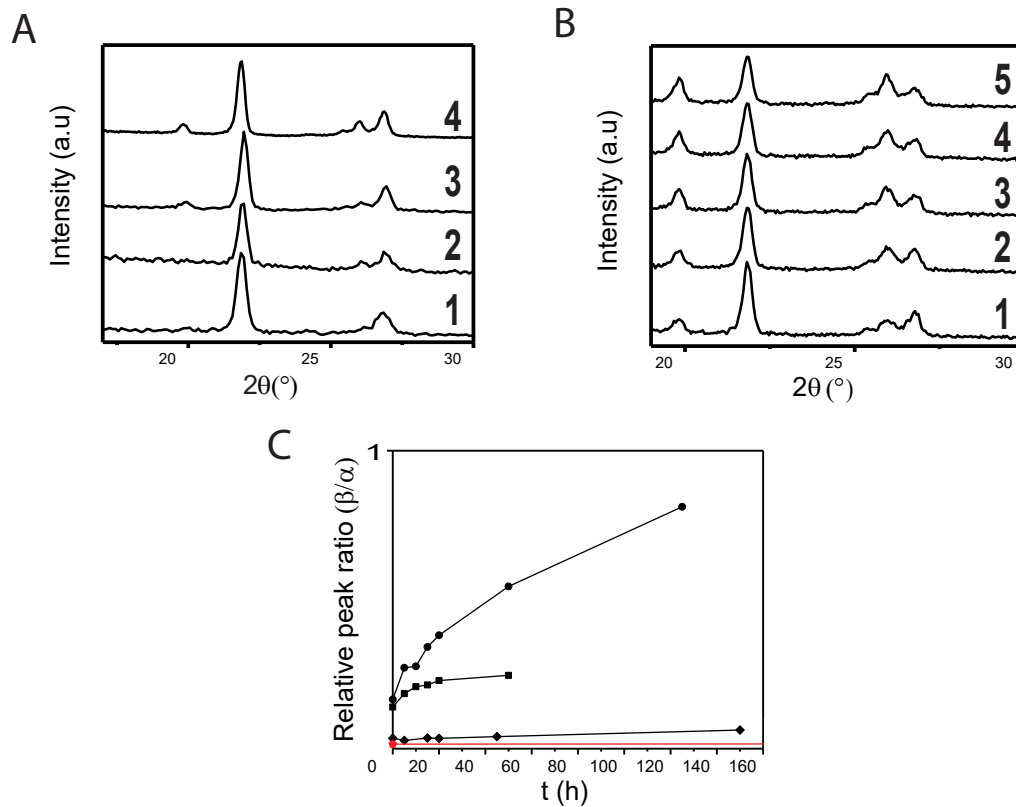


Figure 3.6: Influence of initial solute concentration on structural stability of spray-dried particles. XRD traces of particles spray-dried from solutions initially containing (A) 10 mM and (B) 100 mM succinic acid. Particles produced from 10 mM succinic acid containing solutions have been characterized at (1) $t=0$ (2) $t=2$ weeks (3) $t=1$ month (4) $t=3$ months. Those produced from solutions initially containing 100 mM succinic acid have been characterized after (1) $t=0$, (2) $t=5$ h, (3) $t=10$ h, (4) $t=15$ h and (5) $t=20$ h. (C) Overview of the evolution of the structure of particles produced from ethanol-based solutions initially containing (●) = 100 mM, (■) = 75 mM, (◆) = 50 mM and (●) = 10 mM succinic acid if stored at ambient conditions.

To quantify the influence of the initial solute concentration on the structural stability, I monitor the ratio of the intensities of the diffraction peaks at $2\theta=20^{\circ}$: $2\theta=22^{\circ}$, corresponding to the stable and metastable phase, respectively. Indeed, the rate of phase transformation increases with increasing initial solute concentration, as shown in Figure 3.6C. These results suggest that with increasing initial saturation concentration, the density of nuclei possessing the stable β phase, present within the predominantly metastable matrix, increases. These nuclei grow over time at

the expense of the metastable phase, until the vast majority of the particles possess the stable β phase.

3.4.4 Influence of Additives on Crystal Structure of Succinic Acid

A key advantage of the spray-drying process is the ability to load matrix materials with well-defined amounts of active ingredients because each drop forms exactly one particle such that the particle composition corresponds to that of the solute concentration [96, 149, 179].

The structure of spray-dried particles often depends on additives present during their formulation [180]. To check if active ingredients also influence the structure of spray-dried succinic acid, I employ vanillin, a volatile low molecular weight compound, as a model encapsulant. If spray-dried from an ethanol-based solution containing 60 mM vanillin and 100 mM succinic acid, I obtain highly irregular particles. Particles made from ethanol-based solutions initially containing 100 mM succinic acid display needle-like structures if stored under ambient conditions for 24 hours.

Noteworthy, particles encompassing vanillin have a higher density of needles than those without vanillin, as shown in Figure 3.7B, suggesting that vanillin acts as a heterogeneous nucleation site. In this case, the needle-like structures must be based on succinic acid. Indeed, if succinic acid is slowly dried at room temperature, I obtain the β phase that exhibits needle-like structures, as shown in Figure 3.8. These results suggest that vanillin acts as heterogeneous nucleation sites for succinic acid crystals. By contrast, spray-dried pure vanillin particles are spherical, as shown in Figure 3.9. These results indicate that by controlling the time of the solidification of succinic acid, for example by tuning the spray-drying conditions, I can control the crystal structure and particle morphology.

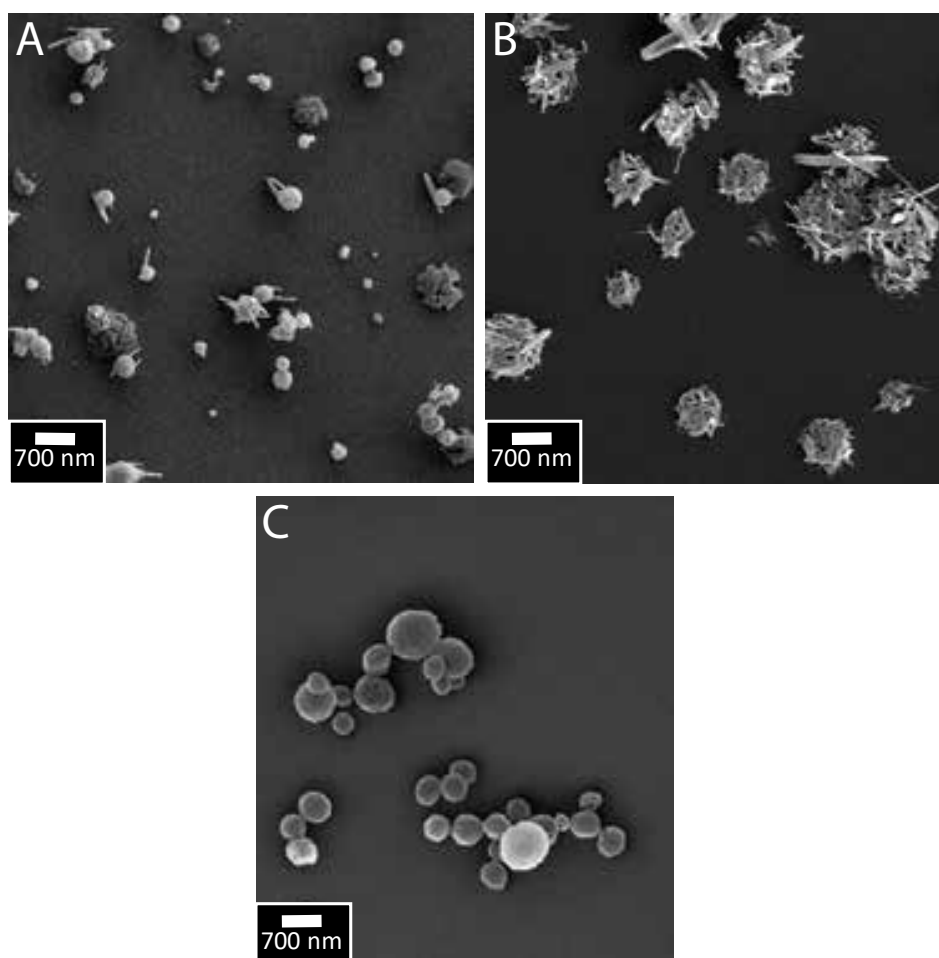


Figure 3.7: SEM image of succinic acid particles spray dried (A) in the absence of vanillin, with 60 mM (B) vanillin and (C) maltol.

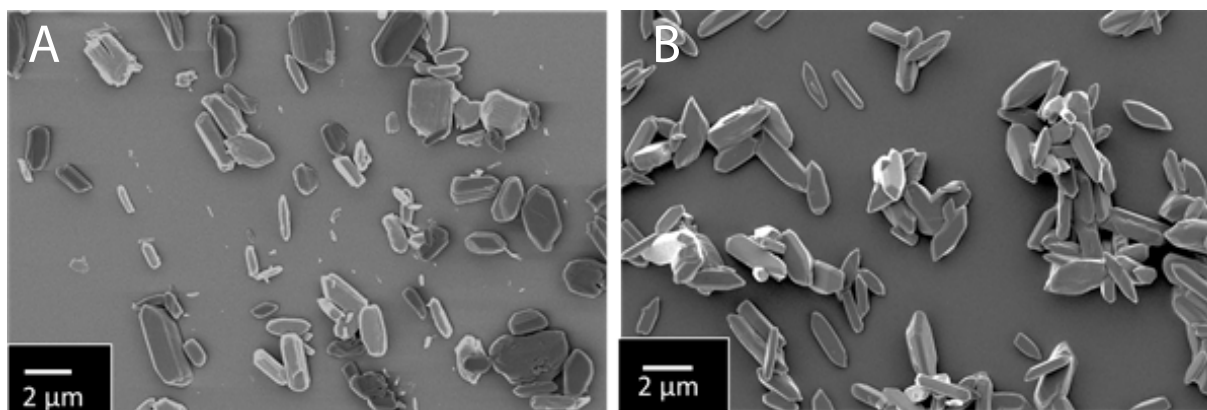


Figure 3.8: SEM images of particles with vanillin after storage at A) 65°C for 10 h and B) ambient conditions for 48h. Particles are produced from ethanol-based solutions containing 80 mM succinic acid and 40 mM vanillin.

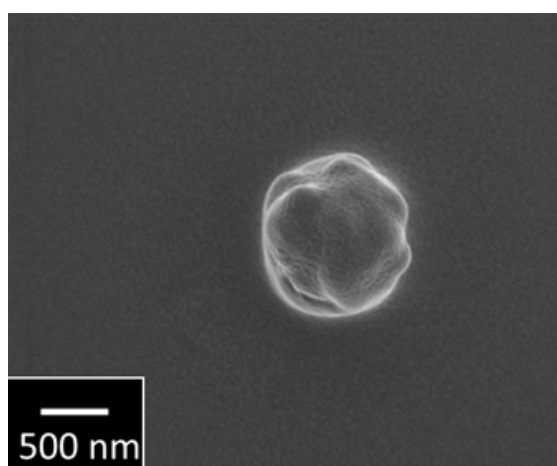


Figure 3.9: SEM image of vanillin nanoparticle sprayed from an ethanol-based solution containing 20 mM vanillin.

The heterogeneous morphology of succinic acid-based particles that have been co-spray dried with vanillin suggests that these two compounds phase separate while the drops dry. I expect this phase separation to only occur if the vanillin to succinic acid concentration exceeds a threshold value. To test this expectation, I vary the initial vanillin concentration from 10 mM to 60 mM, corresponding to a saturation concentration of 3 to 20% while keeping the initial succinic acid concentration constant at 100 mM, corresponding to a supersaturation concentration of 20%. To monitor the phase separation, I perform XRD analysis on the spray-dried samples. I observe a diffraction peak at $2\theta=13^\circ$, characteristic for vanillin, if the initial vanillin concentration exceeds 15 mM, suggesting that macroscopic phase separations start to occur at this concentration. Note that the rate of phase transformation of the metastable α into the stable β phase increases with increasing amount of vanillin present in these particles, as shown in Figure 3.10B. These results confirm that vanillin acts as heterogeneous nucleation sites, thereby promoting the formation of succinic acid nuclei possessing the stable phase.

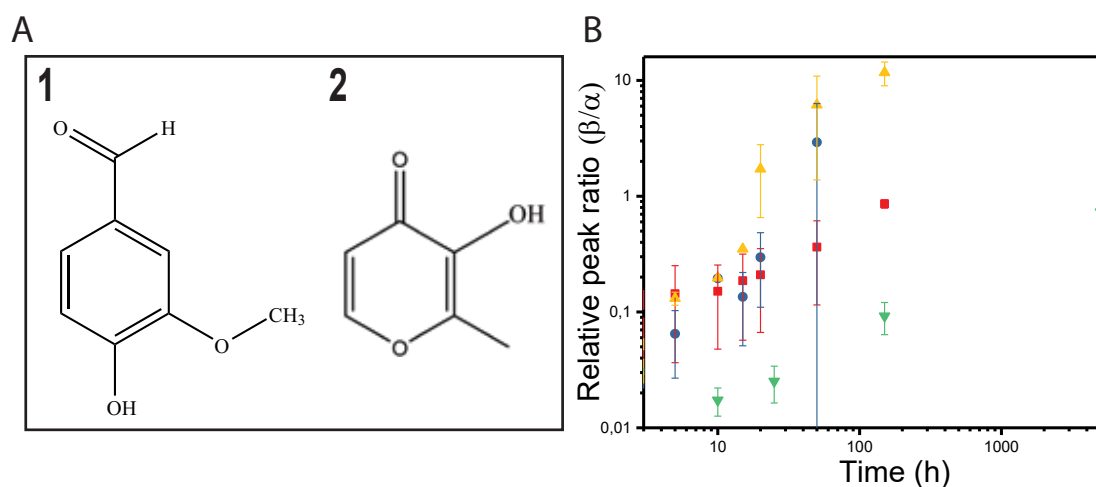


Figure 3.10: A) Molecular structures of 1) vanillin 2) maltol. (B) Evolution of the crystal structure of vanillin loaded succinic acid particles initially containing 100 mM succinic acid and (\blacktriangle) 60 mM, (\bullet) 20 mM, (\blacksquare) 0 mM of vanillin and (\blacktriangledown) 60 mM of maltol.

Phase separations are typically system specific such that they must be assessed case-by-case. However, to demonstrate that SAW-based spray-drying is a suitable technique to formulate volatile-loaded succinic acid, I co-spray dry succinic acid

with another volatile, maltol. Remarkably, by contrast to vanillin, maltol increases the stability of the metastable α phase of succinic acid such that it remains in this form for at least one week if produced from ethanol-based solutions initially containing 60 mM maltol and 100 mM succinic acid, as shown in Figure 3.10B. These results indicate that SAW-based spray-drying enables the formulation of succinic acid-based particles that can efficiently be loaded with different types of volatiles.

3.5 Conclusion

I demonstrate that the structure and the structural stability during storage of a model low molecular weight organic matrix material, succinic acid, strongly depends on its processing conditions. SAW-based spray-drying enables the formulation of succinic acid into the metastable α phase without the need for any crystallization inhibiting additives. This is achieved by minimizing the time during which succinic acid can solidify within the drying drops. These findings open up new possibilities to tune the dissolution kinetics of matrix materials composed of low molecular weight organic compounds that efficiently retain volatile substances and thereby their release kinetics by adjusting spray-drying conditions.

4 Implementation of Crystallization Control: Vanillin Encapsulation in Crystalline Particles

In this chapter, I evaluate the influence of the microfluidic spray dry processing parameters on retention of volatile vanillin within crystalline succinic acid nanoparticles. I demonstrate that vanillin can controllably be retained within crystalline succinic acid particles with a high loading efficiency and I can control the release kinetics by controlling the initial solute concentration.

This chapter is adapted from the paper entitled “Succinic acid-based particles as carriers of volatile substances” accepted in *ACS Sustainable Chemistry & Engineering* and authored by Aysu Ceren Okur, Philipp Erni, Lahoussine Ouali, Daniel Benczedi, and Esther Amstad. A. Okur performed all the experiments. A. Okur and E. Amstad analyzed all data and wrote the manuscript.

Contents

| | | |
|---------|--|----|
| 4.1 | Abstract | 64 |
| 4.2 | Introduction | 65 |
| 4.3 | Experimental Section | 67 |
| 4.3.1 | Solution Preparation | 67 |
| 4.3.2 | Particle Formation | 67 |
| 4.3.3 | Characterization | 67 |
| 4.3.3.1 | Scanning Electron Microscopy (SEM) | 67 |
| 4.3.3.2 | X-Ray Diffraction (XRD) | 69 |
| 4.3.3.3 | Thermogravimetric Analysis (TGA) | 69 |
| 4.4 | Results & Discussion | 69 |
| 4.4.1 | Influence of Solute Concentration on Size & Morphology | 69 |
| 4.4.2 | Influence of Solute Concentration on Phase Separation | 72 |
| 4.4.3 | Vanillin Retention in Crystalline Particles | 75 |
| 4.4.3.1 | Vanillin Loading in Succinic Acid and Tartaric Acid Particles | 75 |
| 4.4.3.2 | Release Kinetics | 78 |
| 4.5 | Conclusion | 80 |

4.1 Abstract

Volatile substances are in high demand especially in cosmetic and pharmaceutical applications. To prolong their shelf-life and prevent their degradation if exposed to air, they are often encapsulated. Most frequently, matrix materials are composed of high molecular weight polymers because some of them can efficiently retain volatiles and meet the safety requirements these applications impose. However, these substances must be processed at high concentrations, resulting in viscous solutions that are difficult to spray or emulsify. To address this shortcoming, I employ a

low molecular weight substance, succinic acid, as matrix material to encapsulate a model volatile, vanillin. To facilitate the encapsulation of low molecular weight substances, such as volatiles, I produce these particles through surface acoustic wave (SAW) based microfluidic spray drying. This technique forms drops with diameters as small as 1-10 μm that dry within a few hundred ms. Thereby, I can kinetically arrest or even suppress phase separations. I demonstrate that vanillin is most efficiently encapsulated and retained over a longer time if succinic acid is formulated from solutions initially containing succinic acid concentrations exceeding 10% of its saturation concentration. If appropriately formulated, these succinic acid-based particles retain volatiles longer than the much more commonly employed high molecular weight dextrin. These results open up a new avenue to encapsulate volatiles in low molecular weight compounds that pack more densely than high molecular weight counterparts and therefore can retain volatiles for a prolonged time.

4.2 Introduction

Fragrances are volatile substances that are used as active ingredients in many food commodities [10, 181], detergents [12, 13], and some textiles [14–16]. The volatility of fragrances makes it difficult to preserve them during storage, thereby limiting the shelf life of products that contain them. To mitigate this limitation, fragrances are often encapsulated within polymeric matrices such as the nature-derived polymer gum acacia [17–19]. However, the cost of this material limits its use to selected high value products. Cheaper more commonly used alternatives include dextrin derivatives such as maltodextrin and cyclodextrin.[20] Maltodextrin is especially attractive because it possesses a neutral taste, has good barrier properties towards many volatiles, and if dissolved at high concentrations in aqueous solutions only moderately increases their viscosity to values between 40 and 100 mPa.s [21]. This low viscosity facilitates the processing of the solutions into drops that serve as templates for particles.

Solutions can be broken into airborne drops through electro-spraying yet, at a limited throughput and under high electric fields. Hence, electro spraying is limited to the formulation of substances that are insensitive to high electric fields and only needed in small quantities [182, 183]. Solutions can also be processed into airborne drops through spray-drying, which is a high throughput, cost-effective

Chapter 4. Implementation of Crystallization Control: Vanillin Encapsulation in Crystalline Particles

process that is often used in industry [22, 23]. However, the release profile of the encapsulated volatiles is difficult to control because it strongly depends on the dimensions of the capsules, a parameter that cannot readily be tuned if produced through conventional spray-drying. Moreover, the permeability of the resulting capsules depends on the molecular weight of the polymer which for nature derived polymers varies from batch to batch.

The properties of capsules can be more closely controlled if they are made from synthetic polymers. For example, volatiles can be loaded into microparticles [33, 34] made of poly(lactic-co-glycolic acid) (PLGA), and capsules [35–37, 184] made of polycaprolactone (PCL), polyurethane and polybutylcyanoacrylate (PBCA) [38]. However, these systems generally use harmful solvents and volatiles tend to diffuse through these amorphous matrices, again limiting the shelf life of these materials. The permeability of capsules towards volatiles typically decreases with increasing density of the matrix material. However, if capsules are made of inorganic nanoparticles such as SiO_2 , $CaCO_3$ or phosphate particles, that are much denser than polymers, volatiles diffuse through the pores that form between adjacent particles, again compromising their shelf life [40–42, 185], even if they interact more strongly with inorganic particles than they typically do with polymers [43, 44]. To reduce the porosity of particle-based capsules, they can be strengthened with polymers such as cyclodextrins [186] and derivatives thereof [121], that act as fillers. However, depending on the processing conditions these fillers partially crystallize into phases which have different barrier properties thereby preventing a good control over the permeability of these capsules [121, 187].

The addition of polymers increases the viscosity of the dispersion, thereby compromising its processability. Processing of reagent-containing solutions is facilitated if low molecular weight compounds that only moderately increase the solution viscosity are employed. For example, erythritol was spray chilled to form limonene-containing microparticles, demonstrating the potential of low molecular weight substances to act as matrix material for the encapsulation of volatiles [45]. However, this process involves elevated temperatures that limit the encapsulation efficiency, which is the percentage of encapsulants contained within spray-dried particles with respect to those added to the feed solution, because a significant fraction of the volatiles evaporates during processing. In addition, the influence of the processing parameters on the matrix material and its permeability remains unknown. Capsules composed of benign materials compatible with cosmetic and food applications

that are easy to be processed and possess a low permeability towards volatile encapsulants remain to be established.

In this chapter, I demonstrate that a model low molecular weight organic compound that has a high propensity to crystallize, succinic acid, can efficiently retain volatiles if appropriately formulated. To control the structure and morphology of succinic acid-based particles, I formulate them with a surface acoustic wave (SAW)-based microfluidic spray dryer that forms small drops with diameters of order 1 μm . These drops rapidly dry even at room temperature, thereby offering an encapsulation efficiency that can reach up to 95%. I demonstrate that the amount of fragrances contained in the resulting particles and their release kinetics strongly depend on the initial solute concentration, a parameter that can conveniently be tuned. These findings open up new possibilities to tune the release kinetics of low molecular weight substances not only through the choice of the matrix material but also through their processing.

4.3 Experimental Section

4.3.1 Solution Preparation

All reagents are used as received. Vanillin, acetone (technical grade), and ethanol (absolute grade) are purchased from Sigma Aldrich, succinic acid from Merck.

4.3.2 Particle Formation

Particles are produced with microfluidic spray dryer as detailed in Section 3.3.2.

4.3.3 Characterization

4.3.3.1 Scanning Electron Microscopy (SEM)

To characterize the size and morphology of particles, they are collected on a one-side polished silicon wafer. To prevent charging effects during the imaging, samples are coated with a 4 nm thick iridium film (Quorum Q 150). Samples are imaged with the scanning electron microscope (Zeiss Merlin field emission SEM) that is

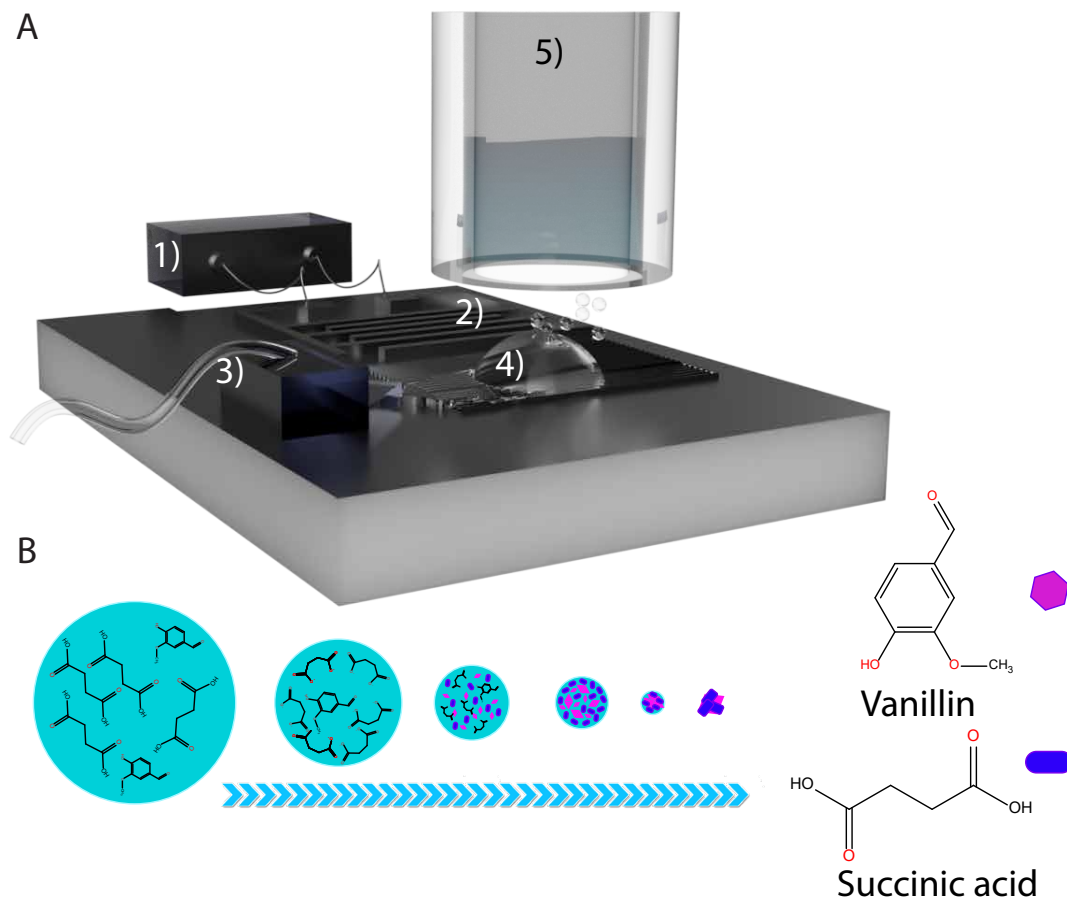


Figure 4.1: (A) Schematic illustration of the microfluidic spray-dryer composed of (1) a SAW generator connected to (2) an IDT pattern on a piezoelectric chip onto which liquid is delivered through a PDMS-based channel (3) before it is atomized into airborne drops that (4) dry within a dedicated drying unit (5). (B) Schematic illustration of the formation of succinic acid particles that are loaded with vanillin within drying drops. The solidification time of reagents contained in the drop is dictated by its drying rate.

operated at an acceleration voltage of 2 kV and 100 pA using an in-lens detector.

4.3.3.2 X-Ray Diffraction (XRD)

XRD analysis is performed on an Empyrean X-ray diffractometer (PANalytical) with a PIXcel-1D detector using a Cu K α source with a wavelength of 1.5405 Å. The measurement is performed with a 1° grazing incident angle configuration over 2θ between 10-30° with a scanning rate of 0.1 degree/sec.

4.3.3.3 Thermogravimetric Analysis (TGA)

The amount of vanillin contained in particles is quantified using thermogravimetry analysis (TGA 4000 from Perkin Elmer). The sample is heated from 30 to 250 °C at a rate of 1 °C/min before it is maintained at this temperature for 2 min. To determine the release kinetics of vanillin, I perform isothermal TGA measurements. The sample is heated from 30 to 65 °C at 35°C/ min and maintained at this temperature for 300 min. To ensure all vanillin is released and to quantify the amount of capsules contained in the crucible, I subsequently heat the sample from 65° to 250° at 1°C/ min.

4.4 Results & Discussion

4.4.1 Influence of Solute Concentration on Size & Morphology

An efficient loading and predictable release of fragrances requires a good control over the particle composition. This parameter can readily be adjusted if particles are produced with the SAW-based spray-dryer because each drop forms exactly one particle. Therefore, the overall composition of spray-dried particles corresponds to that of the solutes contained in the initial drop [149]. I leverage this feature to produce succinic acid-based particles that are loaded with a model volatile substance, vanillin, by spray-drying an ethanol-based solution containing succinic acid and vanillin.

The solute-containing ethanol solution is broken into small drops using SAWs that are excited at a frequency of 64.5 MHz. Ethanol-based drops produced under these conditions have diameters between 1-10 μm , as is shown in Figure 4.2D, well in agreement with previous reports [149]. These drops are dried by co-flowing air. The

Chapter 4. Implementation of Crystallization Control: Vanillin Encapsulation in Crystalline Particles

speed of the drops within the drying unit is close to that of the co-flowing air, such that the surrounding air does not significantly accelerate the solvent evaporation. I hence neglect evaporative cooling effects. Under these conditions, ethanol drops with diameters between 1-10 μm dry within a few hundred ms and deposit within 2 seconds on the collecting substrate as has previously been shown [96, 149, 179].

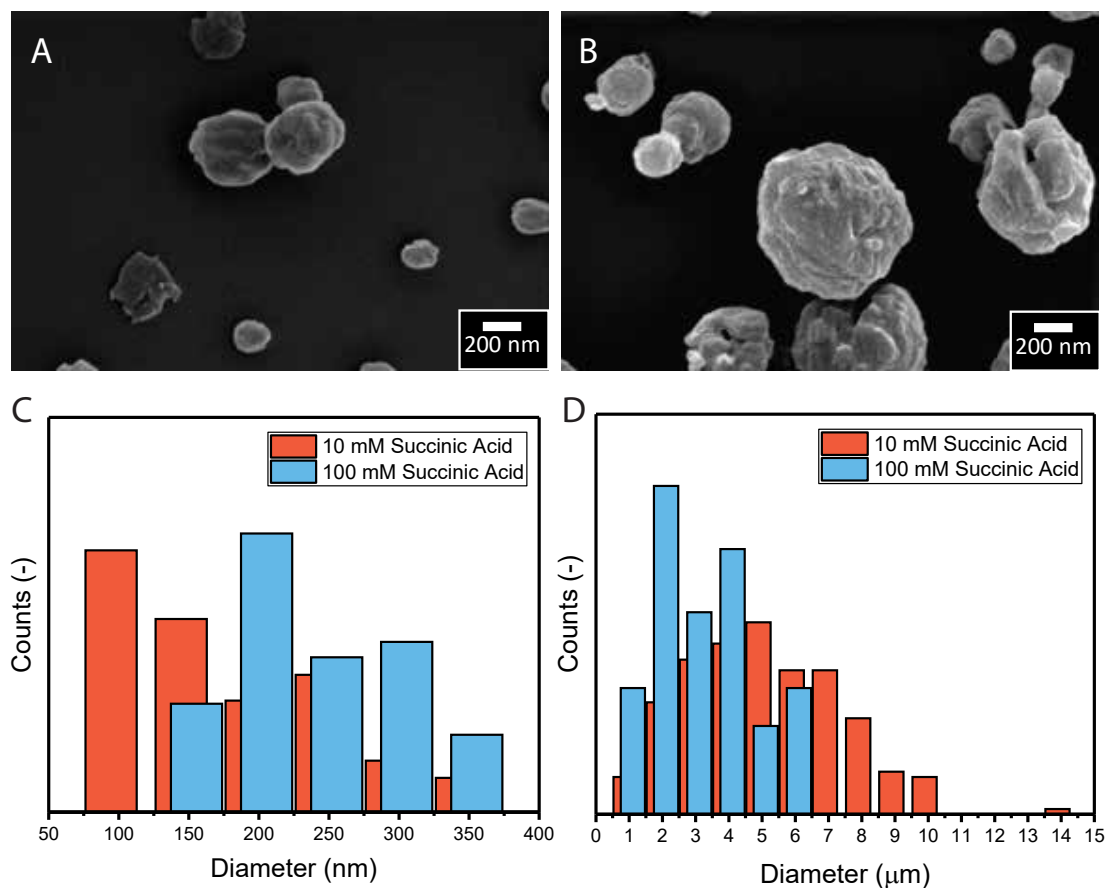


Figure 4.2: Morphology of succinic acid particles. SEM image of succinic acid particles spray-dried from ethanol-based solutions containing (A) 10 mM and (B) 100 mM succinic acid. (C) Size distribution of particles sprayed from solutions containing 10 mM (orange) and 100 mM (blue) succinic acid. (D) The initial size distribution of the corresponding ethanol-based drops initially containing 10 mM (orange) and 100 mM (blue) succinic acid.

This fast drying allows to kinetically arrest phase separations and crystallization reactions on a time scale of milliseconds. To leverage this feature, I produce succinic acid particles from an ethanol-based solution containing 10 mM of succinic acid,

which corresponds to 2% of its saturation concentration. The resulting succinic acid particles have an average diameter of 240 nm, as shown in the SEM images in Figure 4.2. The time required for low molecular weight substances to diffuse the length of the radius of the initial drop is similar to the time required to dry the drop. Hence, I approximate the solute concentration within the drops to be homogeneous such that I expect the resulting spray-dried particles to be solid.

In this case, the size of spray-dried particles should increase with increasing initial succinic acid concentration. To test this expectation, I increase the initial succinic acid concentration ten-fold to 100 mM. Indeed, this increase in initial solute concentration increases the average particle diameter from 240 nm to 450 nm, as shown in Figure 4.2C. To test if the size of the initial drops depends on the initial solute concentration, I calculate the drop size from the measured particle size and the known initial solute concentration, assuming a succinic acid density of 1.56 g cm^{-3} . Indeed, the calculated initial drop size is within experimental error independent of the initial solute concentration (Figure 4.2D). This finding demonstrates that I can neglect mass transport limitations within the drying drops such that the size of spray-dried particles can conveniently be tuned with the initial solute concentration. This behaviour is well in agreement with reports on the size-dependence of other types of particles produced with the SAW-based spray-dryer [149].

4.4.2 Influence of Solute Concentration on Phase Separation

Succinic acid is a biocompatible low molecular weight substance that easily crystallizes such that I expect it to efficiently retain volatiles contained in it. To assess this potential, I dissolve 100 mM succinic acid and different amounts of vanillin in ethanol before spray-drying this solution. The addition of vanillin introduces surface pores into the spray-dried particles, as shown in SEM images in Figure 4.3.

To investigate the influence of the initial succinic acid concentration on the degree of macroscopic surface pores, I fix the vanillin concentration to 30 mM and vary the succinic acid concentration from 50 mM to 80 mM. The degree of surface pores decreases with increasing initial succinic acid concentration, as shown in Figure 4.4. I assign this observation to the change of the onset of solidification of succinic acid in the drying drop: With increasing initial succinic acid concentration, the degree of supersaturation at the point where a significant amount of succinic acid solidifies increases, resulting in the formation of more but smaller succinic acid crystallites. Our images hint at an increase in surface pores with increasing vanillin concentration and decreasing succinic acid concentration, as shown in Figure 4.3 and Figure 4.4.

Vanillin contained within pores that are in proximity to the particle surface can readily evaporate such that it is rapidly lost. To test if I can reduce the surface pores and thereby improve the vanillin retention of succinic acid-based particles, I lower the initial vanillin concentration to 10 mM while keeping the succinic acid concentration constant at 100 mM. Remarkably, these particles possess much fewer surface pores, as visualized with SEM in Figure 4.3A.

I assign the formation of these pores to macroscopic phase separations that occur during the drying of the drop: With increasing initial concentration of vanillin, its saturation concentration is reached earlier during the drop drying process such that the time it has to solidify and phase separate increases [179]. If vanillin-rich phases are located in proximity to the surface, vanillin readily evaporates especially if particles are exposed to low pressures, which is the case during their visualization with SEM, resulting in surface pores.

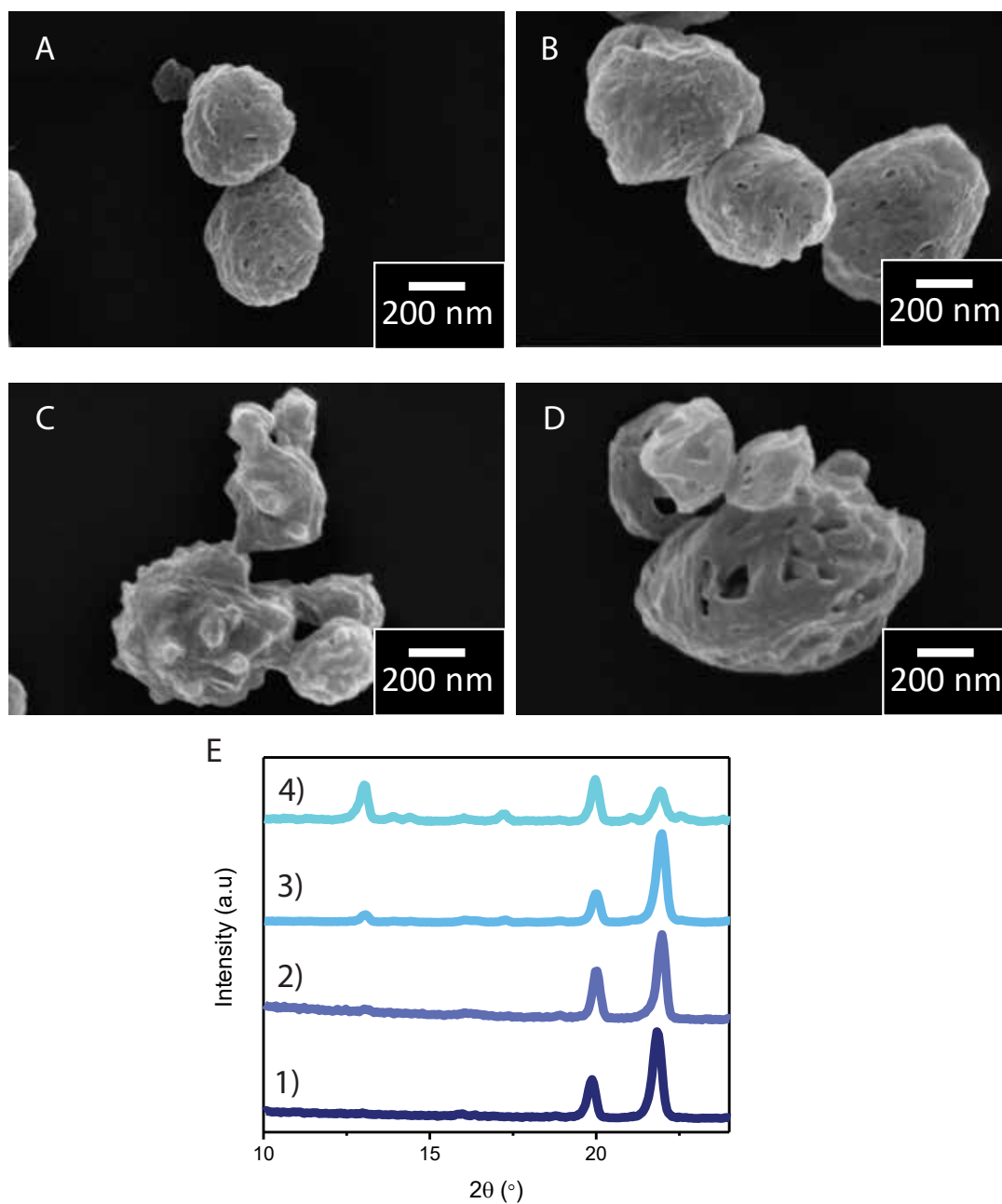


Figure 4.3: SEM image of spray-dried particles composed of a mixture of succinic acid (S) and vanillin (V) produced from solutions initially containing 100 mM succinic acid and (A) 10 mM (B) 15 mM, (C) 20 mM, and (D) 60 mM vanillin. (E) XRD traces of vanillin loaded succinic acid particles spray-dried from a solution initially containing (1) 10 mM, (2) 15 mM, (3) 20 mM, and (4) 60 mM vanillin. The succinic acid concentration is kept constant at 100 mM.

Chapter 4. Implementation of Crystallization Control: Vanillin Encapsulation in Crystalline Particles

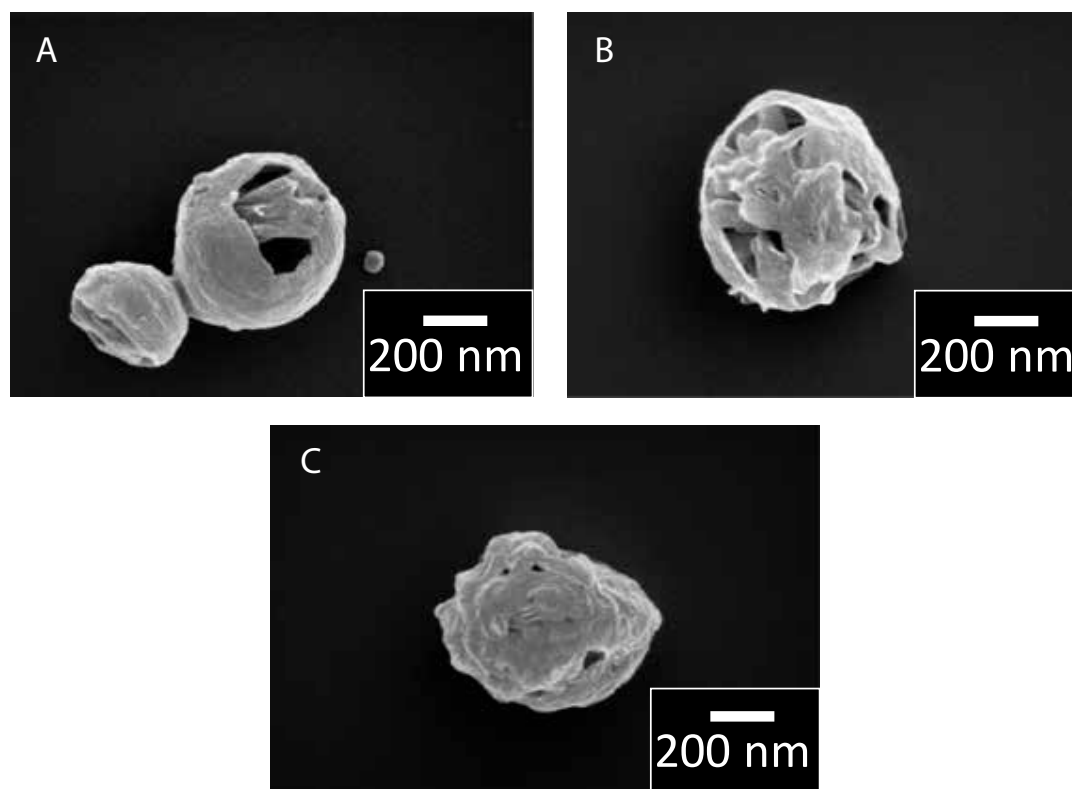


Figure 4.4: SEM image of spray-dried particles composed of a mixture of succinic acid (S) and vanillin (V) produced from solutions initially containing (A) 10 mM S, 10mM V (B) 50 mM S, 30 mM V (C) 80 mM S and 30 mM V.

Our results suggest that vanillin and succinic acid phase separate within drops if the vanillin to succinic acid molar ratio exceeds a threshold value. In this case, I expect vanillin and succinic acid to crystallize within different areas. To test this expectation, I assess the crystallinity of vanillin and succinic acid within particles produced from an ethanol-based solution containing 100 mM succinic acid as a function of the vanillin concentration using X-ray diffraction (XRD). I do not measure any clear diffraction peak of vanillin if its concentration is below 15 mM. By contrast, a clear peak at $2\theta = 13^\circ$ can be seen if the vanillin concentration exceeds 15 mM (Figure 4.3E). The full width of half maximum (FWHM) of the diffraction peak increases with increasing vanillin concentration suggesting that the size of vanillin crystallites decreases. For example, an increase of the vanillin concentration from 20 to 60 mM results in a decrease in the average vanillin crystallite diameter from 35 ± 6 nm to 26 ± 4 nm. These results support our expectation that with increasing vanillin concentration, I create more but smaller vanillin crystals. Trend

of decrease in crystallite size is also deduced from the increased FWHM for succinic acid crystallites with increasing vanillin concentrations. Moreover, if the vanillin concentration exceeds a threshold value of 15 mol%, corresponding to 16 wt%, I obtain macroscopic phase separations.

4.4.3 Vanillin Retention in Crystalline Particles

4.4.3.1 Vanillin Loading in Succinic Acid and Tartaric Acid Particles

An important parameter that determines the suitability of spray-dried succinic acid particles as carriers of volatile substances is their encapsulation efficiency, defined as the percentage of encapsulants that are contained within spray-dried particles with respect to those added to the feed solution. I quantify this parameter using thermogravimetric analysis (TGA).

I expect the amount of vanillin that is lost during the spray-drying process to depend on the time when succinic acid and vanillin precipitate during the drying of the drops. To test this expectation, I dissolve vanillin and succinic acid at the same relative saturation concentrations and vary their absolute concentrations. Indeed, the vanillin encapsulation efficiency increases with increasing vanillin concentration present in the initial solution: It is approximately 70% if the vanillin concentration is 50 mM, corresponding to a relative supersaturation of 0.16 and increases to almost 100% if I increase the vanillin concentration to 60 mM (Figure 4.5A). Hence, the highest encapsulation efficiency is observed for solutions containing 60 mM vanillin and the highest processable succinic acid concentration, 100 mM. Note that particles produced with the SAW based microfluidic spray-drier do not encompass significant amounts of solvent, as indicated by TGA results, although I cannot exclude that traces of solvents are trapped within them.

Our results suggest that the initial concentration of vanillin influences its encapsulation efficiency. To test if this is indeed the case, I fix the succinic acid concentration to 80 mM and vary the vanillin concentration. Indeed, the encapsulation efficiency increases with increasing vanillin concentration, reaching 80% for an initial vanillin concentration of 80 mM. Independent of the initial vanillin concentration, approximately 15 mM vanillin is lost during the spray-drying process, as exemplified for particles sprayed from a solution initially containing 80 mM succinic acid (Figure 4.5B). This is much less than what has been previously reported

Chapter 4. Implementation of Crystallization Control: Vanillin Encapsulation in Crystalline Particles

for vanillin spray drying [188, 189]. Note, that if the same solution is processed with a commercial spray-drier where drops are dried at elevated temperatures, approximately 90% of vanillin is lost (Figure 4.6). Vanillin degradation in the particles sprayed from commercial spray-dryer is observed at lower temperatures compared to vanillin reference. This result might indicate that vanillin has been partially thermally degraded or oxidated if processed with commercial spray dryers at elevated temperatures.

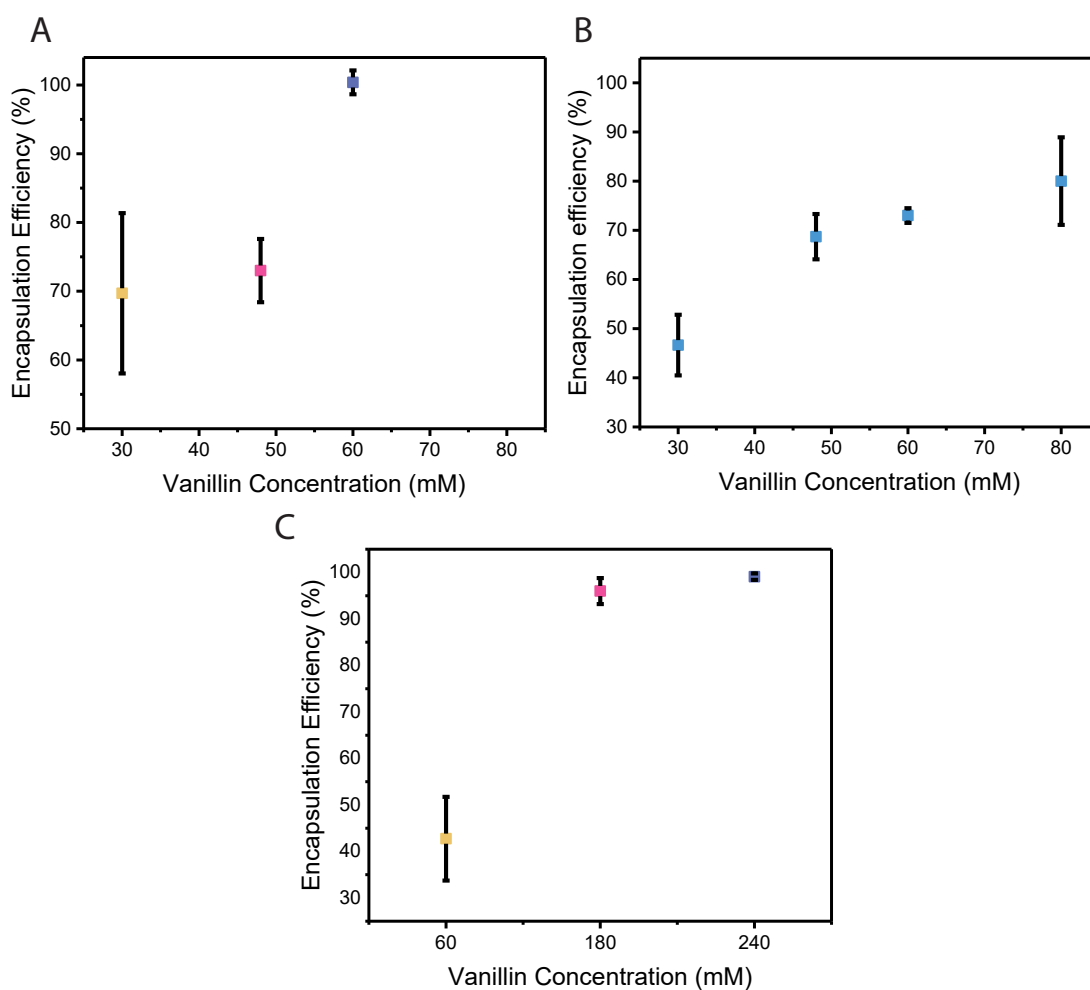


Figure 4.5: Vanillin encapsulation efficiency. (A, B) Encapsulation efficiency of vanillin as a function of its concentration (A) for a constant molar ratio of succinic acid: vanillin of 5:3 and (B) constant succinic acid concentration of 80 mM. (C) Encapsulation efficiency of vanillin within tartaric acid-based particles as a function of the vanillin concentration. The tartaric concentration is kept constant at 15 mM.

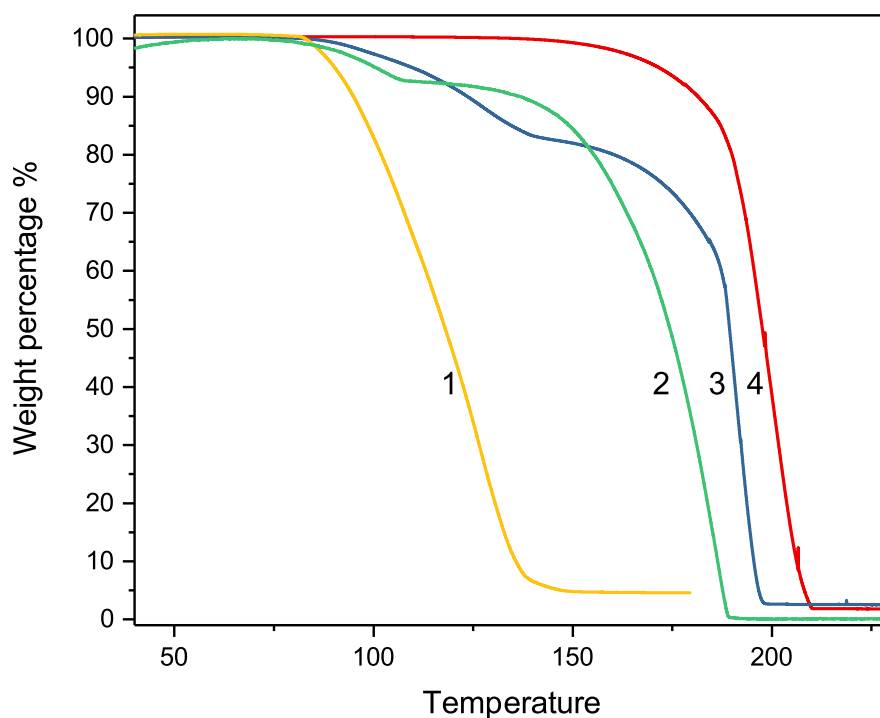


Figure 4.6: TGA of 1) control bulk vanillin, (2,3) particles sprayed from DI water containing 100 mM succinic acid and 60 mM vanillin with a 2) commercial spray dryer and 3) microfluidic spray dryer. 4) Control of bulk succinic acid.

To test the generality of our approach of using low molecular weight organic substances as matrix materials for the encapsulation of volatile substances, I form particles from tartaric acid, another low molecular weight substance that has a high propensity to crystallize. The encapsulation efficiency of vanillin is also high if contained in tartaric acid particles formed from solutions containing high vanillin concentrations: The encapsulation efficiency is 99% if particles are produced from an ethanol-based solution containing 15 mM tartaric acid and 240 mM vanillin (Figure 4.5C). This result demonstrates that our findings are not limited to succinic acid but apply to other low molecular weight organic compounds that possess a high propensity to crystallize.

Chapter 4. Implementation of Crystallization Control: Vanillin Encapsulation in Crystalline Particles

4.4.3.2 Release Kinetics

Smaller polydisperse, or more spherical crystallites typically pack more densely than larger, anisotropic, counterparts formed from more dilute solutions. Hence, I expect particles made from more concentrated solutions where more but smaller crystallites form to retain volatiles more efficiently. To test this expectation, I quantify the amount of released vanillin as a function of the initial vanillin concentration. To accelerate the vanillin release, I heat the samples to 65°C and monitor their release for 7 h. Indeed, the vanillin release rate decreases with increasing initial vanillin concentration and hence, decreasing crystallite size (Figure 4.7A-C), in good agreement with our expectation.

These results demonstrate the potential of crystalline low molecular weight substances as matrix materials for the encapsulation of volatile substances. Note that, while I exclusively test solid volatiles, this method is not limited to them but can also be expanded to liquid volatiles, if process parameters are adjusted, as has been shown with conventional spraying methods [45].

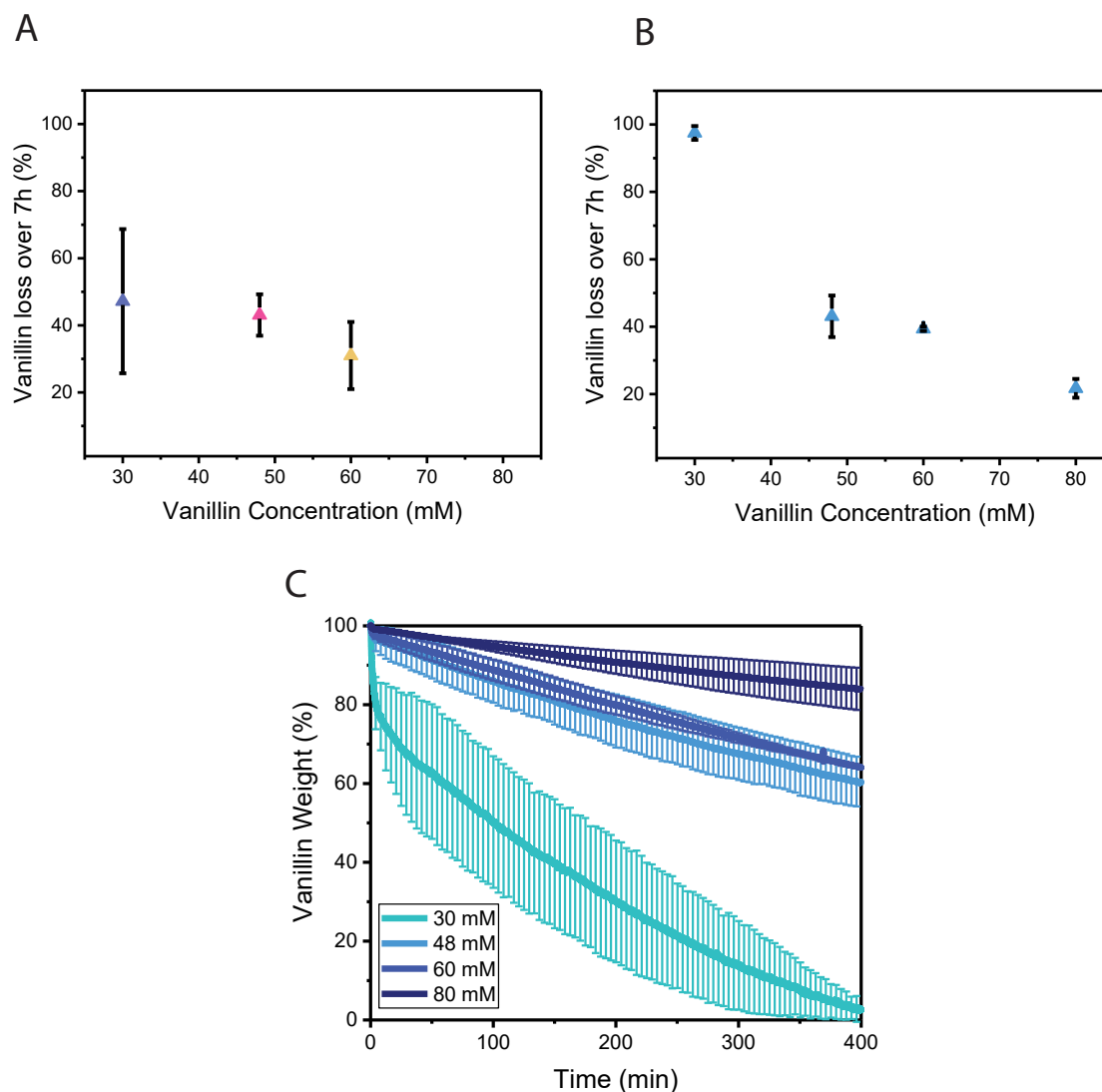


Figure 4.7: Vanillin release kinetics. Weight percentage of vanillin released if particles are stored at 65 °C as a function of the vanillin concentration contained in the initial solution if (A) the molar ratio of succinic acid to vanillin is kept constant at 5:3 and (B) the succinic acid concentration is fixed at 80 mM. (C) Release kinetics of vanillin from succinic acid particles as a function of the vanillin concentration if the succinic acid concentration is kept constant at 80 mM.

4.5 Conclusion

Low molecular weight substances that have a high propensity to crystallize such as succinic acid are well-suited matrix materials for volatiles as they are typically composed of densely packed molecules that have a low permeability towards volatile substances such that they retain them for a prolonged time. Low molecular weight substances add an additional advantage: They do not significantly increase the viscosity of the solvent they are dissolved in, even if added at high concentrations, thereby facilitating the processing of this solution for example through spray-drying. Note that the concept presented here is not limited to succinic acid but can be expanded to other organic low molecular weight substances such as tartaric acid or even liquid volatiles. These findings open up new possibilities to tune the encapsulation efficiency and release kinetics of volatile substances not only through the composition of the matrix material but also through its processing.

5 Emulsion Templated Crystallization

In this chapter, I present the feasibility of various microfluidic techniques to achieve control over crystallization of biogenic crystals. I show that the single and double emulsions produced by microfluidics allow to grow biogenic crystals if pH or the salt concentrations are changed.

This chapter is formed with the collaboration of Luc Monnier for crystal formation in single emulsions under supervision of Esther Amstad and of Nina Wittig for crystal formation in trapping devices under the supervision of Henrik Birkedal and Esther Amstad.

Contents

| | | |
|---------|---|----|
| 5.1 | Abstract | 82 |
| 5.2 | Introduction | 83 |
| 5.3 | Experimental Section | 85 |
| 5.3.1 | Materials | 85 |
| 5.3.2 | Methods | 85 |
| 5.3.2.1 | Single Emulsion Production via Tip Sonication | 85 |
| 5.3.2.2 | Production of Single Emulsions and Their Trapping | 85 |
| 5.3.2.3 | Microfluidic Device Production for Double Emulsions | 86 |
| 5.3.2.4 | Double Emulsion Production | 86 |
| 5.4 | Results & Discussion | 87 |
| 5.4.1 | Crystal Formation in Single Emulsions | 87 |
| 5.4.2 | Crystal Formation in Trapping Device | 88 |
| 5.4.3 | Crystal Formation in Double Emulsions | 89 |
| 5.4.4 | Influence of Reactant Concentration on Morphology & Size | 91 |
| 5.4.5 | Influence of Osmotic Pressure on DE Core Size & Morphology of the Particles | 94 |
| 5.5 | Conclusion | 96 |

5.1 Abstract

Crystals found in nature, whose formation conditions are usually well-defined, exhibit unique and extraordinary material properties and performance. A tight structural control is often achieved through crystallization in small volumes which is very difficult to achieve via bulk crystallization techniques. Crystallization can be achieved under confined conditions, however, to simultaneously control all crystallization parameters is challenging. To address this challenge, microfluidic tools that present or form picoliter-sized vessels can be used to study the formation of biogenic crystals. Miniaturization of the volume limits the impurities, and

decreases the crystallization rate such that it opens up room to observe short-lived metastable phases and analyze influences of process parameters on crystal size, morphology and structure. In this chapter, I present the use of single and double emulsions to study biogenic crystal formation. These emulsions can be formed with microfluidic devices that also allow monitoring the crystallization in them. I use microfluidics to screen the influence of many processing parameters such as pH, stoichiometric ratio, initial solute concentration, crystallization vessel size and additives. In addition, double emulsions are shown to be suitable for reaction induced crystallization as they are selectively permeable to certain reactants. These results open up new routes to use emulsions as micro compartments to study, control and initiate reactions in picoliter-sized cell-mimetic compartments.

5.2 Introduction

Nature produces crystals in living objects with very intricate morphologies [190, 191], well defined arrangement and orientation [76, 192, 193] that constitute materials displaying extraordinary properties such as photonic crystals with excellent optical properties [1, 2, 194], composites with superior mechanical properties towards high load bearing applications [8, 73, 195], and toughness [196, 197]. These crystals are formed via templates of controlled sizes and dimensions, which helps to determine the crystal orientation, structure and size. For example, amorphous calcium phosphate is an important part of bones where its crystallization is templated through collagen molecules forming gaps with sizes of several tens of nanometers whose crystals can form. The ACP crystals that form within these gaps are oriented apatite structures that display a fibrillary phase, which contributes to the excellent mechanical properties of bone [9, 195, 198]. Similar models are also observed in other crystals such as $CaCO_3$ and guanine, as cells are used to control the crystallization [77, 199–201]. It is still not fully understood how living organisms achieve such tight control over crystallization. While it is necessary to have in-depth understanding to obtain high performance materials through biomimetics, such information can also be used in therapeutics. For instance, calcium oxalate is the main constituent of kidney stones, which require painful and costly invasive treatments [202, 203]. To formulate drugs or other non-invasive techniques, one useful way is to prevent its crystallization by preventing nucleation or delaying the growth. However, calcium oxalate is an organic crystal that presents multiple short-

lived metastable phases with different hydration levels and many morphologies [203, 204]. Hence, in depth systematic studies on what parameters influence the formation and structure of the crystals are difficult to design.

The level of control nature possesses is today not possible to obtain in synthetic systems through bulk crystallization techniques. To gain a better control over the morphology and structure of forming crystals, methods that allow to closely control the crystallization reactions and thereby to systematically and independently vary different crystallization parameters are warranted.

Microfluidic tools are well suited to study reactions in small volumes. For example, the crystallization of proteins has been studied in picoliter-sized drops [101, 102]. To advance drug design, crystallization of proteins that display the appropriate conformation has to be achieved. However, proteins that display the desired functionalities do not always exhibit the most stable phases that can readily be obtained via bulk methods. Moreover, phase diagrams that present a roadmap for the synthesis of the desired form are missing for many proteins. Hence, to formulate proteins that are arranged into the desired structure often involves screening of crystallization parameters as well as means to observe and analyze metastable phases. Drops formed with microfluidics have been used to address these limitations, as they enable the formation of crystals in small volumes such that risks for impurities are lower and the crystallization kinetics is slowed down. Hence, these tools have been used to crystallize proteins, and thanks to the high throughput production of emulsions, they have been used for high throughput screening assays.

In this chapter, I demonstrate that biogenic crystals can controllably be grown within single and double emulsions with picoliter-sized volumes. Drops of controlled sizes can be formed with microfluidics. These calibrated drops can be trapped in microfluidic devices to monitor crystallization reactions. Unfortunately, harsh crystallization conditions can compromise the stability of single emulsions. This shortcoming can be overcome if double emulsions that are more stable than single emulsions are used. I show that the size and morphology of various biogenic crystals can be directed with the size of emulsions, stoichiometric ratio of reactants and pH. These results suggest new strategies to gain in-depth understanding on crystallization parameters that enable tuning the structure and morphology of crystals that might enable novel applications.

5.3 Experimental Section

5.3.1 Materials

All chemical reagents were used as received. Oxalic acid ($\geq 99\%$), guanine (99%), triethylamine (TEA, $\geq 99.5\%$), ethanol (absolute alcohol, without additive), poly vinyl alcohol (PVA, M.W. 13–23 kDa, 87%–89% hydrolyzed) were purchased from Sigma–Aldrich. D (+) saccharose (sucrose, $\geq 99.7\%$), sodium hydroxide ($NaOH$, $\geq 99\%$), poly (ethylene glycol) (PEG, M.W. 5–7 kDa), Calcium chloride ($CaCl_2$, $> 98\%$), hydrochloric acid (HCl 37%) were purchased from Carl Roth. DL tartaric acid (99%) was purchased from Alfa Aesar. Deionized water (18.2 M Ω cm) was collected from Direct Q, Merck Millipore system.

5.3.2 Methods

5.3.2.1 Single Emulsion Production via Tip Sonication

Varying concentrations of $CaCl_2$ are dissolved in EtOH (filtered with $<0.45 \mu\text{m}$ pore size) and then mixed with $6.33 \mu\text{L}$ of oleic acid and 1 mL of citral. 30 mM $NaHCO_3$ was dissolved in 5 mL of DI water and injected into a citral solution via a syringe pump (Cronus Sigma 1000, Labhut) at a flow rate of $166.67 \mu\text{L s}^{-1}$ while the solution was tip-sonicated with alternate 1s ON/OFF pulses for 30s.

5.3.2.2 Production of Single Emulsions and Their Trapping

Single emulsion drops were formed with a microfluidic flow focusing device and trapped with a microfluidic device containing surface energy wells. The inner phase containing 0.1 M HCl and 0.3 mg/mL guanine was injected through the innermost inlet at a rate of $300 \mu\text{L/h}$, while a continuous phase of HFE–7500 containing 1% (w/w) surfactant (diFSH–PEG600) was injected through a second inlet at a rate of $2000 \mu\text{L/h}$. After formation and trapping, the inner phase was pulled back slightly to stop inflow and then continuously retracted at $-20 \mu\text{L/h}$. The surfactant-containing phase was used to carefully push out untrapped drops, and its injection was discontinued when all untrapped drops were removed. This method resulted in reproducible formation and trapping of single emulsion drops with a uniform size distribution [105].

5.3.2.3 Microfluidic Device Production for Double Emulsions

Double emulsions were produced using 3D microfluidic flow focusing devices, as schematically illustrated in Figure 5.1, and described in further detail in section 2. These devices were fabricated from poly(dimethyl siloxane) using soft lithography [151, 205]. To ensure a stable operation of the microfluidic device, the surface of the first junction was modified to be hydrophobic and the second junction to be hydrophilic. To achieve this, the first junction was treated with a HFE 7500-based solution containing 1% (v/v) perfluorinated trichlorosilane and the second junction with an aqueous solution containing 1% (v/v) poly(diallyldimethylammonium chloride) (400–500 kDa) and 2 M NaCl as described in previously reported protocols[205].

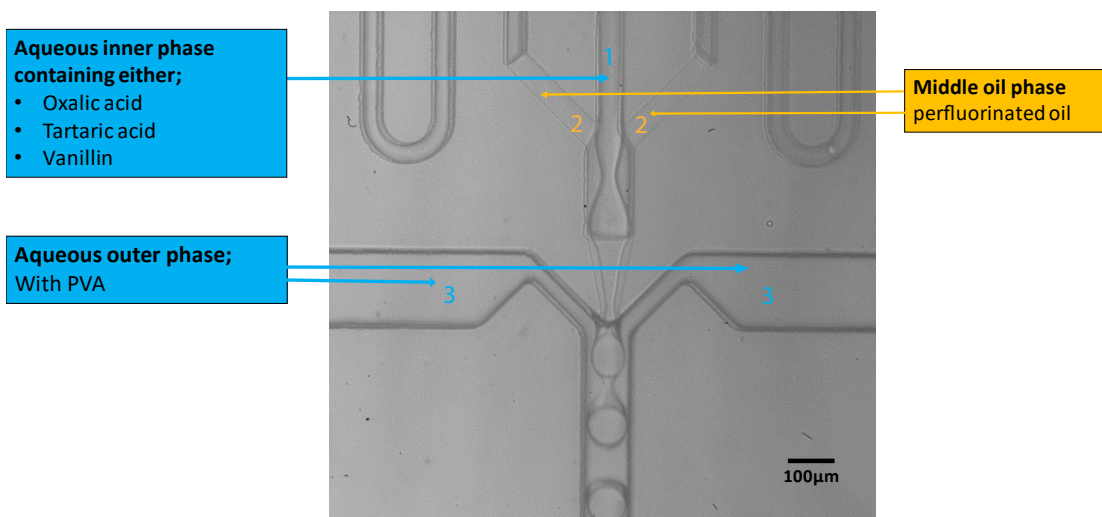


Figure 5.1: Image of flow focusing microfluidic device forming double emulsions.

5.3.2.4 Double Emulsion Production

Inner phase that composes the core of the DEs is based on an aqueous solution of either oxalic acid, tartaric acid or PEG and delivered from the #1 inlet as shown in Figure 5.1. The middle phase is delivered from microchannels labeled as #2. This phase is the fluorinated oil, HFE 7500, that contains 1×10^{-3} M of a functionalized surfactant (diFSH-PEG900) that forms the shell of double emulsions. Finally, the continuous phase, an aqueous solution containing 10% (w/w) PVA (M.W. 13–23 kDa) was delivered from the horizontal channels, labelled as #3. The flow is controlled by syringe pumps (Cronus Sigma 1000, Labhut).

To avoid osmotic pressure gradients, that would result in a change in the dimensions

of the double emulsions, the osmolarity of the inner and outer phase is matched using D(+)-saccharose (Carl Roth, Germany); the osmolarity of the solutions is quantified with an osmometer (Advanced Instruments, Fiske 210).

5.4 Results & Discussion

5.4.1 Crystal Formation in Single Emulsions

Single emulsions can be used as crystallization templates since they constitute picoliter-sized reaction vessels that minimize the risk for having impurities that act as heterogeneous nucleation sites. One route to trigger crystallization is to use the oil/water interface in emulsions as a platform for heterogeneous crystal nucleation. To leverage this potential, we studied the formation of $CaCO_3$ as a well-established model system within single emulsion drops. To form the $CaCO_3$ crystals we dissolved 200 mM $CaCl_2$ into ethanol which is miscible in the citral-based oil phase, and dissolved 30 mM $NaHCO_3$ into the aqueous phase. The two phases were tip sonicated for 30 seconds to form micron size droplets as shown in Figure 5.2C. To ensure the formation of stable emulsions within 30 s, 0.6% (v/v) oleic acid is added to the citral phase. To test the influence of the stoichiometric ratio on the crystallite size, we varied the ratio of $Ca : HCO_3$ between 1:5 to 1:10. Indeed, we observe the formation of crystals within the emulsion drops. The crystals found within the drops displayed similar sizes even if formed with different stoichiometric ratios, indicating that the amount of carbonate ions present in the system, that remains constant in this experimental series, determines the size of the resulting crystals, as seen in Figure 5.2A-B. However, the drops were polydisperse, such that we could not systematically study the influence of the drop size on the crystal size.

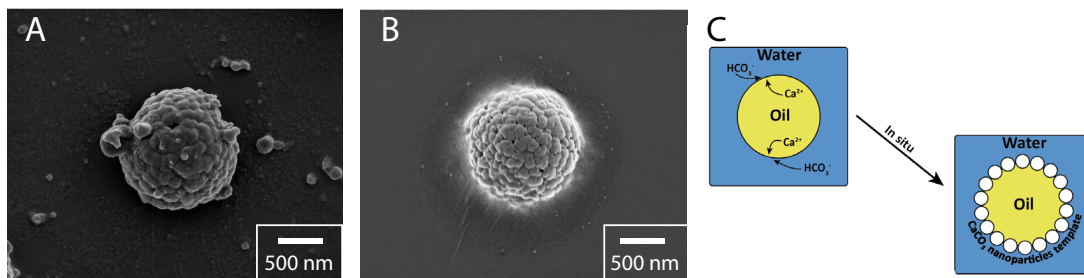


Figure 5.2: SEM image of CaCO_3 formed in single emulsions containing stoichiometric ratios of A) Ca^{+2} : HCO_3 B) Ca^{+2} :2 HCO_3 C) Schematic illustration of CaCO_3 formation on the oil/water interface.

5.4.2 Crystal Formation in Trapping Device

Biogenic guanine crystals that exhibit distinct phases and hence optical properties are difficult to obtain with conventional techniques, complicating the studies on their formation. To gain in-depth understanding of their formation, the use of emulsion drops that can slow down the crystallization due to confinement effects is attractive.

To study the guanine crystallization, we dissolved 0.3 mg/mL guanine in 0.1 M HCl which was injected through the innermost inlet at a rate of 300 $\mu\text{L/h}$, while a continuous phase of HFE-7500 containing 1% (w/w) surfactant (diFSH-PEG600) was injected through the second inlet at a rate of 2000 $\mu\text{L/h}$. To induce crystallization, TEA is used to increase the pH; an increase in pH decreases the solubility of guanine such that it starts to nucleate once its concentration exceeds its saturation concentration. However, under such basic conditions, the single emulsions are not sufficiently stable to visualize the crystallization for several days. To prevent coalescence of emulsion drops, we spatially separated them using the microfluidic trapping device.

To test the influence of the nucleation rate of guanine on the formation of crystals within drops, we varied the TEA concentration within the oil phase. We trapped guanine loaded emulsions and injected the oil, HFE-7500, under constant flow into the trapping device. We varied the TEA concentration contained in the oil between 0-1 wt% and let the experiment run over 4 days. As expected, the rate of crystal growth increases with the amount of TEA contained in the oil, as can be seen in

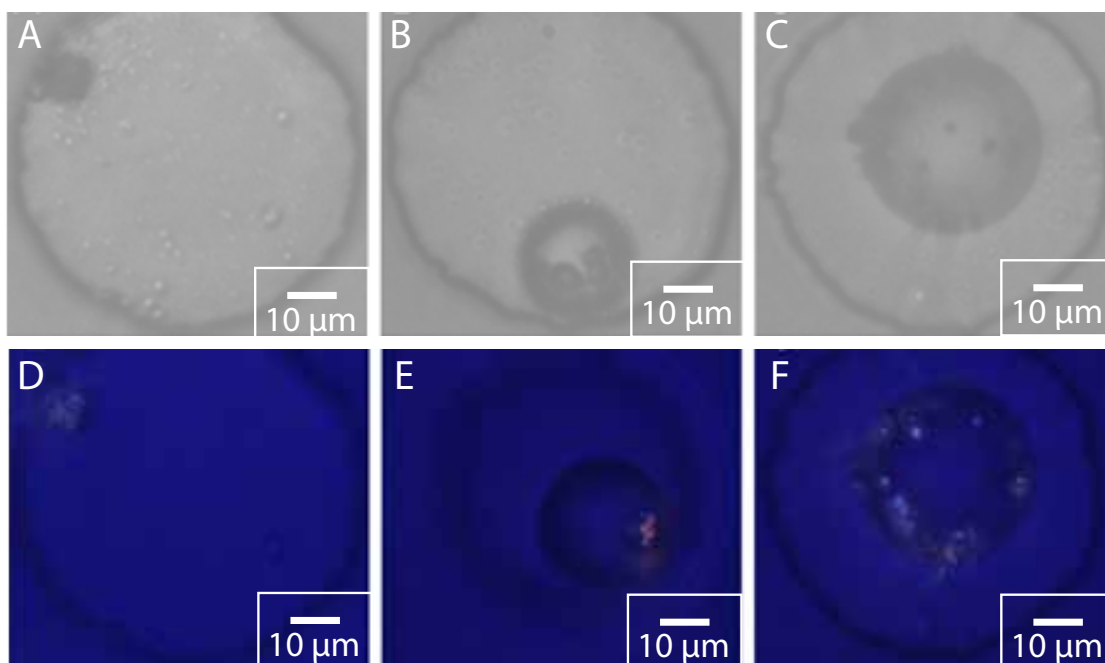


Figure 5.3: Optical microscopy images taken (A-C) without and (E-H) with crossed polars revealing guanine crystals formed in trapped single emulsion drops. HFE-7500 was constantly injected during incubation for A,D) a few minutes with no TEA (B,E) for 16 hours containing 0.5% (v/v) TEA (C,F) for 5 hours containing 1% (v/v) TEA.

Figure 5.3. These results demonstrated that the nucleation rate is pH dependent and can hence conveniently be tuned with the TEA concentration.

5.4.3 Crystal Formation in Double Emulsions

Harsh crystallization conditions can compromise the stability of single emulsions. To address this limitation, I formed double emulsions that are more stable, especially if stored at extreme pHs or high ion concentrations [206, 207]. Double emulsions (DEs), where each one was composed of an acidic aqueous core that is surrounded by a shell composed of HFE-7500 containing 1 wt% Di-FSH-PEG600 surfactants were dispersed in an aqueous continuous phase containing 10% PVA. These double emulsions were stable over a week even if incubated in solutions containing high salt concentrations which are known to be destabilizing emulsions stabilized with most polymeric surfactants. I use this feature to produce organic salt crystals, calcium oxalate, to test the potential to controllably grow them within the small reaction vessels.

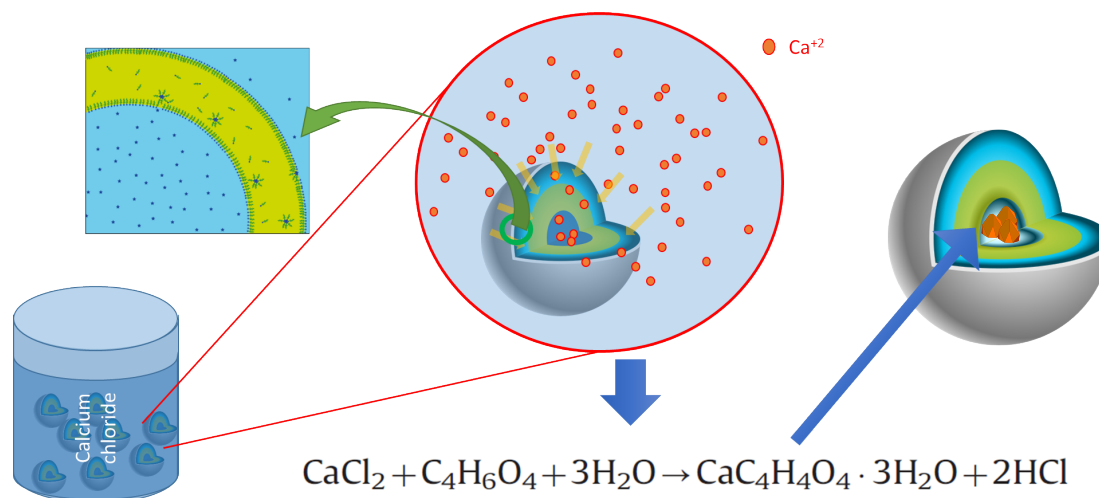


Figure 5.4: Schematic illustration of the formation of calcium oxalate crystals within double emulsions.

The emulsions are formed within a flow focusing microfluidic device, where the inner, middle and outer phases are delivered with flow rates of 1000 $\mu\text{L/h}$, 500 $\mu\text{L/hr}$, 3400 $\mu\text{L/h}$ respectively. The size of these emulsions is dictated by the outlet channel width which is 100 μm . Upon collection, the DEs are transferred into isolated and closed wells that contain an aqueous solution containing CaCl_2 to observe the crystal formation over 24h. Because there is a chemical gradient between the inner core of the DE and the outer environment which is an aqueous CaCl_2 containing solution, Ca^{+2} ions are expected to diffuse into the core, even if the osmolality of the cores of DEs and the incubation solution is balanced through the addition of sucrose, and react with oxalate ions to form calcium oxalate, as shown in Figure 5.4. Once the calcium oxalate reaches a critical concentration, it is expected to nucleate and grow to yield micron size crystals.

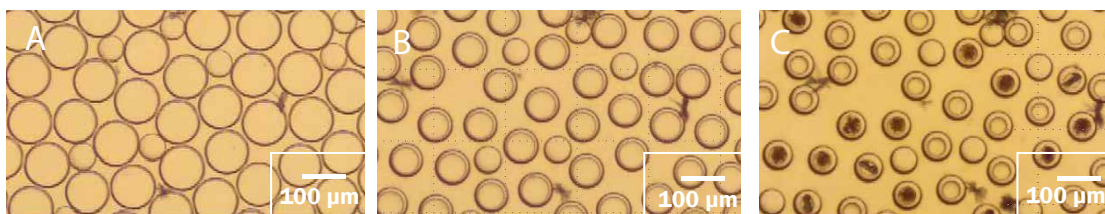


Figure 5.5: Formation of calcium oxalate crystals in double emulsions containing 250 mM oxalic acid within their cores upon incubation in an aqueous solution containing 325 mM CaCl_2 over the timeframe of A) $t = 0$ B) $t = 5\text{h}$ C) $t = 20\text{h}$.

The diffusion of ions is expected to start almost immediately due to the chemical potential difference between the two aqueous phases. While Ca^{+2} ions were transferred into the core of DEs, water can also be transported out of DEs if they are subjected to an osmotic pressure difference such that it should change the size of the emulsion. To test this expectation, the DEs with a diameter of $100\ \mu\text{m}$, containing 250 mM oxalic acid in their aqueous core are incubated in DI water containing 325 mM $CaCl_2$. DEs shrunk during incubation such that the core is contracted and the shell thickness increased. Eventually the aqueous cores are sufficiently densified to observe the onset of crystal formation, as seen in Figure 5.5A-C.

5.4.4 Influence of Reactant Concentration on Morphology & Size

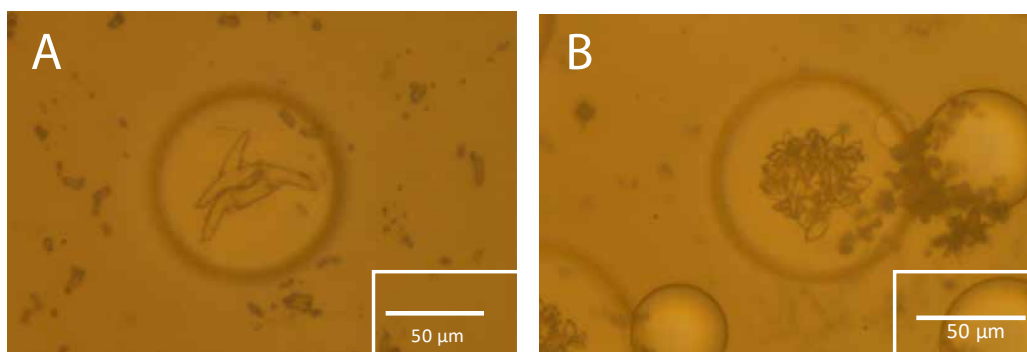


Figure 5.6: Morphology of calcium oxalate crystals formed in double emulsions containing A) 250 mM, B) 100 mM oxalic acid in their cores. $C[CaCl_2] = 325\ \text{mM}$.

The reactant concentrations and their stoichiometric ratio determine the reaction rate and hence the calcium oxalate concentration over time. A change in ion concentrations reflects on the evolution of the supersaturation and hence, the rate of nucleation and growth of calcium oxalate crystals. To investigate the influence of the reactant concentration on the crystal size and morphology, I fixed the $CaCl_2$ concentration in the incubation solution to 325 mM, and varied the oxalic acid concentration. Incubated DEs possessing aqueous cores containing oxalic acid with concentrations varying from 50 to 250 mM are observed with optical microscopy over 20 h. The size of the crystals formed in DEs decreased with increasing

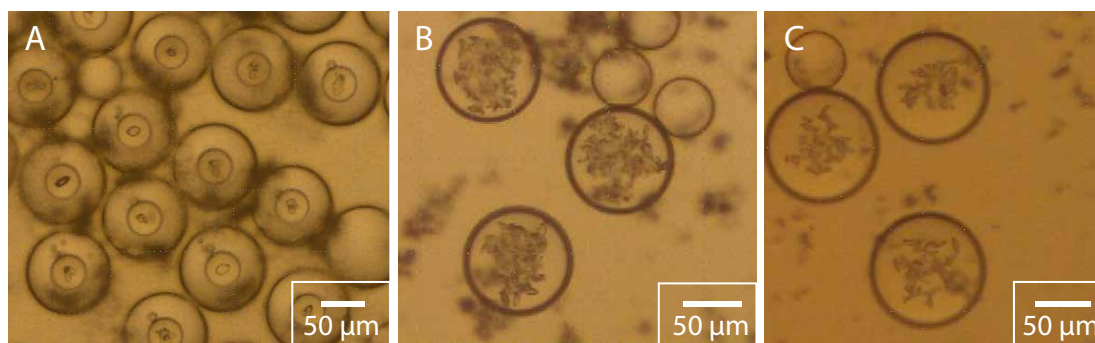


Figure 5.7: Morphology of calcium oxalate crystals formed in double emulsions containing A) 250 mM, B) 100 mM. and C) 50 mM oxalic acid in their cores upon incubation in DI water containing 325 mM of $CaCl_2$ over 20h.

concentration of oxalic acid as seen in Figure 5.7. This observation suggests that at higher oxalic acid concentrations more but smaller calcium oxalate crystals form. I found 250 mM oxalic acid containing DEs to be the optimum system for further analysis. If I kept the oxalic acid concentration constant and varied the calcium concentration such that oxalic acid was in excess, I did not observe significant differences in morphology or size of the crystals as shown in Figure 5.8A-C. These results suggest that the crystal size and morphology is mainly dependent on the concentration of oxalic acid.

The observed decrease in core size upon crystal formation can be due to a decreased ion density occurring after crystals formed, which would reduce the osmolarity of the DE core and cause water to diffuse out of the double emulsions. To test if the reaction has an impact on the size of double emulsion cores, I incubated DEs whose cores contain 250 mM oxalic acid within aqueous solutions containing $CaCl_2$ concentrations varying between 32 to 325 mM. I fixed the osmotic pressure by adjusting it with sucrose such that in all sets, the osmotic pressure difference between the aqueous core and outer phase is 660 mOsm/kg. Under these conditions, I obtained crystals with diameters of approximately 15 μm displaying an atypical morphology that is similar to that of reported kidney stone crystals [202, 203] at the end of a 20h incubation (Figure 5.8A-C). The core size has reduced to approximately 50% of the DE's initial core, independent of the calcium concentration (Figure 7D). To test if calcium ions are transported into the aqueous core, I incubated

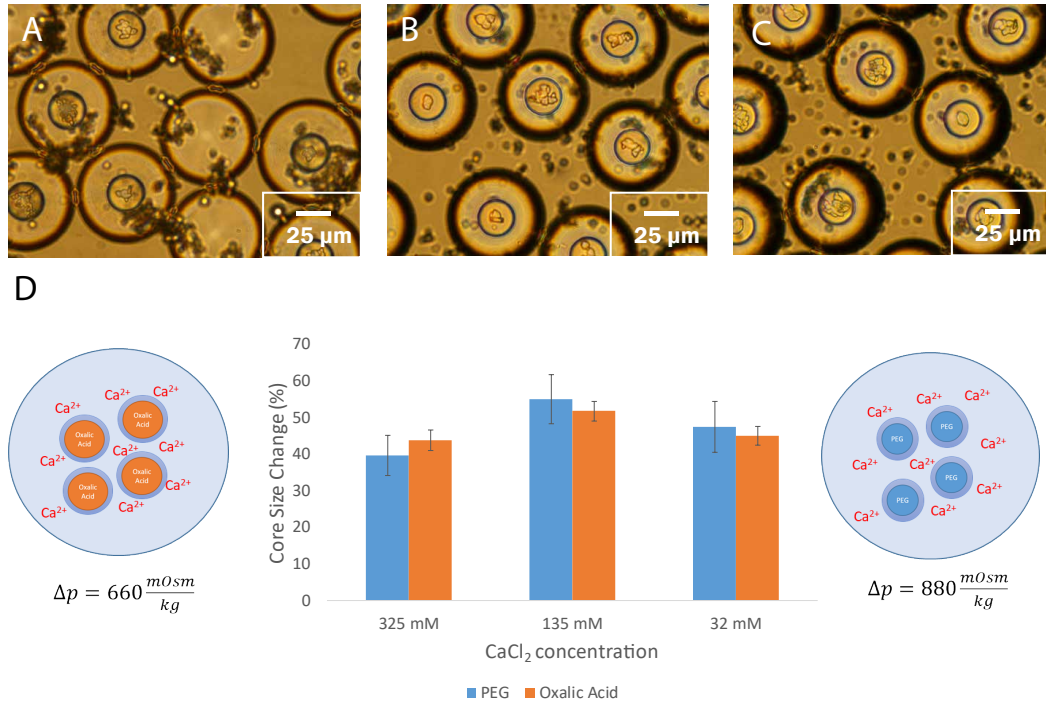


Figure 5.8: Influence of CaCl_2 concentration on the core size change and crystal morphology. 250 mM oxalic acid containing double emulsions incubated in DI water containing A) 325 mM, B) 135 mM, C) 32 mM CaCl_2 . Δp is kept constant at 660 mOsm/kg D) Core size change of double emulsions containing 250 mM oxalic acid or 10 wt% PEG as a function of the CaCl_2 concentration.

DEs containing 10 wt% PEG in the cores in an aqueous solution containing CaCl_2 concentrations varying between 32 to 325 mM with a fixed osmotic pressure difference between the cores of DEs and the outer phase to 880 mOsm/kg. By analogy to DEs loaded with oxalic acid, those loaded with PEG also shrank upon incubation in aqueous solutions containing different amounts of CaCl_2 . Indeed, the size of the cores of DEs loaded with oxalic acid and PEG was within experimental error the same after they have been incubated in a respective aqueous solution (Figure 5.9 D). These results indicate that the shrinkage of emulsions is not considerably influenced by the formation of calcium oxalate crystals but is related to the osmotic pressure difference.

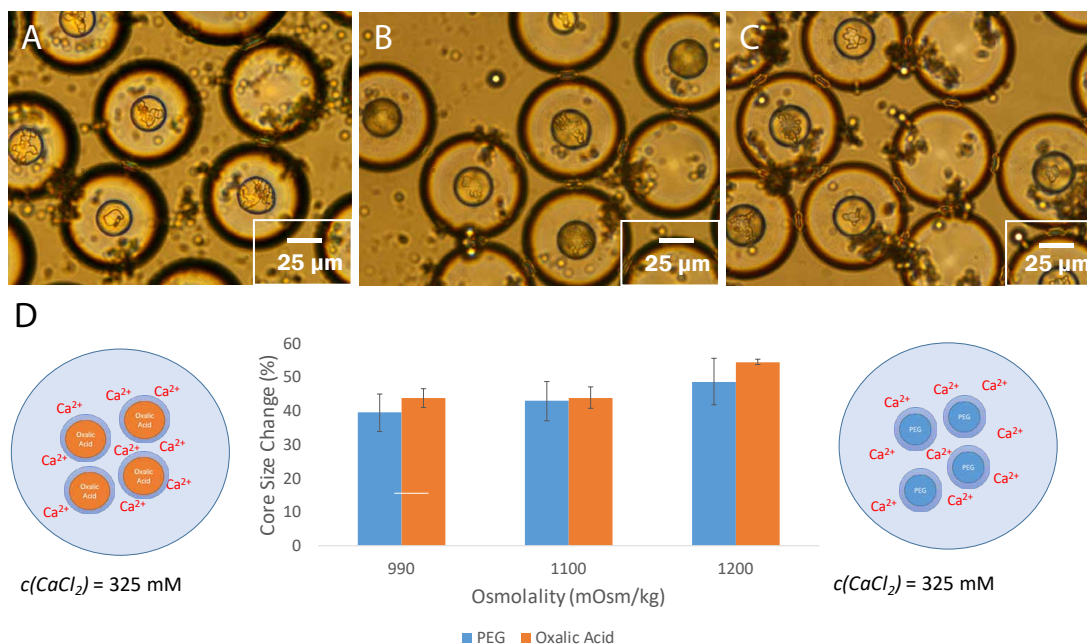


Figure 5.9: Influence of the osmotic pressure on the change of the core size of DEs. DEs containing 250 mM oxalic acid in their cores are incubated over 20h in DI water containing 325 mM CaCl_2 where the osmotic pressure has been adjusted with sucrose to A) $\Delta p = 200 \text{ mOsm/kg}$ B) $\Delta p = 100 \text{ mOsm/kg}$, C) $\Delta p = 0 \text{ mOsm/kg}$ D) Core size change of double emulsions containing 250 mM oxalic acid or 10 wt% PEG that have been incubated in aqueous solutions possessing varying osmolarities.

5.4.5 Influence of Osmotic Pressure on DE Core Size & Morphology of the Particles

The presence of ions in the incubation solution exerts an osmotic pressure on the DEs resulting in a reduction of their core size. To test the effect of the osmotic pressure on the shrinkage of the DE cores, I fixed the oxalic acid and CaCl_2 concentrations and varied the osmolality of the incubation solution. DEs containing 250 mM oxalic acid in their cores are incubated in a solution containing 325 mM CaCl_2 possessing different osmolarities. I added sucrose to controllably vary the osmolality between 900–1200 mOsm/kg. DEs shrunk by approximately 40% at the end of a 20 h incubation independent of the osmotic pressure difference (Figure 8D). The up-concentration of the reagents contained in their cores results in the formation of crystals that display atypical morphologies of aggregates (Figure 5.9 A–C).

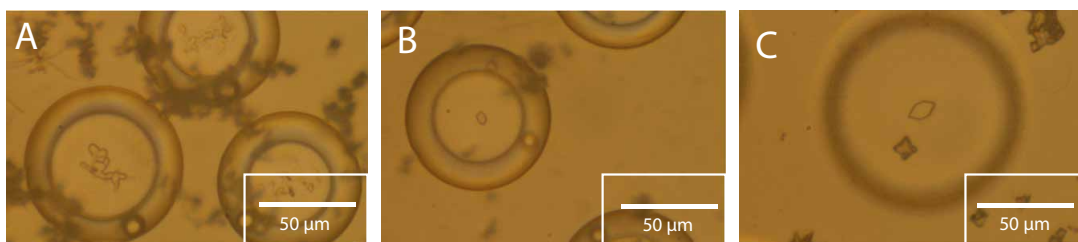


Figure 5.10: Morphology of calcium oxalate crystals when co-precipitated with vanillin. Crystals were formed in double emulsions initially containing 250 mM oxalic acid and 13 mM vanillin in their cores upon their incubation in an aqueous solution containing A) 325 mM B) 250 mM C) 100 mM $CaCl_2$ over 20h.

This result indicates that oxalic acid is not leaking from the emulsions hence its contribution to the osmotic pressure does not change over time.

Additives can influence the crystallization rates significantly. To test if I can monitor the effect of additives, I co-precipitated calcium oxalate with vanillin within DEs. DEs loaded with 13 mM vanillin and 250 mM oxalic acid are incubated in aqueous solutions containing $CaCl_2$ with concentrations varying between 100 – 325 mM. Note that emulsions with higher vanillin concentrations were also produced yet, their stability is compromised upon incubation. Dendritic calcium oxalate crystals formed within DEs that were incubated in aqueous solutions containing 325 mM $CaCl_2$ for 20 h. By contrast, lower calcium concentrations resulted in the formation of single monoclinic prismatic crystals with sizes around 5 μm . This difference in morphology could be attributed to the presence of vanillin that acts as crystallization inhibitor and hence, decreases the nucleation or growth rate. The optical images strongly suggest that both dendritic and monoclinic prismatic crystals are composed of calcium oxalate monohydrate [202], yet the structure of these crystals has to be confirmed with scattering experiments.

5.5 Conclusion

Organic and inorganic crystals can be produced controllably in emulsion drops. Drops with a narrow size distribution formed with microfluidics present a confined environment that enables a controllable formation of crystals. Double emulsions are more stable than single emulsions such that they offer more flexibility in tuning the crystallization conditions. However, the amount of crystals formed within emulsions is small, thereby making the characterization of these crystals tedious.

6 Conclusion

Drop-templated crystallization can be a powerful technique to mimic the confinement under which many biogenic crystals and biominerals form. In particular, drops enable to systematically vary individual crystallization parameters and study their effect on the crystallization. In this thesis, I used drops to study the formation of micro- and nanoparticles that can be used as matrix materials for the encapsulation of volatile actives.

The crystallization within picoliter-sized drops is slower than in the bulk due to the confinement effect and the reduced risk for impurities that can influence the crystallization. Therefore, drops allow monitoring the early crystallization stages, which are very challenging to access through bulk crystallization. Depending on the fabrication method, the produced drops show variable size distributions. If drops can rapidly be dried, they can be used to control crystallization of the solutes within them. The time crystals have to form within drying drops can be tuned with the drop size, initial solute concentration and choice of solvent. In this thesis, I use a microfluidic SAW-based spray-dryer to produce tiny airborne drops with diameters of only a few micrometers out of solutions containing reagents that form crystalline nanoparticles once the solvent is evaporated. Through this technique I demonstrate that the structure and the structural stability during storage of a model low molecular weight organic matrix material, succinic acid, strongly depends on its processing conditions. SAW-based spray-drying enables the formulation of succinic acid into the metastable phase without the need for any crystallization inhibiting additives. These findings open up new possibilities to tune the dissolution kinetics of matrix materials composed of low molecular weight organic compounds.

Once the important processing parameters are determined, they can be applied to formulate novel materials such as high density matrices that have the potential to possess a low permeability even towards volatile substances. Organic crystals that have a high propensity to crystallize such as succinic acid are well-suited matrix materials for volatiles as they are typically composed of densely packed molecules that have a low permeability towards volatile substances such that they retain them for a prolonged time. This concept is not limited to succinic acid but can be expanded to other organic low molecular weight substances such as tartaric acid and liquid volatiles. These findings open up new possibilities to tune the encapsulation efficiency and release kinetics of volatile substances not only through the composition of the matrix material but also through its processing.

In summary, microfluidic spray-drying is a tool that can be used to formulate crystals possessing well-defined and tunable structures that might enable new applications. I showed the feasibility to use succinic acid as a matrix material for the encapsulation of vanillin, a model volatile substance. However, I deem my system to be much more generally applicable. For example, I consider it to be well suited to study the drug polymorphism, and overcome the pharmaceutical challenges such as phase separation of drugs and excipients. Compared to the other encapsulants, volatiles are difficult to retain, hence, I foresee crystalline capsules composed of low molecular weight substances to be well suited encapsulation materials for such compounds.

The studies in this thesis can be further advanced if the present technical challenges are addressed. For instance, the collection of nanoparticles requires an advanced collection system, since the nanoparticle impaction to any substrate is very limiting, making their characterization challenging. Obviously, this issue does not apply to industrial scale applications, as such collectors are already present. Therefore, the coupling of the SAW-based nebulization to nanospray-drying systems could increase the collection yield and thereby enable us to deepen our understanding on the influence of processing parameters on the structure of spray dried particles and screen further parameters such as temperature or even pressure. Another challenge is the characterization of porosity in these particles. The porosity of succinic acid particles containing vanillin must be further characterized. The characterization of phase separation on particles via imaging techniques such as TEM were challenging due to the sensitivity of organic crystals to the electron beam and the low contrast between organic crystals and volatile moieties. Therefore, with more advanced

characterization tools, crystallization mechanisms could be further elucidated for example using the platform I employed, which eventually could open up new possibilities to produce materials that display a performance that is similar to natural counterparts.

A different approach to use of drops to control the crystallization of solutes within them is to confine crystallization within emulsions. If microfluidics is used, monodisperse emulsions with diameters of 100 μm can be formed. Within these drops, I produced crystals with sizes up to 20 μm . Single emulsion water in oil drops have a limited stability especially if the aqueous phase contains a high concentration of ions or extreme pHs, conditions which are frequently met during crystallization. To overcome this limitation, I employed double emulsions that are more stable than single emulsions. However, the amount of crystals formed within emulsions is small, thereby making the characterization of these crystals tedious.

Bibliography

- [1] Gur, D., Palmer, B. A., Weiner, S. & Addadi, L. Light Manipulation by Guanine Crystals in Organisms: Biogenic Scatterers, Mirrors, Multilayer Reflectors and Photonic Crystals. *Advanced Functional Materials* **27**, 1603514 (2017).
- [2] Palmer, B. A. *et al.* A highly reflective biogenic photonic material from core-shell birefringent nanoparticles. *Nature Nanotechnology* **15**, 138–144 (2020).
- [3] Palyanov, Y. N., Kupriyanov, I. N., Khokhryakov, A. F. & Borzdov, Y. M. High-pressure crystallization and properties of diamond from magnesium-based catalysts. *CrystEngComm* **19**, 4459–4475 (2017).
- [4] Flicker, F., Eberle, V. A. & Betz, G. Recrystallization of commercial carbamazepine samples-a strategy to control dissolution variability. *Pharmaceutics* **4**, 58–70 (2012).
- [5] Pudipeddi, M. & Serajuddin, A. T. Trends in Solubility of Polymorphs. *Journal of Pharmaceutical Sciences* **94**, 929–939 (2005).
- [6] Savjani, K. T., Gajjar, A. K. & Savjani, J. K. Drug Solubility: Importance and Enhancement Techniques. *ISRN Pharmaceutics* **2012**, 195727 (2012).
- [7] Cantaert, B., Beniash, E. & Meldrum, F. C. Nanoscale Confinement Controls the Crystallization of Calcium Phosphate: Relevance to Bone Formation. *Chemistry – A European Journal* **19**, 14918–14924 (2013).
- [8] Dorozhkin, S. V. Nanodimensional and Nanocrystalline Apatites and Other Calcium Orthophosphates in Biomedical Engineering, Biology and Medicine. *Materials* **2**, 1975–2045 (2009).

Bibliography

- [9] Posner, A. S. & Betts, F. Synthetic amorphous calcium phosphate and its relation to bone mineral structure. *Accounts of Chemical Research* **8**, 273–281 (1975).
- [10] Majeed, H. *et al.* Essential oil encapsulations: Uses, procedures, and trends. *RSC Advances* **5**, 58449–58463 (2015).
- [11] Kale, R., Kadam, P. & Hashmi, S. Effect of different varieties of date palm paste incorporation on quality characteristics of yoghurt. *Carpathian J Food Sci Technol* **3**, 28–38 (2011).
- [12] Li, Y. *et al.* Properties of Chitosan-Microencapsulated Orange Oil Prepared by Spray-Drying and Its Stability to Detergents. *Journal of Agricultural and Food Chemistry* **61**, 3311–3319 (2013).
- [13] Yazar, K., Johnsson, S., Lind, M.-L., Boman, A. & Lidén, C. Preservatives and fragrances in selected consumer-available cosmetics and detergents. *Contact Dermatitis* **64**, 265–272 (2011).
- [14] Sharkawy, A., Fernandes, I. P., Barreiro, M. F., Rodrigues, A. E. & Shoeib, T. Aroma-Loaded Microcapsules with Antibacterial Activity for Eco-Friendly Textile Application: Synthesis, Characterization, Release, and Green Grafting. *Industrial & Engineering Chemistry Research* **56**, 5516–5526 (2017).
- [15] Zhao, D. *et al.* Preparation of high encapsulation efficiency fragrance microcapsules and their application in textiles. *RSC Advances* **6**, 80924–80933 (2016).
- [16] Ghayempour, S. & Montazer, M. Micro/nanoencapsulation of essential oils and fragrances: Focus on perfumed, antimicrobial, mosquito-repellent and medical textiles. *Journal of Microencapsulation* **33**, 497–510 (2016).
- [17] Chranioti, C. & Tzia, C. Arabic Gum Mixtures as Encapsulating Agents of Freeze-Dried Fennel Oleoresin Products. *Food and Bioprocess Technology* **7**, 1057–1065 (2014).
- [18] Gabas, A., Telis, V., Sobral, P. & Telis-Romero, J. Effect of maltodextrin and arabic gum in water vapor sorption thermodynamic properties of vacuum dried pineapple pulp powder. *Journal of Food Engineering* **82**, 246–252 (2007).

-
- [19] Ahmed, A. A. 16 - Health Benefits of Gum Arabic and Medical Use. In Mariod, A. A. (ed.) *Gum Arabic*, 183–210 (Academic Press, 2018).
- [20] McNamee, B. F., O’Riorda, E. D. & O’Sullivan, M. Effect of Partial Replacement of Gum Arabic with Carbohydrates on Its Microencapsulation Properties. *Journal of Agricultural and Food Chemistry* **49**, 3385–3388 (2001).
- [21] Chavan, R., Khedkar, C. & Bhatt, S. Fat Replacer. In Caballero, B., Finglas, P. M. & Toldrá, F. (eds.) *Encyclopedia of Food and Health*, 589–595 (Academic Press, Oxford, 2016).
- [22] Yoshii, H. *et al.* Flavor release from spray-dried maltodextrin/gum arabic or soy matrices as a function of storage relative humidity. *Innovative Food Science & Emerging Technologies* **2**, 55–61 (2001).
- [23] Siccama, J. W. *et al.* Maltodextrin improves physical properties and volatile compound retention of spray-dried asparagus concentrate. *LWT* **142**, 111058 (2021).
- [24] Klinjapo, R. & Krasaekoopt, W. Chapter 14 - Microencapsulation of Color and Flavor in Confectionery Products. In Grumezescu, A. M. & Holban, A. M. (eds.) *Natural and Artificial Flavoring Agents and Food Dyes*, 457–494 (Academic Press, 2018).
- [25] Hung, S. & Zayas, J. Emulsifying Capacity and Emulsion Stability of Milk Proteins and Corn Germ Protein Flour. *Journal of Food Science* **56**, 1216–1218 (1991).
- [26] Wang, S., Langrish, T. & Leszczynski, M. The Effect of Casein as a Spray-Drying Additive on the Sorption and Crystallization Behavior of Lactose. *Drying Technology* **28**, 422–429 (2010).
- [27] Huppertz, T. & Gazi, I. Lactose in dairy ingredients: Effect on processing and storage stability¹. *Journal of Dairy Science* **99**, 6842–6851 (2016).
- [28] Rehman, A. *et al.* Pectin polymers as wall materials for the nano-encapsulation of bioactive compounds. *Trends in Food Science & Technology* **90**, 35–46 (2019).
- [29] Carneiro, H. C. F., Tonon, R. V., Grosso, C. R. F. & Hubinger, M. D. Encapsulation efficiency and oxidative stability of flaxseed oil microencapsulated

- by spray drying using different combinations of wall materials. *Journal of Food Engineering* **115**, 443–451 (2013).
- [30] Charve, J. & Reineccius, G. A. Encapsulation Performance of Proteins and Traditional Materials for Spray Dried Flavors. *Journal of Agricultural and Food Chemistry* **57**, 2486–2492 (2009).
- [31] Crittenden, R. G. & Bennett, L. E. Cow’s milk allergy: A complex disorder. *Journal of the American College of Nutrition* **24**, 582S–591S (2005).
- [32] Misselwitz, B. *et al.* Lactose malabsorption and intolerance: Pathogenesis, diagnosis and treatment. *United European gastroenterology journal* **1**, 151–159 (2013).
- [33] Lee, P. W. & Pokorski, J. K. Poly(lactic-co-glycolic acid) devices: Production and applications for sustained protein delivery. *Wiley interdisciplinary reviews. Nanomedicine and nanobiotechnology* 10.1002/wnan.1516 (2018).
- [34] Zhu, Z., Min, T., Zhang, X. & Wen, Y. Microencapsulation of Thymol in Poly(lactide-co-glycolide) (PLGA): Physical and Antibacterial Properties. *Materials* **12** (2019).
- [35] Ephrem, E., Greige-Gerges, H., Fessi, H. & Charcosset, C. Optimisation of rosemary oil encapsulation in polycaprolactone and scale-up of the process. *Journal of Microencapsulation* **31**, 746–753 (2014).
- [36] Hu, J. *et al.* Preparation of polybutylcyanoacrylate encapsulated rose fragrance nanocapsule. *Gongneng Cailiao/Journal of Functional Materials* **41**, 225–228 (2010).
- [37] Jacquemond, M., Jeckelmann, N., Ouali, L. & Haeffliger, O. P. Perfume-containing polyurea microcapsules with undetectable levels of free isocyanates. *Journal of Applied Polymer Science* **114**, 3074–3080 (2009).
- [38] Bruyninckx, K. & Dusselier, M. Sustainable Chemistry Considerations for the Encapsulation of Volatile Compounds in Laundry-Type Applications. *ACS Sustainable Chemistry & Engineering* **7**, 8041–8054 (2019).
- [39] Kundu, J., Pati, F., Hun Jeong, Y. & Cho, D.-W. Chapter 2 - Biomaterials for Biofabrication of 3D Tissue Scaffolds. In Forgacs, G. & Sun, W. (eds.) *Biofabrication*, 23–46 (William Andrew Publishing, Boston, 2013).

- [40] Fujiwara, M., Shiokawa, K., Morigaki, K., Zhu, Y. & Nakahara, Y. Calcium carbonate microcapsules encapsulating biomacromolecules. *Chemical Engineering Journal* **137**, 14–22 (2008).
- [41] Wang, J.-X., Wang, Z.-H., Chen, J.-F. & Yun, J. Direct encapsulation of water-soluble drug into silica microcapsules for sustained release applications. *Materials Research Bulletin* **43**, 3374–3381 (2008).
- [42] Radulova, G. M. *et al.* Encapsulation of oils and fragrances by core-in-shell structures from silica particles, polymers and surfactants: The brick-and-mortar concept. *Colloids and Surfaces A: Physicochemical and Engineering Aspects* **559**, 351–364 (2018).
- [43] Pagliaro, M. *Silica-Based Materials for Advanced Chemical Applications* (The Royal Society of Chemistry, 2009).
- [44] Ciriminna, R. & Pagliaro, M. Sol–gel microencapsulation of odorants and flavors: Opening the route to sustainable fragrances and aromas. *Chemical Society Reviews* **42**, 9243–9250 (2013).
- [45] Sillick, M. & Gregson, C. M. Spray chill encapsulation of flavors within anhydrous erythritol crystals. *LWT - Food Science and Technology* **48**, 107–113 (2012).
- [46] Kim, A. I., Akers, M. J. & Nail, S. L. The Physical State of Mannitol after Freeze-Drying: Effects of Mannitol Concentration, Freezing Rate, and a Noncrystallizing Cosolute. *Journal of Pharmaceutical Sciences* **87**, 931–935 (1998).
- [47] Dimick, K. P. & Benjamin, M. Process for preparing a solid flavoring composition (1959).
- [48] Kanig, J. L. Properties of Fused Mannitol in Compressed Tablets. *Journal of Pharmaceutical Sciences* **53**, 188–192 (1964).
- [49] Zajc, N., Obreza, A., Bele, M. & Srčič, S. Physical properties and dissolution behaviour of nifedipine/mannitol solid dispersions prepared by hot melt method. *Proceedings of the 5th Central European Symposium on Pharmaceutical Technology and Biotechnology* **291**, 51–58 (2005).

Bibliography

- [50] Martínez-Frías, M. L. The thalidomide experience: Review of its effects 50 years later. *Medicina clínica* **139**, 25–32 (2011).
- [51] Censi, R. & Di Martino, P. Polymorph Impact on the Bioavailability and Stability of Poorly Soluble Drugs. *Molecules (Basel, Switzerland)* **20**, 18759–18776 (2015).
- [52] Rodriguez-Aller, M., Guillarme, D., Veuthey, J.-L. & Gurny, R. Strategies for formulating and delivering poorly water-soluble drugs. *In Honor of Prof. Dominique Duchêne* **30**, 342–351 (2015).
- [53] Aguiar, A. J., Krc Jr, J., Kinkel, A. W. & Samyn, J. C. Effect of polymorphism on the absorption of chloramphenicol from chloramphenicol palmitate. *Journal of pharmaceutical sciences* **56**, 847–853 (1967).
- [54] Aggarwal, M. D., Wang, W. S., Shields, A. W., Penn, B. G. & Frazier, D. O. A versatile low-cost Czochralski crystal growth system for nonlinear optical organic materials. *Review of scientific instruments* **63**, 5481–5482 (1992).
- [55] Zellnitz, S., Narygina, O., Resch, C., Schroettner, H. & Urbanetz, N. A. Crystallization speed of salbutamol as a function of relative humidity and temperature. *International Journal of Pharmaceutics* **489**, 170–176 (2015).
- [56] Fan, Z. & Zhang, H. Crystal phase-controlled synthesis, properties and applications of noble metal nanomaterials. *Chemical Society Reviews* **45**, 63–82 (2016).
- [57] Yadav, V. K. *et al.* Synthesis and Characterization of Amorphous Iron Oxide Nanoparticles by the Sonochemical Method and Their Application for the Remediation of Heavy Metals from Wastewater. *Nanomaterials* **10**, 1551 (2020).
- [58] Cölfen, H. & Mann, S. Higher-Order Organization by Mesoscale Self-Assembly and Transformation of Hybrid Nanostructures. *Angewandte Chemie International Edition* **42**, 2350–2365 (2003).
- [59] Sear, R. P. The non-classical nucleation of crystals: Microscopic mechanisms and applications to molecular crystals, ice and calcium carbonate. *International Materials Reviews* **57**, 328–356 (2012).

-
- [60] Meldrum, F. C. & Cölfen, H. Controlling Mineral Morphologies and Structures in Biological and Synthetic Systems. *Chemical Reviews* **108**, 4332–4432 (2008).
- [61] Lee, J., Yang, J., Kwon, S. G. & Hyeon, T. Nonclassical nucleation and growth of inorganic nanoparticles. *Nature Reviews Materials* **1**, 16034 (2016).
- [62] De Yoreo, J. J. *et al.* Crystallization by particle attachment in synthetic, biogenic, and geologic environments. *Science* **349** (2015).
- [63] Zhang, H. *et al.* Pressure-controlled crystallization of stereocomplex crystals in enantiomeric polylactides with remarkably enhanced hydrolytic degradation. *CrystEngComm* **20**, 7337–7347 (2018).
- [64] Suzuki, Y. *et al.* Protein crystallization under high pressure. *Biochimica et Biophysica Acta (BBA) - Protein Structure and Molecular Enzymology* **1595**, 345–356 (2002).
- [65] Neumann, M. A., van de Streek, J., Fabbiani, F. P. A., Hidber, P. & Grassmann, O. Combined crystal structure prediction and high-pressure crystallization in rational pharmaceutical polymorph screening. *Nature Communications* **6**, 7793 (2015).
- [66] Ostrowska, K., Kropidłowska, M. & Katrusiak, A. High-Pressure Crystallization and Structural Transformations in Compressed R,S-Ibuprofen. *Crystal Growth & Design* **15**, 1512–1517 (2015).
- [67] Chan, H. K. & Doelker, E. Polymorphic Transformation of Some Drugs Under Compression. *Drug Development and Industrial Pharmacy* **11**, 315–332 (1985).
- [68] Judge, R. A., Jacobs, R. S., Frazier, T., Snell, E. H. & Pusey, M. L. The Effect of Temperature and Solution pH on the Nucleation of Tetragonal Lysozyme Crystals. *Biophysical Journal* **77**, 1585–1593 (1999).
- [69] Falini, G., Albeck, S., Weiner, S. & Addadi, L. Control of aragonite or calcite polymorphism by mollusk shell macromolecules. *Science* **271**, 67–69 (1996).
- [70] Ma, Y. R., Weiner, S. & Addadi, L. Mineral Deposition and Crystal Growth in the Continuously Forming Teeth of Sea Urchins. *Advanced Functional Materials* **17**, 2693–2700 (2007).

Bibliography

- [71] Kim, D., Lee, B., Thomopoulos, S. & Jun, Y.-S. The role of confined collagen geometry in decreasing nucleation energy barriers to intrafibrillar mineralization. *Nature Communications* **9**, 962 (2018).
- [72] Meldrum, F. C. & O'Shaughnessy, C. Crystallization in Confinement. *Advanced Materials* **32**, 2001068 (2020).
- [73] Ishimoto, T., Nakano, T., Umakoshi, Y., Yamamoto, M. & Tabata, Y. Degree of biological apatite c-axis orientation rather than bone mineral density controls mechanical function in bone regenerated using recombinant bone morphogenetic protein-2. *Journal of Bone and Mineral Research* **28**, 1170–1179 (2013).
- [74] Gur, D. *et al.* Guanine Crystallization in Aqueous Solutions Enables Control over Crystal Size and Polymorphism. *Crystal Growth & Design* **16**, 4975–4980 (2016).
- [75] Levy-Lior, A. *et al.* Guanine-Based Biogenic Photonic-Crystal Arrays in Fish and Spiders. *Advanced Functional Materials* **20**, 320–329 (2010).
- [76] Palmer Benjamin A. *et al.* The image-forming mirror in the eye of the scallop. *Science* **358**, 1172–1175 (2017).
- [77] Funt, N., Palmer, B. A., Weiner, S. & Addadi, L. Koi Fish-Scale Iridophore Cells Orient Guanine Crystals to Maximize Light Reflection. *ChemPlusChem* **82**, 914–923 (2017).
- [78] Takiyama, H. Nucleation and Crystal Growth in Limited Crystallization Field. In Tamura, R. & Miyata, M. (eds.) *Advances in Organic Crystal Chemistry: Comprehensive Reviews 2015*, 55–72 (Springer Japan, Tokyo, 2015).
- [79] Capper, P. Bulk Crystal Growth – Methods and Materials. In Kasap, S. & Capper, P. (eds.) *Springer Handbook of Electronic and Photonic Materials*, 231–254 (Springer US, Boston, MA, 2007).
- [80] Darr, J. A., Zhang, J., Makwana, N. M. & Weng, X. Continuous hydrothermal synthesis of inorganic nanoparticles: Applications and future directions. *Chemical reviews* **117**, 11125–11238 (2017).

-
- [81] Demirer, G. S., Okur, A. C. & Kizilel, S. Synthesis and design of biologically inspired biocompatible iron oxide nanoparticles for biomedical applications. *Journal of Materials Chemistry B* **3**, 7831–7849 (2015).
- [82] Scheel, H. J. Historical aspects of crystal growth technology. *Journal of Crystal Growth* **211**, 1–12 (2000).
- [83] Feng, S.-H. & Li, G.-H. Chapter 4 - Hydrothermal and Solvothermal Syntheses. In Xu, R. & Xu, Y. (eds.) *Modern Inorganic Synthetic Chemistry (Second Edition)*, 73–104 (Elsevier, Amsterdam, 2017).
- [84] Grey, J. L. & Thompson, D. H. Challenges and opportunities for new protein crystallization strategies in structure-based drug design. *Expert opinion on drug discovery* **5**, 1039–1045 (2010).
- [85] Snell, E. H. *et al.* Optimizing crystal volume for neutron diffraction: D-xylose isomerase. *European Biophysics Journal* **35**, 621–632 (2006).
- [86] Chayen, N. E. Comparative studies of protein crystallization by vapour-diffusion and microbatch techniques. *Acta Crystallographica Section D: Biological Crystallography* **54**, 8–15 (1998).
- [87] Ward, K. & Fan, Z. H. Mixing in microfluidic devices and enhancement methods. *Journal of micromechanics and microengineering : structures, devices, and systems* **25**, 094001 (2015).
- [88] Zeng, Y. *et al.* Insights into the Confined Crystallization in Microfluidics of Amorphous Calcium Carbonate. *Crystal Growth & Design* **18**, 6538–6546 (2018).
- [89] Grossier, R., Tishkova, V., Morin, R. & Veessler, S. A parameter to probe microdroplet dynamics and crystal nucleation. *AIP Advances* **8**, 075324 (2018).
- [90] Cavanaugh, J., Whittaker, M. L. & Joester, D. Crystallization kinetics of amorphous calcium carbonate in confinement. *Chemical Science* **10**, 5039–5043 (2019).
- [91] Zheng, B., Tice, J. D., Roach, L. S. & Ismagilov, R. F. A droplet-based, composite PDMS/glass capillary microfluidic system for evaluating protein crystallization conditions by microbatch and vapor-diffusion methods with

- on-chip X-ray diffraction. *Angewandte chemie international edition* **43**, 2508–2511 (2004).
- [92] Zou, Z. *et al.* On the Phase Diagram of Calcium Carbonate Solutions. *Advanced Materials Interfaces* **4**, 1600076 (2017).
- [93] Juarez-Martinez, G. Macromolecular Crystallization Using Nano-volumes. In Bhushan, B. (ed.) *Encyclopedia of Nanotechnology*, 1235–1248 (Springer Netherlands, Dordrecht, 2012).
- [94] Du, W., Li, L., Nichols, K. P. & Ismagilov, R. F. SlipChip. *Lab on a Chip* **9**, 2286–2292 (2009).
- [95] Perry, S. L., Roberts, G. W., Tice, J. D., Gennis, R. B. & Kenis, P. J. A. Microfluidic Generation of Lipidic Mesophases for Membrane Protein Crystallization. *Crystal Growth & Design* **9**, 2566–2569 (2009).
- [96] Du, H. *et al.* Amorphous CaCO₃: Influence of the Formation Time on Its Degree of Hydration and Stability. *Journal of the American Chemical Society* **140**, 14289–14299 (2018).
- [97] Shi, H.-h. *et al.* Progress of crystallization in microfluidic devices. *Lab on a Chip* **17**, 2167–2185 (2017).
- [98] Wang, J., Cao, W., Wang, J. & Zhu, L. A novel Spherical Crystallization Method Using Pickering Emulsions. *Journal of Pharmaceutical Sciences* (2021).
- [99] Wang, X., Wang, S.-J., Nan, Y. & Liu, G.-Q. The effects of oil type and crystallization temperature on the physical properties of vitamin C-loaded oleogels prepared by an emulsion-templated approach. *Food & Function* **11**, 8028–8037 (2020).
- [100] Kashchiev, D., Kaneko, N. & Sato, K. Kinetics of Crystallization in Poly-disperse Emulsions. *Journal of Colloid and Interface Science* **208**, 167–177 (1998).
- [101] Zhu, D., Zhou, X. & Zheng, B. A Double Emulsion-Based, Plastic-Glass Hybrid Microfluidic Platform for Protein Crystallization. *Micromachines* **6**, 1629–1644 (2015).

-
- [102] Akella, S. V., Mowitz, A., Heymann, M. & Fraden, S. Emulsion-Based Technique To Measure Protein Crystal Nucleation Rates of Lysozyme. *Crystal Growth & Design* **14**, 4487–4509 (2014).
- [103] Li, N. *et al.* Water-Induced Phase Separation of Spray-Dried Amorphous Solid Dispersions. *Molecular pharmaceuticals* **17**, 4004–4017 (2020).
- [104] Lucaioli, P. *et al.* Serendipitous isolation of a disappearing conformational polymorph of succinic acid challenges computational polymorph prediction. *CrystEngComm* **20**, 3971–3977 (2018).
- [105] Kessler, M. *et al.* Everything in its right place: Controlling the local composition of hydrogels using microfluidic traps. *Lab on a Chip* **20**, 4572–4581 (2020).
- [106] Dangla, R., Lee, S. & Baroud, C. N. Trapping microfluidic drops in wells of surface energy. *Physical review letters* **107**, 124501 (2011).
- [107] Gregson, F. K. A., Robinson, J. F., Miles, R. E. H., Royall, C. P. & Reid, J. P. Drying and Crystallization of Evaporating Sodium Nitrate Aerosol Droplets. *The Journal of Physical Chemistry B* **124**, 6024–6036 (2020).
- [108] Hudait, A. & Molinero, V. Ice Crystallization in Ultrafine Water–Salt Aerosols: Nucleation, Ice–Solution Equilibrium, and Internal Structure. *Journal of the American Chemical Society* **136**, 8081–8093 (2014).
- [109] Bertoni, S., Dolci, L. S., Albertini, B. & Passerini, N. Spray congealing: A versatile technology for advanced drug-delivery systems. *Therapeutic Delivery* **9**, 833–845 (2018).
- [110] Wagner, R., Höhler, K., Möhler, O., Saathoff, H. & Schnaiter, M. Crystallization and immersion freezing ability of oxalic and succinic acid in multicomponent aqueous organic aerosol particles. *Geophysical Research Letters* **42**, 2464–2472 (2015).
- [111] Madene, A., Jacquot, M., Scher, J. & Desobry, S. Flavour encapsulation and controlled release – a review. *International Journal of Food Science & Technology* **41**, 1–21 (2006).
- [112] Henao, J. *et al.* Deposition mechanisms of metallic glass particles by Cold Gas Spraying. *Acta Materialia* **125**, 327–339 (2017).

Bibliography

- [113] Sun, C., Zhou, X. & Xie, C. Effect of processing conditions on Al-based amorphous/nanocrystalline coating by cold-spraying. *Surface and Coatings Technology* **362**, 97–104 (2019).
- [114] Nguyen, D. N., Clasen, C. & Van den Mooter, G. Pharmaceutical Applications of Electrospraying. *Journal of Pharmaceutical Sciences* **105**, 2601–2620 (2016).
- [115] Radacsi, N., Stankiewicz, A. I., Creighton, Y. L. M., van der Heijden, A. E. D. M. & ter Horst, J. H. Electrospray Crystallization for High-Quality Submicron-Sized Crystals. *Chemical Engineering & Technology* **34**, 624–630 (2011).
- [116] Wang, M., Rutledge, G. C., Myerson, A. S. & Trout, B. L. Production and Characterization of Carbamazepine Nanocrystals by Electrospraying for Continuous Pharmaceutical Manufacturing. *Journal of Pharmaceutical Sciences* **101**, 1178–1188 (2012).
- [117] Radacsi, N. *et al.* Electrospray Crystallization for Nanosized Pharmaceuticals with Improved Properties. *Crystal Growth & Design* **12**, 3514–3520 (2012).
- [118] De La Mora, J. F. & Loscertales, I. G. The current emitted by highly conducting Taylor cones. *Journal of Fluid Mechanics* **260**, 155–184 (1994).
- [119] Perge, L. *et al.* Concurrent Antisolvent Electrospraying: A Novel Continuous Crystallization Technique. *Journal of Pharmaceutical Sciences* **109**, 3027–3034 (2020).
- [120] Xiao, Z., Liu, W., Zhu, G., Zhou, R. & Niu, Y. A review of the preparation and application of flavour and essential oils microcapsules based on complex coacervation technology. *Journal of the Science of Food and Agriculture* **94**, 1482–1494 (2014).
- [121] Shrestha, M., Ho, T. M. & Bhandari, B. R. Encapsulation of tea tree oil by amorphous beta-cyclodextrin powder. *Food Chemistry* **221**, 1474–1483 (2017).
- [122] Abd Manaf, M., Jai, J., Raslan, R., Subuki, I. & Mustapa, A. N. Microencapsulation Methods of Volatile Essential Oils - A Review. In *Material Science Technology and Global Sustainability*, vol. 1113 of *Advanced Materials Research*, 679–683 (Trans Tech Publications Ltd, 2015).

-
- [123] Ali, H., Al-Khalifa, A. R., Aouf, A., Boukhebt, H. & Farouk, A. Effect of nanoencapsulation on volatile constituents, and antioxidant and anticancer activities of Algerian *Origanum glandulosum* Desf. essential oil. *Scientific Reports* **10**, 2812 (2020).
- [124] Yang, G. *et al.* Comparison of Effects of Sodium Chloride and Potassium Chloride on Spray Drying and Redispersion of Cellulose Nanofibrils Suspension. *Nanomaterials* **11**, 439 (2021).
- [125] Sinquefeld, S., Ciesielski, P. N., Li, K., Gardner, D. J. & Ozcan, S. Nanocellulose Dewatering and Drying: Current State and Future Perspectives. *ACS Sustainable Chemistry & Engineering* **8**, 9601–9615 (2020).
- [126] Arpagaus, C., John, P., Collenberg, A. & Ruetli, D. Nanocapsules formation by nano spray drying. In *Nanoencapsulation Technologies for the Food and Nutritional Industries*, 346–401 (2017).
- [127] Al-Zoubi, N., Gharaibeh, S., Aljaberi, A. & Nikolakakis, I. Spray Drying for Direct Compression of Pharmaceuticals. *Processes* **9** (2021).
- [128] Al-Zoubi, N., Odeh, F. & Nikolakakis, I. Co-spray drying of metformin hydrochloride with polymers to improve compaction behavior. *Powder technology* **307**, 163–174 (2017).
- [129] Ullah, M., Hussain, I. & Sun, C. C. The development of carbamazepine-succinic acid cocrystal tablet formulations with improved in vitro and in vivo performance. *Drug Development and Industrial Pharmacy* **42**, 969–976 (2016).
- [130] Chistyakov, D. & Sergeev, G. The Polymorphism of Drugs: New Approaches to the Synthesis of Nanostructured Polymorphs. *Pharmaceutics* **12**, 34 (2020).
- [131] Santos, D. *et al.* Spray Drying: An Overview (2018).
- [132] Woo, M. & Bhandari, B. 2 - Spray drying for food powder production. In Bhandari, B., Bansal, N., Zhang, M. & Schuck, P. (eds.) *Handbook of Food Powders*, 29–56 (Woodhead Publishing, 2013).
- [133] Arpagaus, C. & Meuri, M. Laboratory scale spray drying of inhalable particles: A review. *Respiratory Drug Delivery* 469–473 (2010).

Bibliography

- [134] Desobry, S. A., Netto, F. M. & Labuza, T. P. Comparison of Spray-drying, Drum-drying and Freeze-drying for β -Carotene Encapsulation and Preservation. *Journal of Food Science* **62**, 1158–1162 (1997).
- [135] Garti, N. & McClements, D. J. *Encapsulation Technologies and Delivery Systems for Food Ingredients and Nutraceuticals* (Elsevier, 2012).
- [136] Lisboa, H. M., Duarte, M. E. & Cavalcanti-Mata, M. E. Modeling of food drying processes in industrial spray dryers. *Food and Bioproducts Processing* **107**, 49–60 (2018).
- [137] Wisniewski, R. S. Spray drying technology review (2015).
- [138] Licht, S. Chapter 5 - Fermentation for Biofuels and Bio-Based Chemicals. In Vogel, H. C. & Todaro, C. M. (eds.) *Fermentation and Biochemical Engineering Handbook (Third Edition)*, 59–82 (William Andrew Publishing, Boston, 2014).
- [139] Dobry, D. E. *et al.* A Model-Based Methodology for Spray-Drying Process Development. *Journal of Pharmaceutical Innovation* **4**, 133–142 (2009).
- [140] Arpagaus, C. Pharmaceutical Particle Engineering via Nano Spray Drying-Process Parameters and Application Examples on the Laboratory-Scale 26 (2019).
- [141] Arpagaus, C., Collenberg, A., Rütli, D., Assadpour, E. & Jafari, S. M. Nano spray drying for encapsulation of pharmaceuticals. *International Journal of Pharmaceutics* **546**, 194–214 (2018).
- [142] Moon, S.-H. *et al.* Effects of Driving Frequency and Voltage on the Performances of Vibrating Mesh Nebulizers. *Applied Sciences* **11** (2021).
- [143] Schmid, K., Arpagaus, C. & Friess, W. Evaluation of a vibrating mesh spray dryer for preparation of submicron particles. *Respiratory Drug Delivery Europe* **30**, 323–326 (2009).
- [144] Merchant, Z. *et al.* Engineering hydrophobically modified chitosan for enhancing the dispersion of respirable microparticles of levofloxacin. *European Journal of Pharmaceutics and Biopharmaceutics* **88**, 816–829 (2014).

-
- [145] Okuyama, K., Abdullah, M., Wuled Lenggoro, I. & Iskandar, F. Preparation of functional nanostructured particles by spray drying. *Advanced Powder Technology* **17**, 587–611 (2006).
- [146] Campbell, C. *Surface Acoustic Wave Devices and Their Signal Processing Applications* (Elsevier, 2012).
- [147] Qi, A., Yeo, L. Y. & Friend, J. R. Interfacial destabilization and atomization driven by surface acoustic waves. *Physics of Fluids* **20**, 074103 (2008).
- [148] Lang, R. J. Ultrasonic Atomization of Liquids. *The Journal of the Acoustical Society of America* **34**, 6–8 (1962).
- [149] Steinacher, M., Du, H., Gilbert, D. & Amstad, E. Production of Additive-Free Amorphous Nanoparticles with a SAW-Based Microfluidic Spray-Dryer. *Advanced Materials Technologies* **4**, 1800665 (2019).
- [150] M. S. Kharusi & G. W. Farnell. On diffraction and focusing in anisotropic crystals. *Proceedings of the IEEE* **60**, 945–956 (1972).
- [151] Xia, Y. & Whitesides, G. M. SOFT LITHOGRAPHY. *Annual Review of Materials Science* **28**, 153–184 (1998).
- [152] Nogueira, B. A., Castiglioni, C. & Fausto, R. Color polymorphism in organic crystals. *Communications Chemistry* **3**, 34 (2020).
- [153] Li, X. *et al.* Rich polymorphism in nicotinamide revealed by melt crystallization and crystal structure prediction. *Communications Chemistry* **3**, 152 (2020).
- [154] Cavallini, M. *et al.* Lithographic Alignment of Discotic Liquid Crystals: A New Time–Temperature Integrating Framework. *Advanced Materials* **21**, 4688–4691 (2009).
- [155] Hildebrandt, L., Dinnebier, R. & Jansen, M. Crystal Structure and Ionic Conductivity of Three Polymorphic Phases of Rubidium Trifluoromethyl Sulfonate, RbSO₃CF₃. *Inorganic Chemistry* **45**, 3217–3223 (2006).
- [156] Sobczak, S., Ratajczyk, P. & Katrusiak, A. High-pressure Nucleation of Low-Density Polymorphs**. *Chemistry – A European Journal* **27**, 7069–7073 (2021).

Bibliography

- [157] Löbmann, K., Grohgan, H., Laitinen, R., Strachan, C. & Rades, T. Amino acids as co-amorphous stabilizers for poorly water soluble drugs–Part 1: Preparation, stability and dissolution enhancement. *European journal of pharmaceuticals and biopharmaceutics* **85**, 873–881 (2013).
- [158] Jensen, K. T., Löbmann, K., Rades, T. & Grohgan, H. Improving co-amorphous drug formulations by the addition of the highly water soluble amino acid, proline. *Pharmaceutics* **6**, 416–435 (2014).
- [159] Modhave, D., Saraf, I., Karn, A. & Paudel, A. Understanding Concomitant Physical and Chemical Transformations of Simvastatin During Dry Ball Milling. *AAPS PharmSciTech* **21**, 152 (2020).
- [160] Wostry, M., Plappert, H. & Grohgan, H. Preparation of co-amorphous systems by freeze-drying. *Pharmaceutics* **12**, 941 (2020).
- [161] Halliwell, R. A. *et al.* Spray Drying as a Reliable Route to Produce Metastable Carbamazepine Form IV. *Journal of Pharmaceutical Sciences* **106**, 1874–1880 (2017).
- [162] Long, B., Walker, G. M., Ryan, K. M. & Padrela, L. Controlling Polymorphism of Carbamazepine Nanoparticles in a Continuous Supercritical-CO₂-Assisted Spray Drying Process. *Crystal Growth & Design* **19**, 3755–3767 (2019).
- [163] Ullah, M., Ullah, H., Murtaza, G., Mahmood, Q. & Hussain, I. Evaluation of Influence of Various Polymers on Dissolution and Phase Behavior of Carbamazepine-Succinic Acid Cocrystal in Matrix Tablets. *BioMed Research International* **2015**, 870656 (2015).
- [164] Patil, S. P., Modi, S. R. & Bansal, A. K. Generation of 1:1 Carbamazepine:Nicotinamide cocrystals by spray drying. *European Journal of Pharmaceutical Sciences* **62**, 251–257 (2014).
- [165] Tawfeek, H. M., Chavan, T. & Kunda, N. K. Effect of Spray Drying on Amorphization of Indomethacin Nicotinamide Cocrystals; Optimization, Characterization, and Stability Study. *AAPS PharmSciTech* **21**, 181 (2020).
- [166] Ferdynand, M. S. & Nokhodchi, A. Co-spraying of carriers (mannitol-lactose) as a method to improve aerosolization performance of salbutamol sulfate dry

- powder inhaler. *Drug Delivery and Translational Research* **10**, 1418–1427 (2020).
- [167] Corrigan, D. O., Corrigan, O. I. & Healy, A. M. Predicting the physical state of spray dried composites: Salbutamol sulphate/lactose and salbutamol sulphate/polyethylene glycol co-spray dried systems. *International Journal of Pharmaceutics* **273**, 171–182 (2004).
- [168] Wu, L. *et al.* Studies on the spray dried lactose as carrier for dry powder inhalation. *Asian Journal of Pharmaceutical Sciences* **9**, 336–341 (2014).
- [169] Buanz, A., Gurung, M. & Gaisford, S. Crystallisation in printed droplets: Understanding crystallisation of D -mannitol polymorphs. *CrystEngComm* **21**, 2212–2219 (2019).
- [170] Guimarães, T. F., Lanchote, A. D., da Costa, J. S., Viçosa, A. L. & de Freitas, L. A. P. A multivariate approach applied to quality on particle engineering of spray-dried mannitol. *Advanced Powder Technology* **26**, 1094–1101 (2015).
- [171] Hulse, W. L., Forbes, R. T., Bonner, M. C. & Getrost, M. The characterization and comparison of spray-dried mannitol samples. *Drug Development and Industrial Pharmacy* **35**, 712–718 (2009).
- [172] Littringer, E. M. *et al.* Spray Drying of Mannitol as a Drug Carrier—The Impact of Process Parameters on Product Properties. *Drying Technology* **30**, 114–124 (2012).
- [173] Dohrn, S. *et al.* Predicting process design spaces for spray drying amorphous solid dispersions. *International Journal of Pharmaceutics: X* **3**, 100072 (2021).
- [174] Tang, Y., Scher, H. B. & Jeoh, T. Volatile Retention and Enteric Release of d-Limonene by Encapsulation in Complex Coacervated Powders Formed by Spray Drying. *ACS Food Science & Technology* **1**, 2086–2095 (2021).
- [175] McGinty, J., Yazdanpanah, N., Price, C., ter Horst, J. H. & Sefcik, J. CHAPTER 1 Nucleation and Crystal Growth in Continuous Crystallization. In *The Handbook of Continuous Crystallization*, 1–50 (The Royal Society of Chemistry, 2020).

Bibliography

- [176] Yu, Q., Dang, L., Black, S. & Wei, H. Crystallization of the polymorphs of succinic acid via sublimation at different temperatures in the presence or absence of water and isopropanol vapor. *Journal of Crystal Growth* **340**, 209–215 (2012).
- [177] Wexler, A. Vapor Pressure Formulation for Water in Range 0 to 100 °C. A Revision. *Journal of research of the National Bureau of Standards. Section A, Physics and chemistry* **80A**, 775–785 (1976).
- [178] Kretschmer, C. B. & Wiebe, R. Liquid-Vapor Equilibrium of Ethanol–Toluene Solutions. *Journal of the American Chemical Society* **71**, 1793–1797 (1949).
- [179] Amstad, E. *et al.* Production of amorphous nanoparticles by supersonic spray-drying with a microfluidic nebulator. *Science* **349**, 956–960 (2015).
- [180] Dixit, M., Kulkarni, P., Kini, A. & Shivakumar, H. Spray drying: A crystallization technique : A review. *International Journal of Drug Formulation and Research* **1**, 1–29 (2010).
- [181] Bhavaniramy, S., Vishnupriya, S., Al-Aboody, M. S., Vijayakumar, R. & Baskaran, D. Role of essential oils in food safety: Antimicrobial and antioxidant applications. *Grain & Oil Science and Technology* **2**, 49–55 (2019).
- [182] Loscertales I. G. *et al.* Micro/Nano Encapsulation via Electrified Coaxial Liquid Jets. *Science* **295**, 1695–1698 (2002).
- [183] Deng, W., Klemic, J. F., Li, X., Reed, M. A. & Gomez, A. Increase of electrospray throughput using multiplexed microfabricated sources for the scalable generation of monodisperse droplets. *Journal of Aerosol Science* **37**, 696–714 (2006).
- [184] Podshivalov, A. V., Bronnikov, S., Zuev, V. V., Jiamrungraksa, T. & Charuchinda, S. Synthesis and characterization of polyurethane–urea microcapsules containing galangal essential oil: Statistical analysis of encapsulation. *Journal of Microencapsulation* **30**, 198–203 (2013).
- [185] Petrov, A. I., Volodkin, D. V. & Sukhorukov, G. B. Protein—Calcium Carbonate Coprecipitation: A Tool for Protein Encapsulation. *Biotechnology Progress* **21**, 918–925 (2005).

-
- [186] Ashraf, M. A., Khan, A. M., Ahmad, M. & Sarfraz, M. Effectiveness of silica based sol-gel microencapsulation method for odorants and flavors leading to sustainable environment. *Frontiers in chemistry* **3**, 42–42 (2015).
- [187] Fülöp, Z., Kurkov, S., Nielsen, T., Larsen, K. & Loftsson, T. Self-assembly of cyclodextrins: Formation of cyclodextrin polymer based nanoparticles. *Journal of Drug Delivery Science and Technology* **22**, 215–221 (2012).
- [188] Aguirre-Alonso, R. *et al.* Effect of process variables of spray drying employing heat pump and nitrogen on aromatic compound yield in powders obtained from vanilla (*Vanilla planifolia* Andrews) ethanolic extract. *Drying Technology* **37**, 1806–1820 (2019).
- [189] Noshad, M., Mohebbi, M., Koocheki, A. & Shahidi, F. Microencapsulation of vanillin by spray drying using soy protein isolate-maltodextrin as wall material: Microencapsulation of vanillin by spray drying. *Flavour and Fragrance Journal* **30**, 387–391 (2015).
- [190] Politi, Y., Arad, T., Klein, E., Weiner, S. & Addadi, L. Sea urchin spine calcite forms via a transient amorphous calcium carbonate phase. *Science* **306**, 1161–1164 (2004).
- [191] Ehrlich, H. Biominerals. In Ehrlich, H. (ed.) *Marine Biological Materials of Invertebrate Origin*, 21–44 (Springer International Publishing, Cham, 2019).
- [192] Warrant, E. J. Visual Optics: Remarkable Image-Forming Mirrors in Scallop Eyes. *Current Biology* **28**, R262–R264 (2018).
- [193] Iwasaka, M. Hidden triangular grating structures in biogenic guanine platelet. *AIP Advances* **10**, 095133 (2020).
- [194] Chen, F., Guo, D., Gao, J. & Ma, Y. Bioinspired Crystallization of Guanine. *The Journal of Physical Chemistry Letters* **12**, 11695–11702 (2021).
- [195] Mahamid, J., Sharir, A., Addadi, L. & Weiner, S. Amorphous calcium phosphate is a major component of the forming fin bones of zebrafish: Indications for an amorphous precursor phase. *Proceedings of the National Academy of Sciences* **105**, 12748–12753 (2008).

Bibliography

- [196] Jackson, A. P., Vincent, J. F. V., Turner, R. M. & Alexander, R. M. The mechanical design of nacre. *Proceedings of the Royal Society of London. Series B. Biological Sciences* **234**, 415–440 (1988).
- [197] Tang, Z., Kotov, N. A., Magonov, S. & Ozturk, B. Nanostructured artificial nacre. *Nature Materials* **2**, 413–418 (2003).
- [198] Beniash, E., Metzler, R. A., Lam, R. S. & Gilbert, P. Transient amorphous calcium phosphate in forming enamel. *Journal of structural biology* **166**, 133–143 (2009).
- [199] Bürki, P. M., Dent Glasser, L. S. & Smith, D. N. Surface coatings on ancient coccoliths. *Nature* **297**, 145–147 (1982).
- [200] Henderiks, J. Coccolithophore size rules—reconstructing ancient cell geometry and cellular calcite quota from fossil coccoliths. *Marine micropaleontology* **67**, 143–154 (2008).
- [201] Hajir, M., Graf, R. & Tremel, W. Stable amorphous calcium oxalate: Synthesis and potential intermediate in biomineralization. *Chem. Commun.* **50**, 6534–6536 (2014).
- [202] Thongboonkerd, V., Semangoen, T. & Chutipongtanate, S. Factors determining types and morphologies of calcium oxalate crystals: Molar concentrations, buffering, pH, stirring and temperature. *Clinica Chimica Acta* **367**, 120–131 (2006).
- [203] Chaplin, A. J. Histopathological occurrence and characterisation of calcium oxalate: A review. *Journal of Clinical Pathology* **30**, 800–811 (1977).
- [204] Franceschi, V. R. & Nakata, P. A. Calcium oxalate in plants: Formation and function. *Annu. Rev. Plant Biol.* **56**, 41–71 (2005).
- [205] Arriaga, L. R., Amstad, E. & Weitz, D. A. Scalable single-step microfluidic production of single-core double emulsions with ultra-thin shells. *Lab on a Chip* **15**, 3335–3340 (2015).
- [206] Kim, J.-W., Kang, H.-H., Suh, K.-D. & Oh, S.-G. Stabilization of water-soluble antioxidant in water-in-oil-in-water double emulsions. *Journal of dispersion science and technology* **24**, 833–839 (2003).

- [207] Chang, J.-C., Swank, Z., Keiser, O., Maerkl, S. J. & Amstad, E. Microfluidic device for real-time formulation of reagents and their subsequent encapsulation into double emulsions. *Scientific reports* **8**, 8143–8143 (2018).

Acronyms

AC Alternating Current

ACC Amorphous Calcium Carbonate

ACP Amorphous Calcium Phosphate

API Active Pharmaceutical Ingredient

CBZ Carbamazepine

DE Dextrose Equivalency

DEs Double Emulsions

DI Deionized

FWHM Full Width Half Maximum

IDT Interdigitating Transducer

MRI Magnetic Resonance Imaging

PBCA Polybutylcyanoacrylate

PCB Printed Circuit Board

PCL Polycaprolactone

PDMS Poly-(dimethylsiloxane)

Pe Peclet Number

PGMEA Propylene Glycol MethylAcetate

PLGA Poly(lactic-co-glycolic acid)

Appendix . Acronyms

PVA Polyvinyl Alcohol

SAW Surface Acoustic Wave

SEM Scanning Electron Microscopy

SPIONs Superparamagnetic Iron Oxide Nanoparticles

TEA Triethylamine

TEM Transmission Electron Microscopy

TGA Thermogravimetric Analysis

UV Ultraviolet

XRD X-ray Diffraction

Symbols

| | |
|--------------|-----------------------------|
| $\Delta\mu$ | Chemical Potential |
| T | Temperature |
| S | Supersaturation |
| k | Boltzmann Constant |
| k_{sp} | Solubility Product |
| ΔG | Gibbs Free Energy |
| r_n | Radius of Nuclei |
| V_m | Volume per molecule |
| γ | Surface tension |
| I | Nucleation Rate |
| n_0 | Number of Nucleation Sites |
| ΔG^* | Critical Gibbs Free Energy |
| v_h | Hopping Velocity |
| u | Growth Rate |
| v | Attachment Frequency |
| ΔG_m | Migration Energy |
| a_0 | Growth Prefactor |
| C_s | Average Solid Concentration |
| ρ | Density |
| d_D | Drop Diameter |
| d_p | Particle Diameter |
| λ | Capillary Wavelength |
| f_c | Frequency of Capillary Wave |
| θ | Diffraction Angle |

List of Figures

| | | |
|-----|--|----|
| 1.1 | Ostwald step rule, adapted with permission from [58]. | 11 |
| 1.2 | Non-classical nucleation pathways adapted with permission from [62]. | 12 |
| 1.3 | Schematic illustration of two different nucleation models for collagen mineralization. a) Extrafibrillar nucleation in unconfined space and b) intrafibrillar nucleation in a confined gap region. c) Geometry of confined amorphous calcium phosphate (ACP) nuclei in the gap region. Adapted with permission from [71] under the license of CC BY 4.0. | 13 |
| 1.4 | Micrographs of scallop eyes where mirrors composed of guanine layers to maximize and manipulate the light reflection. Adapted with permission from [76]. | 15 |
| 1.5 | (i) koifish (ii) koifish scale and iridophores composed of guanine crystals from the skin of koifish. Reproduced with permission from [77]. | 16 |
| 1.6 | Crystallization operation scheme. Adapted with permission from [78]. | 17 |
| 1.7 | Verneuil method adapted with permission from [79]. | 18 |
| 1.8 | Estimated share of the world production of 20000t of bulk crystals (1999). Adapted with permission from [82]. | 19 |

List of Figures

| | | |
|------|---|----|
| 1.9 | Schematics of seed crystallization. Two regimes of crystallization where Profile A shows a poor control over the size distribution and Profile B good control growth over on the size. Adapted with permission from [78]. | 19 |
| 1.10 | Scheme of protein crystallization routes for controlled precipitation and growth. Adapted with permission of the International Union of Crystallography from [86]. | 20 |
| 1.11 | Optical micrograph of a microfluidic chip capable of mixing lipids (L) and aqueous protein (Pr) solutions by pneumatic actuation. Adapted with permission from [95]. | 22 |
| 1.12 | Step-by-step 3D schematic drawings with cross-sectional views that describe the operation of the SlipChip. (a) Off-set view that shows the preloaded wells of the bottom plate, the ducts of the bottom plate, and the wells of the top plate. (b) View of the device available to the user, in which the top and bottom plates are aligned. (c) and (d) Loading of a single sample through the overlapping ducts of the bottom plate and wells of the top plate. (e) Slipping of the top plate relative to the bottom plate disconnects the sample wells of the top plate from the ducts of the bottom plate, and then exposes the sample wells to the wells of the bottom plate containing reagents. (f) The red well schematically shows a reaction taking place after mixing and incubation. Adapted with permission from [94]. | 22 |
| 1.13 | Design of drop generation structures in microfluidics based on (a) capillaries; (b) flow-focusing; (c) Y-junctions; and (d) T-junctions. Adapted with permission from [97]. | 23 |
| 1.14 | Formation of branched ACC at the center of the Y-junction when directly mixing solutions containing equimolar concentrations of $CaCl_2$ and Na_2CO_3 (20 mM) in microfluidics. Adapted with permission from [88]. | 24 |

| | |
|--|----|
| 1.15 (i) Nucleation and growth of a crystal from a protein dense aggregate at (a) $t = 0$, (b) $t = 15$ s, (c) $t = 45$ s, (d) $t = 75$ s, (e) $t = 120$ s, and (f) $t = 300$ s. (ii) (a) Drop generation using a co-flow microfluidic device fabricated using PDMS (b) Detected drops with crystals highlighted in green and without crystals highlighted in red. Reproduced with permission from [102]. Copyright 2014, American Chemical Society | 25 |
| 1.16 (i) (A) Schematic drawing of the trapping device. In the oil channel, drops display an ellipsoidal shape (B), but can relax on entering the wells (C). (D) Plot of stoichiometric equivalents of CO_2 and NH_3 delivered to the drop versus time, predicted by finite element modeling. (ii) Observed phase transformations in the trapping device. Raman spectroscopy demonstrates the potential to observe multiple short-lived metastable phases. Adapted with permission from [90]. | 26 |
| 1.17 Protein crystallization using the double emulsion-based approach on various compounds including (a) Lysozyme; (b) Thaumatin; (c) Trypsin; (d) Horseradish peroxidase. Scale bars: 300 μm . Adapted with permission from [101]. | 27 |
| 1.18 Fine crystalline particles formed by spraying (A) pure erythritol and (B) an erythritol/limonene emulsion as imaged by slightly uncrossed (75°) polarized light. While several gas bubbles are seen within one of the particles of A, particles in B also contain a multitude of fine oil droplets dispersed throughout the structure. Adapted with permission from [45]. | 28 |
| 1.19 Schematics of electrospray process, adapted with permission from [117]. | 29 |
| 1.20 The photo of a spraydryer. | 30 |
| 1.21 Statistics demonstrating the processes of flavor encapsulation, adapted with permission from [135]. | 31 |

List of Figures

| | | |
|------|---|----|
| 1.22 | Schematics of drying process demonstrating the main processing parameters and time scale of drying, adapted with permission from [139]. | 32 |
| 1.23 | Schematics of drying process demonstrating the main processing parameters and time scale of drying, adapted with permission from [126]. | 33 |
| 1.24 | Process parameters and formulation variables for the production of bioactive food-loaded nanoparticles by nano spray drying, adapted with permission from [141]. | 34 |
| 1.25 | SAW propagation along a piezoelectric substrate. (a) Configuration of the SAW device and the IDT electrode deposited on the piezoelectric substrate to generate the SAW. (b) Interaction of the SAW with a fluid causes drop deformation through acoustic streaming. The SAW amplitude is reduced by the interaction with the drop due to viscous dissipation. (c) Schematic representation of atomization occurring from the free surface of the drop. Adapted with permission from [147]. | 38 |
| 3.1 | Schematic illustration of succinic acid particles spray dried from solvents with different vapor pressures that result in particles displaying different crystal structures. Solvent delivered onto the SAW device is broken into (1) aerosols (2) that are guided into the drying unit (3) where solutes start to solidify to form spray-dried particles that are deposited on a substrate (4). | 51 |
| 3.2 | Structure and morphology of succinic acid particles. SEM image of succinic acid particles produced from ethanol-based solutions initially containing (A) 10 mM and (B) 100 mM succinic acid. (C) Crystal structure of spray-dried particles produced from solutions initially containing (1) 10 mM and (2) 100 mM succinic acid. . . . | 52 |

| | | |
|-----|---|----|
| 3.3 | (A-C and D-F) Morphology of spray-dried succinic acid particles produced from (A, D) DI water, (B, E) ethanol, and (C, F) acetone. The initial succinic acid concentration is (A-C) 10 mM and (E-G) 100 mM. | 53 |
| 3.4 | XRD of crystals that is precipitated under ambient conditions from ethanol solution containing 10 mM succinic acid. | 54 |
| 3.5 | XRD traces of succinic acid particles spray-dried from (1) acetone, (2) ethanol and (3) DI water with initial succinic acid concentrations of (A) 10 mM and (B) 100 mM | 55 |
| 3.6 | Influence of initial solute concentration on structural stability of spray-dried particles. XRD traces of particles spray-dried from solutions initially containing (A) 10 mM and (B) 100 mM succinic acid. Particles produced from 10 mM succinic acid containing solutions have been characterized at (1) t=0 (2) t= 2 weeks (3) t= 1 month (4) t= 3 months. Those produced from solutions initially containing 100 mM succinic acid have been characterized after (1) t=0, (2) t=5 h, (3) t=10 h, (4) t= 15 h and (5) t= 20 h. (C) Overview of the evolution of the structure of particles produced from ethanol-based solutions initially containing (●) = 100 mM, (■) = 75 mM, (◆) = 50 mM and (●) =10 mM succinic acid if stored at ambient conditions. | 57 |
| 3.7 | SEM image of succinic acid particles spray dried (A) in the absence of vanillin, with 60 mM (B) vanillin and (C) maltol. | 59 |
| 3.8 | SEM images of particles with vanillin after storage at A) 65°C for 10 h and B) ambient conditions for 48h. Particles are produced from ethanol-based solutions containing 80 mM succinic acid and 40 mM vanillin. | 60 |
| 3.9 | SEM image of vanillin nanoparticle sprayed from an ethanol-based solution containing 20 mM vanillin. | 60 |

List of Figures

| | | |
|------|---|----|
| 3.10 | A) Molecular structures of 1) vanillin 2) maltol. (B) Evolution of the crystal structure of vanillin loaded succinic acid particles initially containing 100 mM succinic acid and (▲) 60 mM, (●) 20 mM, (■) 0 mM of vanillin and (▼) 60 mM of maltol. | 61 |
| 4.1 | (A) Schematic illustration of the microfluidic spray-dryer composed of (1) a SAW generator connected to (2) an IDT pattern on a piezoelectric chip onto which liquid is delivered through a PDMS-based channel (3) before it is atomized into airborne drops that (4) dry within a dedicated drying unit (5). (B) Schematic illustration of the formation of succinic acid particles that are loaded with vanillin within drying drops. The solidification time of reagents contained in the drop is dictated by its drying rate. | 68 |
| 4.2 | Morphology of succinic acid particles. SEM image of succinic acid particles spray-dried from ethanol-based solutions containing (A) 10 mM and (B) 100 mM succinic acid. (C) Size distribution of particles sprayed from solutions containing 10 mM (orange) and 100 mM (blue) succinic acid. (D) The initial size distribution of the corresponding ethanol-based drops initially containing 10 mM (orange) and 100 mM (blue) succinic acid. | 70 |
| 4.3 | SEM image of spray-dried particles composed of a mixture of succinic acid (S) and vanillin (V) produced from solutions initially containing 100 mM succinic acid and (A) 10 mM (B) 15 mM, (C) 20 mM, and (D) 60 mM vanillin. (E) XRD traces of vanillin loaded succinic acid particles spray-dried from a solution initially containing (1) 10 mM, (2) 15 mM, (3) 20 mM, and (4) 60 mM vanillin. The succinic acid concentration is kept constant at 100 mM. | 73 |
| 4.4 | SEM image of spray-dried particles composed of a mixture of succinic acid (S) and vanillin (V) produced from solutions initially containing (A) 10 mM S, 10mM V (B) 50 mM S, 30 mM V (C) 80 mM S and 30 mM V. | 74 |

| | | |
|-----|---|----|
| 4.5 | Vanillin encapsulation efficiency. (A, B) Encapsulation efficiency of vanillin as a function of its concentration (A) for a constant molar ratio of succinic acid: vanillin of 5:3 and (B) constant succinic acid concentration of 80 mM. (C) Encapsulation efficiency of vanillin within tartaric acid-based particles as a function of the vanillin concentration. The tartaric concentration is kept constant at 15 mM. | 76 |
| 4.6 | TGA of 1) control bulk vanillin, (2,3) particles sprayed from DI water containing 100 mM succinic acid and 60 mM vanillin with a 2) commercial spray dryer and 3) microfluidic spray dryer. 4) Control of bulk succinic acid. | 77 |
| 4.7 | Vanillin release kinetics. Weight percentage of vanillin released if particles are stored at 65 °C as a function of the vanillin concentration contained in the initial solution if (A) the molar ratio of succinic acid to vanillin is kept constant at 5:3 and (B) the succinic acid concentration is fixed at 80 mM. (C) Release kinetics of vanillin from succinic acid particles as a function of the vanillin concentration if the succinic acid concentration is kept constant at 80 mM. | 79 |
| 5.1 | Image of flow focusing microfluidic device forming double emulsions. | 86 |
| 5.2 | SEM image of $CaCO_3$ formed in single emulsions containing stoichiometric ratios of A) Ca^{+2} : HCO_3^- B) Ca^{+2} :2 HCO_3^- C) Schematic illustration of $CaCO_3$ formation on the oil/water interface. | 88 |
| 5.3 | Optical microscopy images taken (A-C) without and (E-H) with crossed polars revealing guanine crystals formed in trapped single emulsion drops. HFE-7500 was constantly injected during incubation for A,D) a few minutes with no TEA (B,E) for 16 hours containing 0.5% (v/v) TEA (C,F) for 5 hours containing 1% (v/v) TEA. | 89 |
| 5.4 | Schematic illustration of the formation of calcium oxalate crystals within double emulsions. | 90 |

List of Figures

| | | |
|------|--|----|
| 5.5 | Formation of calcium oxalate crystals in double emulsions containing 250 mM oxalic acid within their cores upon incubation in an aqueous solution containing 325 mM $CaCl_2$ over the timeframe of A) $t = 0$ B) $t = 5h$ C) $t = 20h$ | 90 |
| 5.6 | Morphology of calcium oxalate crystals formed in double emulsions containing A) 250 mM, B) 100 mM oxalic acid in their cores. $C[CaCl_2] = 325$ mM. | 91 |
| 5.7 | Morphology of calcium oxalate crystals formed in double emulsions containing A) 250 mM, B) 100 mM. and C) 50 mM oxalic acid in their cores upon incubation in DI water containing 325 mM of $CaCl_2$ over 20h. | 92 |
| 5.8 | Influence of $CaCl_2$ concentration on the core size change and crystal morphology. 250 mM oxalic acid containing double emulsions incubated in DI water containing A) 325 mM, B) 135 mM, C) 32 mM $CaCl_2$. Δp is kept constant at 660 mOsm/kg D) Core size change of double emulsions containing 250 mM oxalic acid or 10 wt% PEG as a function of the $CaCl_2$ concentration. | 93 |
| 5.9 | Influence of the osmotic pressure on the change of the core size of DEs. DEs containing 250 mM oxalic acid in their cores are incubated over 20h in DI water containing 325 mM $CaCl_2$ where the osmotic pressure has been adjusted with sucrose to A) $\Delta p = 200$ mOsm/kg B) $\Delta p = 100$ mOsm/kg, C) $\Delta p = 0$ mOsm/kg D) Core size change of double emulsions containing 250 mM oxalic acid or 10 wt% PEG that have been incubated in aqueous solutions possessing varying osmolarities. | 94 |
| 5.10 | Morphology of calcium oxalate crystals when co-precipitated with vanillin. Crystals were formed in double emulsions initially containing 250 mM oxalic acid and 13 mM vanillin in their cores upon their incubation in an aqueous solution containing A) 325 mM B) 250 mM C) 100 mM $CaCl_2$ over 20h. | 95 |



Aysu Ceren Okur

Materials Science Engineer

CONTACT

+41 78 729 25 15
okurceren.90@gmail.com
linkedin.com/in/aysuokur/
Swiss B permit
Lausanne, Switzerland

SUMMARY

I am a materials science engineer specialized in spray drying, volatile encapsulation, crystalline nanopowders, release kinetics and microfluidics. I have an interdisciplinary background bridging the bioinspired materials and functional technologies to acquire high-performance sustainable systems & products.

COMPETENCES

Spray Drying
Microfluidics
Spectroscopy
Electron & Confocal
Microscopy
Emulsions
Crystallization
Volatile Encapsulation
Bioinspired Materials
Powder Technologies
C++ Autocad Matlab
Latex
Image and Data Analysis

LANGUAGES

English C1
French B1
Turkish Native

TRAININGS

Body language
Presentation skills
Stress management
Research & publication

INTEREST & HOBBIES

Marbling
Squash
Swimming

EDUCATION

EPFL

PhD - Soft Matter (2017-2022)

Thesis: "Drops: Controlled Crystallization of Organic Crystals and Their Use as Matrix Materials for the Encapsulation of Volatiles"

Koc University

M.Sc. - Biomedical Engineering (2008-2013)

Thesis: "Synthesis of PEG-Hydrogel Particles through Water-in Water Emulsion for Cancer Cell Targeting Therapy"

Sabanci University

B.Sc. - Materials Science & Engineering w/ Chemistry Minor (2008-2013)

GPA: 3.59/4.0 Graduated as 1st ranked among the department

EXPERIENCE

Doctoral Assistant

EPFL (2017-2022)

Projects

Funded by and collaborated with Firmenich

- Encapsulation of volatiles in organic crystals via microfluidic spray drying
- Influence of spray-drying processing conditions on crystal structure, phase separation and volatile retention in crystals
- Confined crystallization in single and double emulsions

Responsibilities:

- Experimental design for optimization of microfluidic spray drying system for maximizing powder collection and processing conditions
- Characterization of crystals and volatile retention via XRD, SEM, TGA, FT-IR
- Regular written and verbal reporting for academic and industry setting on site of EPFL and Firmenich
- Supervision of master students for thesis and semester projects

Research Intern

University of California, Davis, USA (2016-2017)

- Preparation of TEM samples of twin boundaries with FIB

Research Assistant

Koc University, Istanbul, Turkey (2014-2016)

- Synthesis of microgels and analysis of cell uptake and viability of cancer cells

Summer Research Intern

John Kepler University, Linz, Austria (06/2012-09/2012)

- Synthesis of pigment precursors and their application on organoelectronic transistor

Peer Tutor & Teaching Assistant

Sabanci University, Koc University, UC Davis & EPFL (2011-2020)

Responsibilities:

- Active learning peer study sessions
- Assisting bachelor and master level courses by holding Q&A sessions and exam preparation, homework and exam assessments

Courses: Calculus I-II, Physics I-II, Introduction to chemistry for engineers, Semiconductors, Soft matter

ACHIEVEMENTS

TUBITAK (The Scientific & Research Council of Turkey) Scholarship for Abroad Graduate Studies

Koc University Full Merit Scholarship

Erasmus Scholarship for Abroad Summer Internship

Dean's honor list

Sakip Sabanci merit scholarship

EXTRACURRICULAR ACTIVITIES

Turkish Student Association, UC Davis

-Organizing events and introductory sessions for new students

Civic involvement project

-Organizing social activities for primary school age children at orphanage

PUBLICATIONS

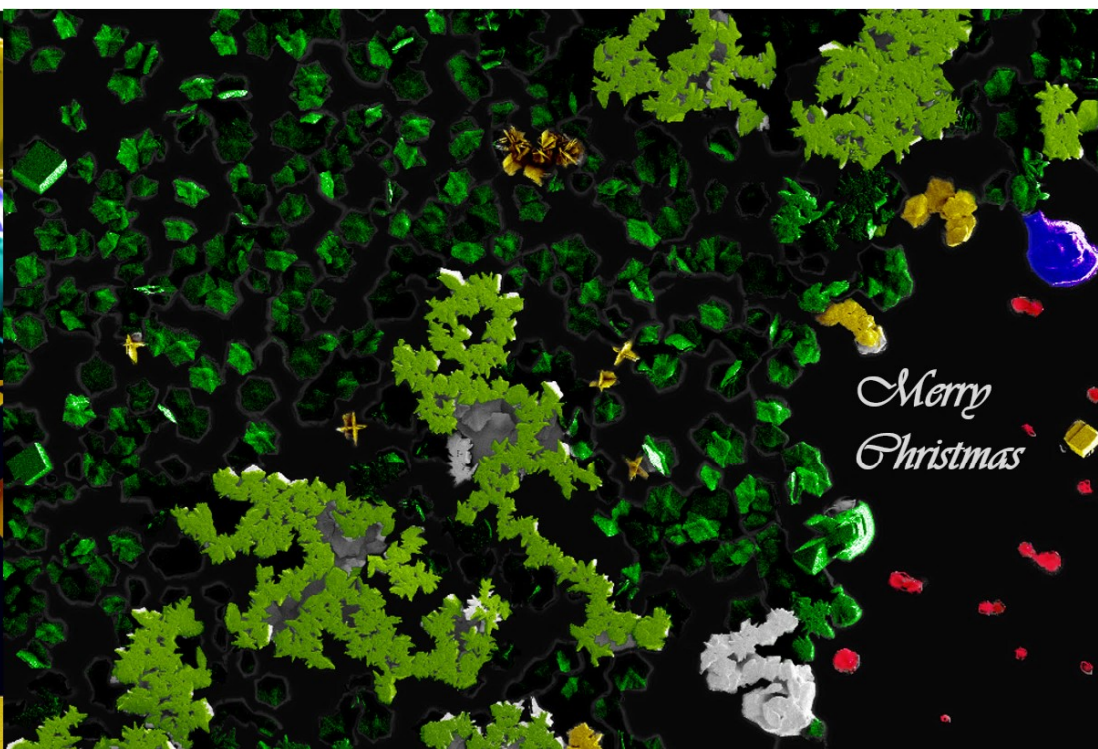
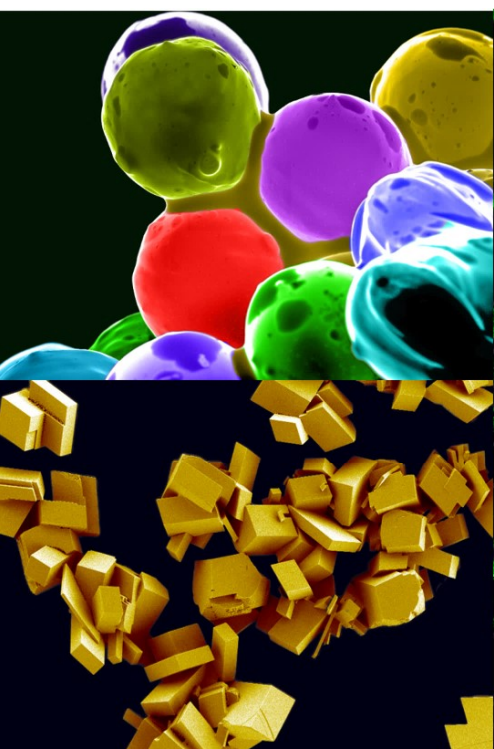
-Succinic acid-based particles as carriers of volatile substances

Sustainable Chemistry & Engineering

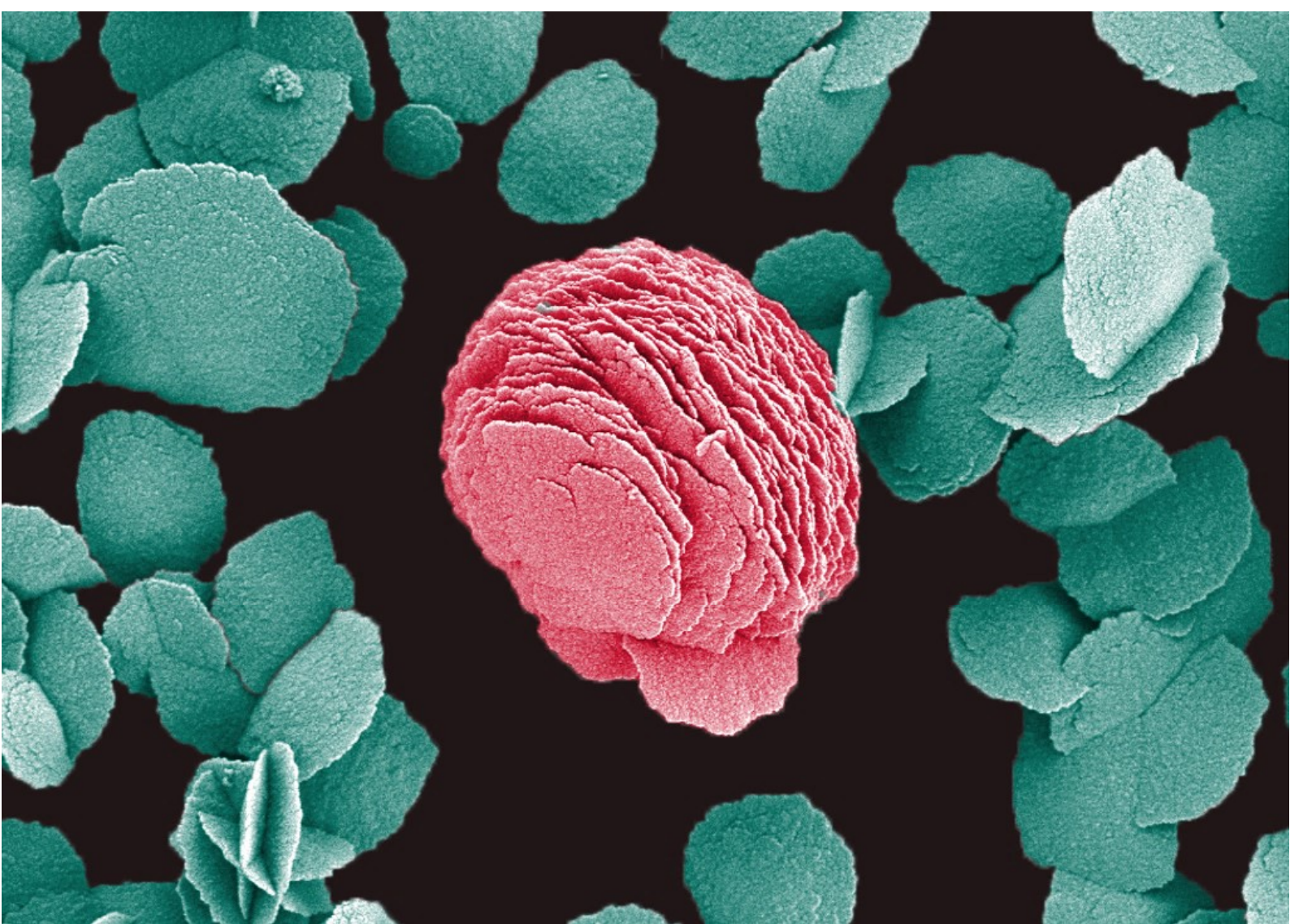
-Controlling the crystal structure of spray-dried succinic acid particles In manuscripting

-Targeting cancer cells via tumor-homing peptide CREKA functional PEG nanoparticles

Colloids and Surfaces B: Biointerfaces

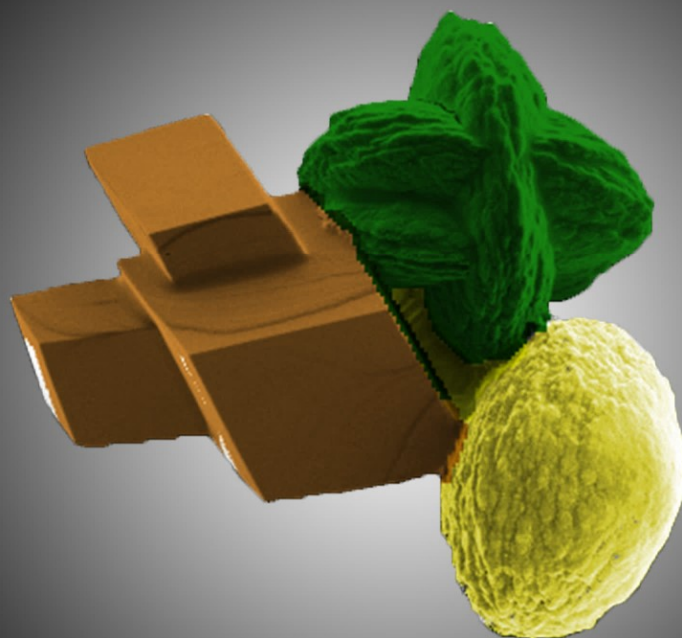




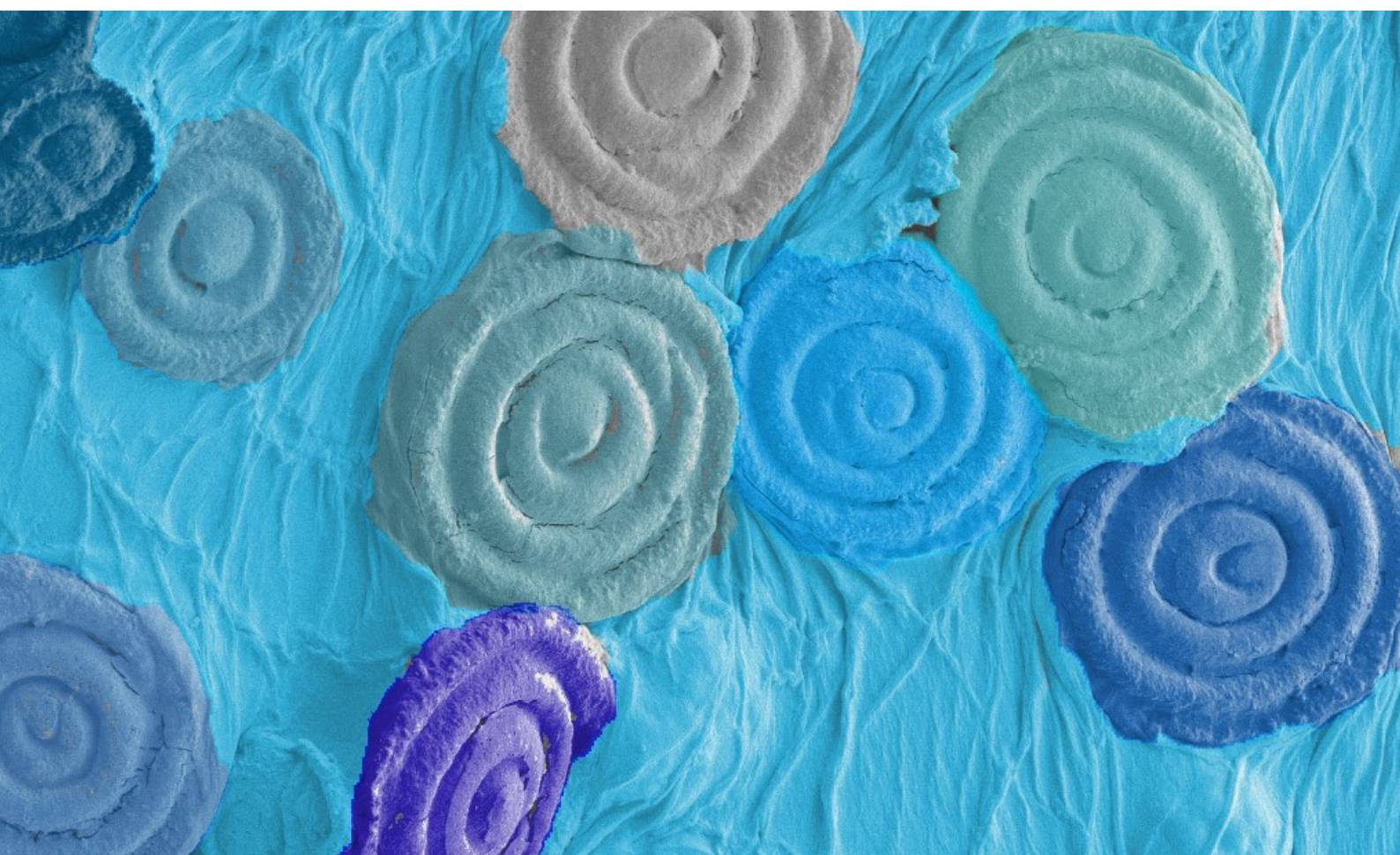








WISH YOU A HAPPY 2021!





Merry Christmas



HAPPY 2022!

